UNIVERSITÉ DE SHERBROOKE

Faculté de génie

Département de génie chimique et de génie biotechnologique

PLA/Starch nanocrystals nanocomposite: study of crystallinity, gas permeability and biodegradability

Étude de la cristallisation, perméabilité et dégradabilité de nanocomposites Poly lactique acide / Nanocristaux d'amidon

Thèse de doctorat

Spécialité : génie chimique et de génie biotechnologique

Somayeh Sharafi Zamir

Jury:

Pr. Mathieu Robert (Directeur)

Pr. Said Elkoun (Directeur)

Pr. Reza Frouzanmehr (Examiner)

Pr. Armand Soldera (Examiner)

Dr. Patrice Cousin (Examiner)

Sherbrooke (Quebec) CANADA **(February 2020)**

To my parents for their love, kindness and supports

به پدر و مادرم برای عشق ومحبت و حمایت بی دریغشان

Résumé

Le mélange d'amidon et de PLA est une approche bien connue et économique permettant d'obtenir les propriétés désirés en fonction des besoins de l'industrie. Le composite PLA/amidon est l'un des mélanges les plus prometteurs offrant de nombreux avantages car le PLA présente des caractéristiques exceptionnelles, telles que des propriétés mécaniques élevées (ex : résistance élevée), une bonne transparence, une biocompatibilité et une biodégradabilité. De plus, le PLA est l'un des polymères bioplastiques le plus largement utilisé, qui convient parfaitement aux applications d'emballages alimentaires. Cependant, le PLA présente certains inconvénients tels que la fragilité, une faible rigidité à l'état fondu, un faible taux de cristallinité, taux d'oxygène élevé et une perméabilité élevée à la vapeur d'eau. Jusqu'à maintenant, des nombreux méthodes différents ont été préparés pour améliorer la cristallinité et les propriétés de barrière du PLA, tels que l'ajout d'agents de nucléation, l'ajout de plastifiants et aussi l'ajout d'une combinaison d'agents de nucléation et de plastifiants. Parmi ceux-ci, l'ajout d'agents de nucléation est l'un des méthodes les plus polyvalents de renforcer non seulement le taux de cristallinité mais aussi d'induire une taille et une structure cristalline plus uniforme qui contrôlent d'autres propriétés. De plus, il a été démontré que l'ajout d'agents de nucléation peut modifier les structures cristallines et d'autres propriétés physiques du PLA, telles que les propriétés mécaniques et les propriétés de barrière aux gaz. L'ajout d'agents de nucléation est une approche efficace et polyvalente pour améliorer non seulement le taux de cristallisation, mais également les propriétés de barrière aux gaz des nanocomposites de PLA. L'ajout d'agent de nucléation crée un obstacle physique au passage des molécules de gaz. Il peut donc être une option unique pour concevoir les propriétés de barrière des nanocomposites de PLA. Au cours des dernières années, on s'intéresse de plus en plus au renfort des propriétés de barrière des PLA par l'ajout de nano-charges bio tels que les nano-cristaux d'amidon (SNCs). Les SCNs sont l'un des nano-bio-matériaux les plus prometteurs qui conservent non seulement les propriétés de l'amidon telles que la renouvelabilité, la non-toxicité et la biodégradabilité, mais aussi une surface spécifique élevée, une homogénéité élevée et donc une énergie de surface élevée. Cependant, PLA et SNCs ont une faible adhésion interfaciale en raison de l'incongruité de leur hydrophilie. En effet, il est nécessaire de renforcer la compatibilité entre deux composants. Le greffage de SNCs avec des molécules biosourcées telles que l'acide lactique (LA) semble produire des matériaux hydrophobes pour SNCs, ce qui peut augmenter l'adhésion interfaciale entre SNCs et PLA. LA est un acide organique avec différents groupes fonctionnels

(ex -COOH). Donc, il peut réagir avec les SNCs pour créer un ester. En utilisant cette méthodologie d'estérification simple, la fonctionnalisation covalente des SNCs permet leur bonne dispersion dans les composites correspondants. Par ailleurs, LA est un monomère de structure cristalline de PLA. Par conséquent, la modification chimique des SNCs avec LA ne conduit pas seulement à un composite entièrement biodégradable, mais augmente également l'adhésion interfaciale entre le PLA et les SNC. Dans ce travail, les SNCs ont été greffées chimiquement avec de l'acide lactique par réaction d'estérification et leur compatibilité avec la matrice PLA a été étudié de manière exhaustive. Dans la deuxième étape, l'effet des SNCs greffées en tant qu'agent de nucléation sur la cinétique de cristallisation (nucléation, taux de croissance de la sphérulite) du PLA a été déterminé. Cela est obtenu en comparant le comportement de cristallisation de nanocomposites PLA/SNCs-g-LA à différentes concentrations de nanoparticules de SNCs-g-LA. Par ailleurs, l'aptitude des SNCs à contrôler les conformations cristallines et les structures cristallines du PLA (α et α') est étudiée. Cette partie ouvre la voie à la recherche de concentrations optimales de nanoparticules de SNCs-g-LA sur la structure cristalline impaire de contrôle. Dans cette étude, on examine l'effet des nanoparticules et de la cristallinité de SNCs-g-LA sur la perméabilité à l'oxygène et à la vapeur d'eau de PLA en raison de la modification de l'épaisseur et de la cristallinité de ses cristaux.

Mots clés: Poly (acide lactique), SNCs, agents de nucléation, cristallisation et propriétés de barrière.

Summary

Blending of Poly (lactic acid) (PLA) with starch is a promising and economical approach to achieve desirable properties according to the needs of the food packaging industry. PLA/starch blend offers several benefits compared to other biodegradable polymer blend because of desirable characteristics of PLA such as high mechanical properties (i.e. high strength), good transparency, biocompatibility and biodegradability. In addition, PLA is one the most widely available bioplastic polymer that is suitable in food packaging applications. However, PLA has some drawbacks such as low melt rigidity, low rate of crystallinity and high oxygen and water vapor permeability. Until now, many different methods have been found to improve the crystallinity and barrier properties of PLA such as adding nucleating agents, adding plasticizers, and adding combination of nucleating agents and plasticizers. Among them, adding nucleating agents is one the most versatile method due to the fact that they not only enhance the rate of crystallinity but also induce a more uniform crystalline size and crystal structures. In addition, it has been shown that the adding of nucleating agents can modify crystalline structures and other physical properties of PLA such as gas barrier properties. This is because of the fact that pure PLA has a higher amorphous to crystalline content, which is known to facilitate gas permeability. Thus, the addition of nucleating agent can create physical obstacle and hindered the passage of the gas molecules and therefore improve the barrier properties of PLA nanocomposite. In recent years there is a growing interest on enhancing crystallinity of PLA by adding natural nano-fillers such as starch nanocrystals (SNCs). SNCs is one of the most promising natural nano-filler that not only retains starch properties such as renewability and biodegradability but also, has high specific surface area, high homogeneity and hence high surface energy. However, PLA and SNCs have a poor interfacial adhesion due to the difference in their hydrophilicity. Therefore, there is a need to enhance the compatibility between two components. Grafting of SNCs with bio-based molecules such as lactic acid (LA) result in hydrophobic SNCs materials which can then increase the interfacial adhesion between SNCs and PLA. LA is an organic acid with different functional groups (i.e.−COOH). Hence, some –OH functional groups of SNCs can replace with −COOH groups to create an ester bond. Using this straightforward esterification methodology, covalent functionalization of SNCs, enables good dispersion of SNCs into the corresponding composites. Moreover, LA is a monomer of PLA crystal structure. Therefore, chemical modification of SNCs with LA not only results in an entirely biodegradable composite but also increase the interfacial adhesion between PLA and

SNCs. In the first step of this work, SNCs were chemically grafted with lactic acid (SNCs-g-LA) through esterification reaction and their compatibility with PLA matrix was studied comprehensively. In the second step, the effect of SNCs-g-LA as a nucleating agent on the kinetics of crystallization (nucleation and spherulite growth rate) of PLA was determined. This was done by comparing crystallization behaviour of PLA/SNCs-g-LA nanocomposites at different concentrations of SNCs-g-LA nanoparticles. Additionally, the ability of SNCs-g-LA nanoparticles to control crystalline conformations ($\alpha \; and \; \alpha'$), phase transition temperature and melting behaviour of PLA from melt state are studied. Finally, the effect of impermeable crystalline regions and $\alpha \; and \; \alpha'$ structures on the oxygen and water vapour permeability of PLA nanocomposites is examined.
Keywords: Poly (lactic acid), SNCs, nucleating agents, crystallization and barrier properties.

Acknowledgement

I would like to thank Prof. Mathieu Robert and Prof. Saïd Elkoun for their support, patience, motivation, and immense knowledge during my PhD program. I really grateful to Prof. Frouzanmehr, Prof. Soldera and Prof. Groleau for evaluation of my thesis. Also, I would like to express my appreciation to Dr. Babak Fathi, and all of my colleagues in Carrefour of Innovative Technologies and Eco-design (CITÉ) who shared their knowledge and information. Finally, I appreciate the help and cooperation of technical staffs at Center for characterization of Materials (CCM) of the Université de Sherbrooke, Mme. Sonia Blais, M. Charles Bertrand, M. Carl St. Louis, and M. Stephane Gutierrez for being great help during my PhD. Most importantly, I would like to thank my family and my Ph.D would have been not possible without the love and patience of my family. My immediate family, to whom this dissertation is dedicated to, has been a constant source of love, concern, support and strength all these years. I warmly appreciate my all of my friends in Sherbrooke for their supports as well.

TABLE OF CONTENTS

LIST OF FIGURES

LIST OF TABLES

List of Symbol

Symbol	*Symbol Definition*
t	Time
X(t)	Degree of crystallinity
$t_{1/2}$	Crystallization half-time
T_m	Melting temperature
T_g	Glass transition temperature
T_s	Partial melting temperature
T_{CC}	Cold crystallization temperature
ΔH_{CC}	Cold crystallization enthalpy
n	Avrami exponent
K	Avrami constant
SGR	Spherulite growth rate
M_n	Number-average molecular weight
M_w	Weight-average molecular weight
WVTR	Water vapor transmission rate
OTR	Oxygen transmission rate
RH	Relative humidity
XPS	X-ray photoelectron spectroscopy
DMA	Dynamic mechanical analysis
OP	Optical microscopy
WAXD	Wide Angel X-ray Diffraction
SAXS	Small Angle X-ray Diffraction
TEM	Transmission Electron Microscopy
TGA	Thermogravimetric analysis
DSC	Differential Scanning Calorimetry
FTIR	Fourier transform infrared spectroscopy
XRD	X-ray Diffraction
SEM	Scanning electron microscopy
ROP	ring-opening polymerization
RAF	rigid amorphous fraction
MAF	Mobil amorphous fraction
NNAs	nanosized nucleating agents
ROP	ring-opening polymerization
RAF	rigid amorphous fraction

List of Acronyms

Acronym	*Definition*
PLA	Poly(lactic acid)
PLLA	PLLA Poly(L-lactic acid)
PDLA	Poly(D-lactic acid)
PP	poly propylene
PEEK	Poly(ether ether ketone)
TPS	Thermoplastic starch
CNC	Cellulose nanocrystals
CNT	Carbon nanotubes
MWCNT	Multiwall carbon nanotube
CB	Carbon black
MCB	Modified carbon black
PEG	Polyethylene glycol
PPG	Polypropylene glycol
CO_2	Carbon dioxide
PP	Polypropylene
PB	Polybutylene
SNCs	Starch nanocrystals
CNCs	Cellules nanocrystals
CNW	Cellulose nano wicker
CNF	Cellulose nano fiber
H_2SO_4	sulfuric acid
MDI	methylenediphenyl diisocyanate
MA	and malic anhydride
TPS	Thermo plastic starch
PS	poly styrene
PET	Poly (ethyleneterephthalate)

Chapter 1

1.1. Introduction

Development of bio-based and bio-degradable polymers is an important step towards replacement of traditional synthetic plastic materials [1–4]. Among the different bio-based and bio-degradable polymers, Poly (lactic acid) (PLA) has been subjected of many previous investigations due to its commercial availability and easy in proccessability [2–5]. In addition, PLA possesses remarkable properties including good tensile (50-70 MPa) and impact (2.5 kJ/m^2) strength, high transparency (equivalent to that of its petroleum-based counterpart) and good biocompatibility [1,2,4,5]. Therefore, these attractive properties of PLA make this polymer as a potential candidate for various applications specifically in food packaging industry where it's global production is currently ~0.20 million tons in 2016 [5]. This figure is likely to be double by 2026 [5]. However, PLA has some shortcomings that do not fulfill all the prerequisites of the food packaging industry. It has been demonstrated that the slow rate of crystallization and low degree of crystallinity of PLA decreases the melting strength that can lead to a failure in polymer processing. In addition, PLA has high oxygen and medium water vapor permeability. The oxygen transmission rate (OTR) of PLA ranges between11000 to 36000 $mL\,\mu m\,m^{-2}day^{-1}$ at 23 ℃ while the water vapor transmission rate (WVTR) of PLA is around 5250 $mL\,\mu m\,m^{-2}day^{-1}$ at 90 RH which is 35% and 43% lower than OTR and WVTR of PET respectively [7]. It has been shown that there is a close relationship between gas permeability (i.e. oxygen and water vapor) and microstructure of semicrystalline polymers such as PLA. Therefore, study of the crystalline organization of PLA is considered as a fundamental step in order to engineer physical properties of PLA such as gas barrier properties. Gas barrier properties has a close relation with the distribution of the amorphous and different crystalline structures. In particular, different crystalline forms of PLA namely $\alpha\ and\ \alpha' -$ crystal structure are observed via using specific thermal history. The disordered $\alpha' -$ structure is considered as a metastable crystalline form and it transformed into more ordered $\alpha -$structure upon heating above 120 ℃. However, below 120 ℃ a mixture of α' and $\alpha -$crystal structure are found to be stable. Therefore, the crystallization temperature is an important parameter to be considered because even a small variation in the thermal history can lead to the development of a different crystalline structure [17]. Moreover, crystallization

behaviour, gas barrier properties and biodegradability are influenced by the crystalline structures. Therefore, a better understanding of the crystallization behaviour of PLA and of its effect on the gas barrier properties are critical steps in order to extend the application of PLA. Several studies have been published with an aim to understand and to control PLA crystallization by the use of proper nucleating agents and processing conditions. Numerous nucleating agents have been suggested to enhance crystallinity and gas barrier properties of PLA such as talc, clay (montmorillonite and kaolinite) and silicate oxides [8].

In recent years there is a growing interest in blending PLA with natural nano-size nucleating agents. Blending of PLA with natural nano-size nucleating agents is a promising technique and has led to development of more efficient PLA nanocomposites with desirable properties for food packaging industry [4,7,9,10]. Among the various natural nano-size nucleating agents, starch nanocrystals (SNCs) is regarded as the most promising candidate for improving PLA properties [4,7,9,10]. SNCs have several advantages over normal starch including greater mechanical stability, easier chemical modification due to the higher surface area which enable SNCs to disperse easily in polymer matrix and decent homogenity compared to native starch [4,7,9,10]. Blending of PLA with SNCs not only reduces the cost of the final products but also, enhances biodegradability of PLA. However, it is well documented that there is a poor interfacial adhesion between PLA and SNCs because of differences in their surface chemistries which results in their incompatibility and limits PLA/SNCs nanocomposites applications [10,11]. Previous studies have shown that the enhancement of interfacial adhesion between SNCs and PLA matrix can lead to substantial improvement in the thermal and mechanical properties [10]. Recently, there has been growing interest on chemical modifications of starch by grafting reactions such as esterification, etherification and double modifications to enhance the compatibility between starch and PLA. However, most of these functional groups are toxic and they are not allowed to be used in food packaging industry. Therefore, there is a need to develop an appropriate and non-toxic grafting method.

A detailed literature review has shown that despite of a number of research works focused on the effect of the modified SNCs on the thermal and mechanical properties of PLA, there is only a handful studies which have reported the effect of renewable and biodegradable polymer materials such as SNCs on the crystallinity and gas barrier properties of PLA. Yet, most of these studies have neglected the presence of both $\alpha' and\ \alpha -$ structures in crystalline PLA and the effect of

these crystalline structures on gas barrier properties. Therefore, a full understanding of the crystallization behaviour, morphology and crystalline conformations of PLA/SNCs is essential to optimize the gas permeability (i.e. oxygen and water vapor) of PLA/SNCs nanocomposites.

1.2. Objectives

1.2.1. Objective 1

The first objective of this work is to chemically modify the SNCs surface by lactic acid (LA) to fabricate a biodegradable and renewable nanocomposite and engineer its thermal and mechanical properties. Grafting of SNCs with an effective bio-based molecules such as LA with different functional groups (i.e. hydroxyl and carboxyl groups) results in hydrophobic SNCs materials which can increase the interfacial adhesion between SNCs and hydrophobic polymer materials. Using this simple esterification methodology, functionalization of SNCs with LA, enhances the dispersion state of SNCs into the corresponding nanocomposite and increases chemical affinity between two components. Moreover, LA is a monomeric unit of PLA crystal structure. Therefore, chemical modification of SNCs with LA (SNCs-g-LA) not only enhances the chemical affinity but also, increases crystallographic interactions or physically interactions between PLA and SNCs-g-LA nanoparticles.

1.2.2. Objective 2

The second objective of this work is to explore the role of SNCs-g-LA nanoparticles as a nucleating agent on the kinetics of crystallization and crystallization behaviour of PLA. We used isothermal thermal analysis to map the nucleation- and the growth-crystallization of PLA/SNCs-g-LA nanocomposites and explore the effect of SNCs-g-LA concentrations on the resulting microstructure. Firstly, the effect of SNCs-g-LA varying in concentrations (3, 5 and 7 wt%) on the crystallization behaviour and half time ($t_{1/2}$) of PLA were studied. Then, crystallization kinetics and the activation energy were quantified using by Avrami equation as a function of T_c (80-130 ℃). In addition, spherulitic growth rate and morphology of PLA nanocomposites were studied for the same range of T_c. Then, the influence of SNCs-g-LA varying in concentrations on the phase transition and melting behaviour were determined. This provided a better insight on the effect of SNCs-g-LA nanoparticles on the promotion of crystalline structures (α and α') of PLA. Finally, the effect of SNCs-g-LA nanoparticles on the oxygen and water vapour permeability of

PLA nanocomposite due to modification in its crystal thickness and α and α'-crystalline structures were quantified.

1.2.3. Objective 3

The third objective is to determine, the effect of $\alpha -$ crystalline structure on the oxygen and water vapor barrier properties. For this purpose, different weight percentage (wt%) of SNCs-g-LA nanoparticles were incorporated into PLA and crystallized above 130 ℃, where α- structure of PLA is observed, for different crystallization time and subsequently oxygen and water vapour permeability of PLA nanocomposites were studied. The obtained results are intended to help us to improve our understanding the effect of induced crystalline structures (i.e. α −structure) on the barrier performance of PLA films. Finally, optimized crystallization conditions were determined and the gas transport properties of the crystallized PLA nanocomposite are discussed.

1.2.4. Objective 4

The fourth objective is to determine the effect of SNCs-g-LA nanoparticles on the soil burial degradation of PLA. The effect of esterification modification of SNCs and soil burial degradation time on the degradation properties of PLA nanocomposites were investigated and compared with the degradation results of neat PLA and PLA/neat SNCs nanocomposite degradation.

1.3. Original Contribution

The present work demonstrates several original and novel ways to improve the crystallinity and permeability of PLA nanocomposites. In the first section, SNCs is grafted by lactic acid (LA) and subsequently, their compatibility with PLA matrices were demonstrated. Additionally, thermal and mechanical properties of PLA/SNCs-g-LA with various concentrations of SNCs-g-LA were investigated. In the second part, the effect of various concentrations of SNCs-g-LA on kinetics of crystallization (nucleation and spherulite growth rate) were shown. While in the third part, the effect of SNCs-g-LA content on the crystalline structures, phase transition temperature and phase content were investigated. The effect of the more ordered crystalline structure from melt state on gas permeability (oxygen and water vapor permeability) were investigated at different crystallization time. Finally, the effect of esterification modification of SNCs and soil burial degradation time on the degradation properties of PLA nanocomposites were examined.

1.4. Organization of the Thesis

The thesis has been organized in the following manner. In chapter 2, a literature review on PLA crystallization has been presented in three parts. A general knowledge on crystallization of PLA, its crystalline phases and the ways that have been employed so far to improve the crystallinity of PLA and barrier properties is reflected in the first section. The second part focused on different chemical surface modifications of SNCs and effect of SNCs on the crystallinity and permeability of PLA. Chapters 3 to 6 cover the four distinct core experimental parts responding to the three main objectives described previously. Chapter 3 presents a study on the chemical compatibility of lactic acid grafted starch nanocrystals (SNCs) with polylactic acid (PLA). In chapter 4, phase transition and crystallization behaviour of grafted starch nanocrystals in PLA nanocomposites is studied. Chapter 5 presents the effect crystallinity and gas permeability of Poly (lactic acid)/ Starch nanocrystals Nanocomposites. In chapter 6 the effect of esterification modification of SNCs and soil burial degradation time on the degradation properties of PLA nanocomposites were studied. Finally, chapter 7 briefly outlines the most significant concluding remarks and presents recommendations for the future works in this area.

Chapter 2

2.2. Literature Review

2.2.1. Lactic Acid (LA)

Lactic acid (2-hydroxypropionic acid) is primary monomer of PLA. Lactic acid is an organic acid with a chiral center. Due to the chiral center, it exists in two enantiomers forms, L-enantiomers and D-enantiomers, allowing the formation of L-lactide, D-lactide and DL-lactide (*meso*-lactide). These enantiomers have different effect on the polarized light (Figure 2.1). The properties of PLA are highly depend upon the conformational variation of lactic acid which allows the tuning of PLA microstructure and subsequently its physical properties. There is a worldwide demand for the lactic acid production due to its usages in the production of poly (lactic acid) (PLA). Presently, 90% of the commercial lactic acid production is made by bacterial fermentation while the remaining is produced synthetically by the hydrolysis of lactonitrile. The fermentation processes to obtain lactic acid depends upon the type of bacteria used. L-lactide is produced in humans and other mammals whereas, D-lactide is obtained by the bacterial fermentation of carbohydrates [12,13].

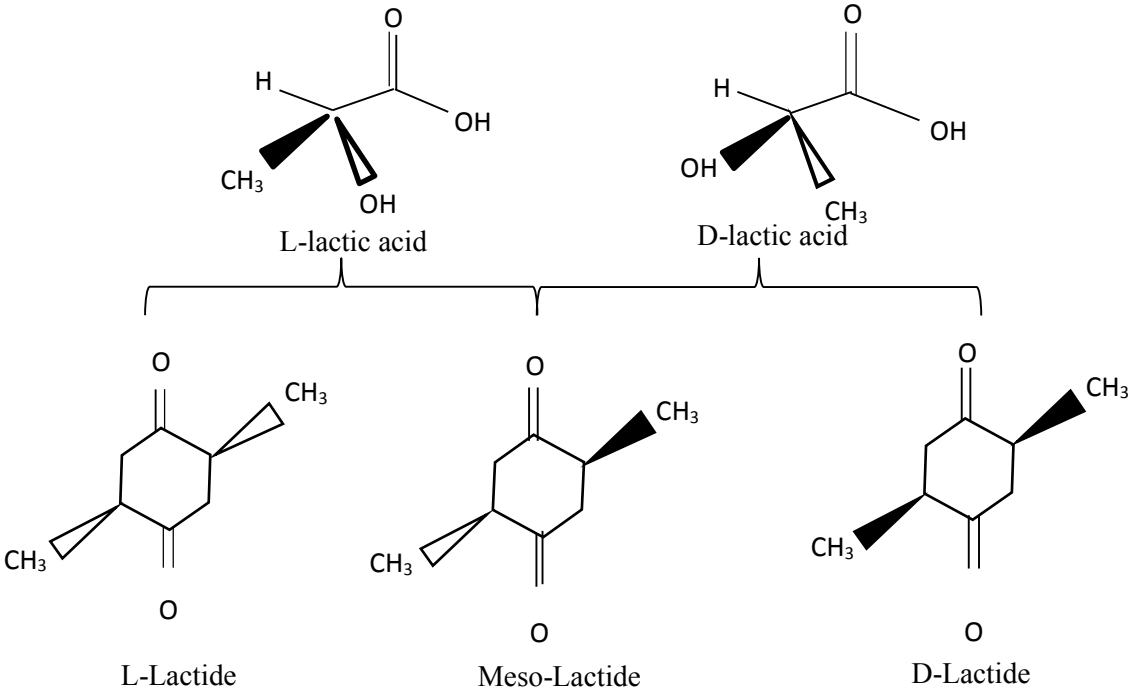

Figure 2.1. The L- and D- enantiomers of lactic acid [2].

2.2.2. Crystal Structures of PLA

PLA can crystallize in three different crystalline structures called α, β and γ − structure. They are characterized by different helical conformations and cell symmetries depending upon different thermal and/or mechanical treatments used [14]. The α −structure develops when PLA is melted or cold crystallized and it has a well-defined XRD diffraction pattern [15]. The α-structure has a unit cell with $a = 1.06$ nm, $b = 1.737$ nm, and $c = 2.88$ nm parameters with a left handed 10_3 helix. The β −structure is shaped upon mechanical stretching of the α-structure [16]. The chain conformation of the β − structure is left handed 3_1 helices and it has a unit cell with $a = 1.031$ nm, $b = 1.821$ nm, and $c = 0.900$ nm. The third crystal structure of PLA (γ −structure) is formed by an epitaxial crystallization of PLA [17]. The γ −structure has two antiparallel helices. It has an orthorhombic unit cell for which the a, b and c lattice parameters are 0.995, 0.625 and 0.88 nm, respectively. Crystal types and parameters of the PLA forms are summarized in Table 2.1.

Recently, a new crystalline structure was observed for PLLA samples which is crystallized below 120 ℃ the melt state. This crystal structure is named as $\boldsymbol{\alpha'}$-structure and has a slightly altered crystal structure compared to $\boldsymbol{\alpha}$-structure. Zhang et al., has been investigated extensively the crystallization of $\boldsymbol{\alpha'}$-structure of PLLA by FTIR,WAXS and DSC [15–17]. In the first study, they prepared PLLA samples by isothermal melt-crystallization process and monitored the structural changes of the samples with real-time IR measurement [15]. They observed, the formation of C-O-C backbone during the both induction period and the growth period of PLLA melt crystallization is due to the interchain interactions between CH_3 and $C = O$ group. These observations not only provided direct evidence that the disordered α'-structure of PLA but also showed that the interchain interactions can control the nucleation and growth of polymer crystallization. In a separate work, they studied the crystallization and structural evaluation of PLLA during isothermal crystallization process by IR spectroscopy and two dimensional correlation analysis. They showed that the C=O band shifts to a higher wavenumber during the crystallization of PLLA and it can be attributed to the appearance of a new peak. They concluded that this new peak with a high wavenumber corresponds to the development of the new crystalline phase [16]. In addition, Zhang et al., studied the crystal structure of PLA from melt state with WAXS and DSC analysis [17]. They found that, the disorder (α') and order (α) crystalline structures of poly (L-lactide) (PLLA) are formed at low ($T_c \leq 100$ ℃) and high ($T_c \geq 120$ ℃) crystallization temperatures respectively.

In addition, they demonstrated that a small exothermic peak around 160 ℃ just prior to the main melting peak can be attributed to the α′-structure, whereas the samples crystallized at T_c above 120 ℃ shows just an endothermic melting peak which is related to the α-structure. In addition, Kawai et al., investigated the effect of the crystallization temperatures on the crystal structure and melting behavior of PLLA by means of WAXS and SAXS analysis [18]. They showed that the ratio of the a- and b-axis lengths of α-structure begins to decrease with T_c below 120 ℃, which suggests a new crystalline form with hexagonal packing, namely, the α′-structure.

Table 2.1. Properties of PLA crystal structures [14,19].

Crystal type	*Crystal structure*	*Cell parameters*						$\rho_{theoretical}$ $(\frac{g}{cm^3})$
		a(nm)	b(nm)	c(nm)	**α**(°)	**β**(°)	**γ**(°)	
α	Pseudo-orthorhombic	1.07	0.645	2.78	90	90	90	1.247
α	orthorhombic	1.05	0.61	2.88	90	90	90	1.297
β	orthorhombic	1.031	1.821	0.90	90	90	90	1.275
β	trigonal	1.052	1.052	0.88	90	120	120	1.277
γ	orthorhombic	0.995	0.625	0.88	90	90	90	1.312
SC	triclinic	0.916	0.916	0.870	109.2	109.2	109.8	1.274
SC	triclinic	1.498	1.498	0.87	90	90	120	1.274

2.2.3. Crystallization Behaviour of PLA

The crystallization of PLLA using both nonisothermal and isothermal crystallizations modes has been quantified over the wide range of temperatures. However, it has been found that the PLLA has a peculiar crystallization behaviour. This was noted for the first time by Vasanthakumari and Pennings [20] who studied the effect of the molecular weight (M_w) and crystallization temperature (T_c) on spherulite growth rate and morphology of PLLA. They observed a clear discontinuity in the spherulite growth rate curve at around 110-120℃. Beside, this discontinuity was observed in the crystallization half-time ($t_{1/2}$) curve of PLLA in the temperature range of $100 - 120$ ℃. Different explanations have proposed in literature for this anomalous behavior [21,22]. Some researchers believed that this phenomenon can be attributed to regime transitions in the crystallinity of PLLA [21]. Regime transition analysis of PLLA demonstrated that transition from regime III to regime II and from regime II to regime I take place around 120 ℃ and 150 ℃ respectively. The transition from regime II to regime I induced trnsformation of spherulites into the hegzagonal lamellar stacking. However, the transition from regime II to regime III, only mirror

changes in morphological structure of spherulite was observed. Nevertheless, others believed that the incredible high rate of crystallization below 120 ℃ is attributed to high radial growth rate of spherulites. This is due to the negligible changes in nucleation rate of PLLA in this range of temperature (100−120 ℃) [22]. Nevertheless, some authors such as Keith et al. believed that the crystal transition is the responsible of the high rate of the crystallization of PLA [23]. Yasuniwa et al., also confirmed that the high rate of the crystallization is attributed to the crystal transition of PLA [24]. They showed, α′-structure is stable at temperature below 120 ℃, whereas, the α-structure is stable above 120 ℃. In addition, Anderson et al., observes a bimodal behaviour in spherulite growth rate and half time of crystallization of PLLA with molecular weight (M_w) of kg/mol containing 0, 2 and 4% D-isomer (Figure 2-2). They showed that the α' to α-crystal structure ratio is maximum in the PLLA containing 2 and 4% D-isomer and this behaviour is not observed in pure PLLA. In addition, and the bimodal crystal growth rate is attributed to spherulite development not to the changes in the nucleation mechanisms [25], [26].

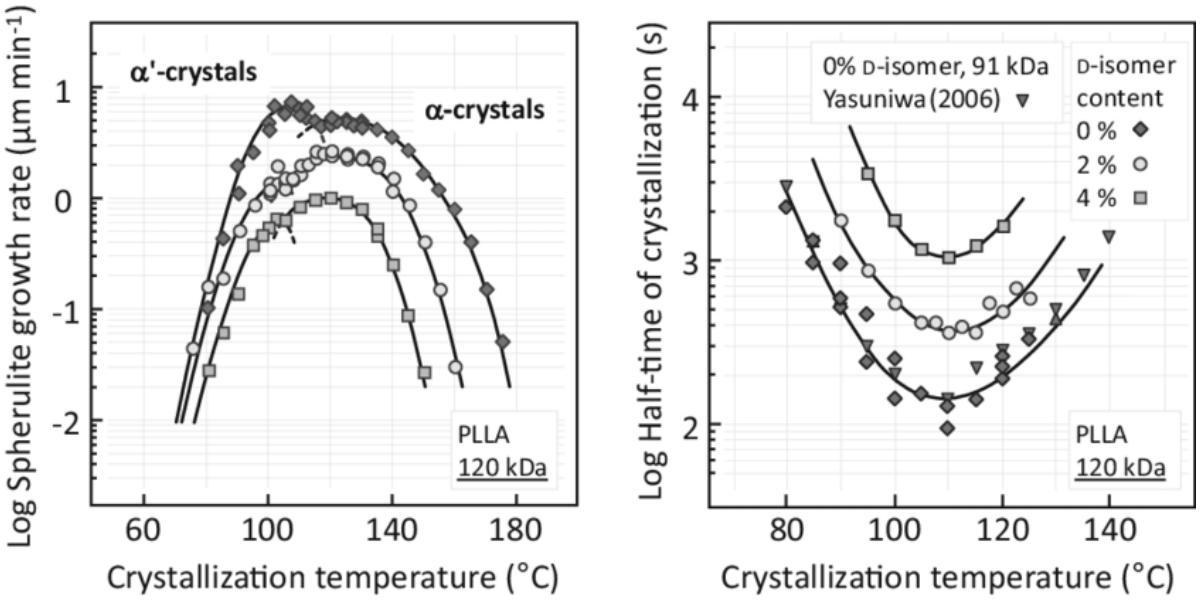

Figure 2.2. Spherulite growth rate and half time of the crystallization of PLA [26].

2.2.4. Dual Melting Behavior of PLA

The presence of the dual melting endotherms is very common in semi crystalline polymers and has been observed in many synthetic semicrystalline polymers, copolymers and composites [27,28]. The origin of this dual melting behaviour was reviewed by Liu et al., [27]. They ascribed this phenomena to various of mechanisms such as; a) melt recrystallization during DSC heating procedure, b) the existence of the more than one crystalline structures, c) variation in lamellar morphology such as lamellar size, thickness, distribution and perfection, d) relaxation of rigid amorphous fraction and finally e) different molecular weight (M_w). However, many studies done in the past ascribe the dual melting endotherms to melt recrystallization mechanism. The low melting peak is assigned to the melting of primary crystals, whereas, the high melting peak is attributed to the crystals formed during the crystallization process. Sometimes, there is an exothermic peak before these double endothermic melting peaks that can be associated with the solid state transition and/or the recrystallization. The melting behavior of PLLA with different M_w has been studied extensively by Jamshidi and his co-workers [29]. They found that, the PLLA with $M_w < 3000\ g/mol$ has a weak and broad melting peak before the main endothermic peak. They attributed this broad peak to the less ordered crystalline structure. Pan et al., also investigated the effect of M_w on the polymorphous and melting behavior of PLLA [30]. They found that PLLA with high M_w crystallized at low T_c (80°C) shows a double endothermic melting peak whereas, PLLA with low M_w which is crystallized at same T_c shows small exothermic peak before the main endothermic peak. They attributed this melting behaviour to the crystalline transformation phenomena. They showed that almost all the α′-structure transform into the α-one in PLLA with high M_w, whereas, α′-structure only partially transform into the α-one PLA with low M_w. Di lorenzo studied the multiple melting behavior of PLLA by DSC in wide range of temperature (Figure 2.3) [31]. They showed that the endothermic peak (Peak II) is due to the fusion of PLLA crystals with low thermal stability whereas, crystal reorganization result in presence of exothermic peak (peak III) before the main endothermic peak (peak IV). The effect of cooling rate on the double melting behavior of the PLLA is studied by Yasuniwa et al., [25]. They showed that the melting peak ratio decreases by increasing the cooling rates. They attributed this behavior to the melt recrystallization mechanism, where imperfect crystals transform to perfect and stable crystals through the melt-recrystallization mechanism. When the melting rate overcomes that of the recrystallization rate, the endothermic peak appears, while the exothermic peak occurs when the

recrystallization rate overwhelms the melting. The double melting behaviors, where the exothermic peak happens before the endothermic peak, were also observed for high molecular weight PLLA (80000 g/mol) [32]. A number of authors attributed this small exothermic peak to a cold crystallization. The double melting behaviors of PLLA were also characterized by X-ray diffraction (XRD). It has been shown that the phase transition from the disorder crystal structure (α') to the ordered crystal structure (α) occurres at the isothermal crystallization temperature of 100 °C or lower [33]. The lattice spacing calculated from the main diffraction peak, for isothermally crystallized samples at 80 °**C** and 100 °**C**, increases with temperature rise by thermal expansion.

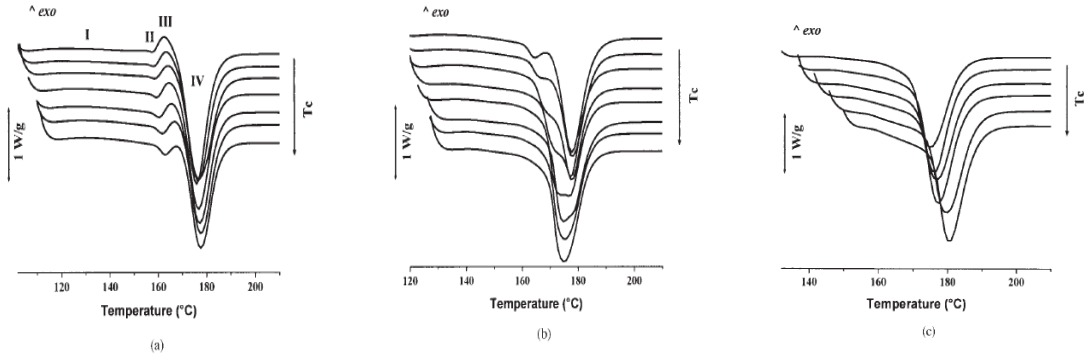

Figure 2.3. Melting behaviour of PLLA isothermally crystallized in a) $\mathbf{96}$℃ $\leq \boldsymbol{T_C} \leq \mathbf{108}$℃, b) $\mathbf{110}$℃ $\leq \boldsymbol{T_C} \leq \mathbf{124}$℃ and c) $\mathbf{126}$℃ $\leq \boldsymbol{T_C} \leq \mathbf{14}$6℃ [31].

2.5. Effect of Nucleating Agents on the PLA Crystallization

Addition of nucleating agents is one of the most important route that can enhance the nucleation density and nuclaetion rate of polymer materials [26]. Therefore, the addition of nucleating agents speed up the final crystallization rate and decreases cold crystallization temperature ($\mathbf{T_{cc}}$) of polymer materials. Nucleating agents can be grouped into three classes: (a) homogeneous nucleation, (b) self-nucleation and (c) heterogeneous nucleation [26]. Among them, heterogeneous nucleating agent is the most applied approach to enhance the crystallization kinetic of polymer materials. Mechanism of heterogeneous nucleating agents defined by the chemical and physical interactions between polymer matrix and nucleating agents. This interaction decreases the interfacial free energy or barrier energy for stable nucleus formation. Generally, the mechanism of the heterogeneous nucleating is divided into four stages: a) primary nucleation b) primary

spherulite growth, c) secondary nucleation and d) secondary spherulite growth. In primary nucleation, a nuclei with a critical size is formed and then the size of this critical nuclei increases with increasing time at a given temperature. In addition free-enthalpy barrier is required for crystal growth of primary nuclei. This nucleus form in the presence of heterogeneous surface area in the case of heterogeneous nucleation. Thus, the total barrier free energy for heterogeneous nucleation is lower than other nucleation. Therefore, using heterogeneous nucleating agent allows to reduce the undercooling temperature, which leads to the formation of smaller crystals and a decrease of process cycle times. Adding nucleating agent also promotes the formation of smaller spherulites and enhances the nucleating density. More importantly, the addition of nucleating agent can determine the type, size and morphology of spherulites of semicrystalline polymers [34].

Heterogeneous nucleating agents for PLA are classified in two different groups; a) chemical nucleating agents and b) physical nucleating agents [35]. Chemical nucleating agents can reduce the nucleation process through a chemical reaction such as organic salts of sodium used in crystallization of PET. However, physical nucleating agents can enhance the kinetic of crystallization by physical interactions. During the last few years, various physical nucleating agents were examined with PLA, including some inorganic nucleating agents such as such as talc [35–37], clay (i.e. MMT, $CaCO_3$ and $BaSO_4$,) [38–40], carbon nanotubes [41], multiwall and carbon black [42]. Additionally, natural nucleating agents have been thoroughly investigated: such as cellulose fibers [43], chitin [44] and starch [45]. An apparent increase in the degree of crystallinity and a reduction in the crystallite size of the PLA were observed after natural nucleating agents were added. In this study we just focused on starch as a nucleating agent for PLA.

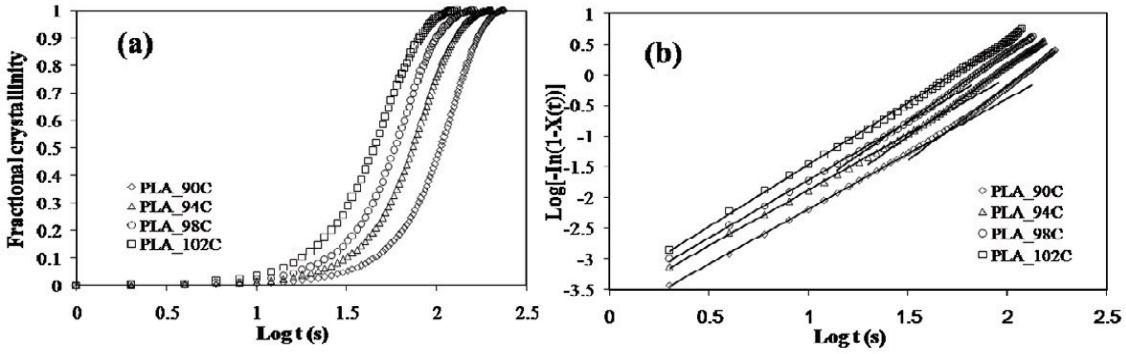

Figure 2.4. Isothermal cold crystallization of PLA at different temperature a) fractional crystallinity vs. time and b) Avrami plots [46].

2.2.6. Nucleating Rate Measurement

Nucleation rate and densities are frequently analyzed by the number and size of spherulites per unit volume through Avrami equation (eq.1.1) [49]:

$$X(t) = 1 - \exp(-kt^n) \qquad (2.1)$$

where k is the crystallization rate constant and n is the Avrami exponent which depends on the nucleation and growth mechanisms of crystallites.

The Avrami parameters (n and k) can be calculated using the following relation (eq.2.2):

$$\ln(-\ln[1 - X(t)]) = n\ln(t) + \ln k \qquad (2.2)$$

Figure 2.4 shows the plot of $\ln[-\ln(1 - X(t)]$ versus $\ln(t)$ of neat PLA at different T_c. In all samples, Avrami plots were found to be linear demonstrating the accuracy of the procedure as shown in Figure 2.4. The slope of line in the plot of $\ln[-\ln(1 - X(t)]$ versus $\ln(t)$ gives the value of n. The exponent is typically between 2 and 4 for polymer crystallization and is associated to the nucleation mechanism (homogeneous or heterogeneous and simultaneous or sporadic. If the nucleation sites are present at the early stage of the nucleation, then this is called simultaneous nucleation. However, when the nuclei form in the polymer matrix at a constant time rate, the nucleation is called sporadic. The higher n values are attributed to three dimensional spherulitic growth with a sporadic or a combination of sporadic and simultaneous nucleation type, whereas the lower amounts are related to two dimensional growth with instantaneous and some sporadic nucleation. Parameter k is a growth rate constant involving both nucleation and growth rate parameters.

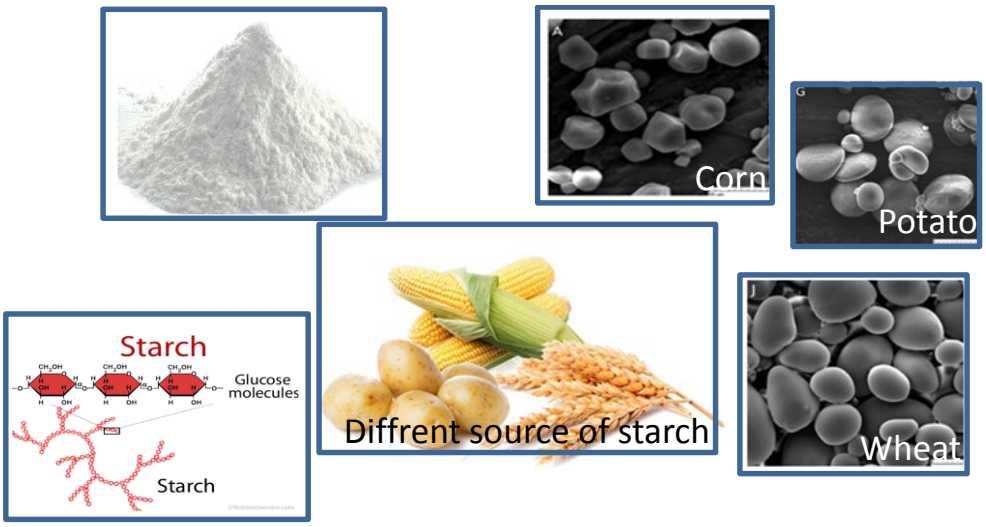

Figure 2.5. Different source of starch and SEM images of corn, wheat and potato starch.

2.2.7. Starch

Starch with chemical formula of $(C_6H_{10}O_6)_n$ is the second most abundant, natural, renewable and biodegradable polymer. Starch is found in a variety of plants as a source of storage energy such as rice, potato, pea, wheat and corn which is termed native starch (Figure 2.5) [7,10,47]. In addition, native starch can be modified using both chemical and physical methods to achieve better properties and is known as modified starch. Depending on the botanical sources, starch granules has diffrent size, shape, crystallinity, and internal molecular organization. Starch is a complex carbohydrate and composed of two main chains namely amylose and amylopectin. Amylose is defined as a linear molecule of glucose units and amylopectin is a branched polymer consisting of relatively short branches of glucose units. Molecular size of amylose ranging from 20 to 800 kg/mol, whereas, the molecular weight of amylopectin ranging from 5000-30,000 kg/mol. Starch is a semicrystalline polymer and its degree of crystallinity, molecular weight, morphology and final product properties deepens upon amylose to amylopectin ratio. Native starch is usually containing 20-30% amylose and 70-80% amylopectin. The crystalline regions are formed by short branched chains in amylopectin whereas, the amorphous regions formed by amylose. Amylopectin is classified into three different types namely, A-, B- and C-type chains. This classification is based on the chain length distribution. Figure 2.6 shows the diffrent levels of organization make up the

starch granule [7,47,48]. As can be seen in Figure 2.6 starch granules organizes as following; a) the granules (2-100 μm), b) amorphous and semicrystalline rings (120-500 nm), c) blocklets (20–50 nm), d) amorphous and crystalline lamella (9-19 nm) and finally e) amylose and amylopectin chains (0.1-1 nm). Within this structure, amylopectin is organized in crystalline clusters of double helices forming stacks of alternating crystalline and amorphous lamellae with a regular repeat distance of 9–10 nm. These are embedded in rounded asymmetric structures named blocklets that have a diameter on the 20-50 nm scale. These blocklets, having different sizes, aggregate in alternating amorphous and semi-crystalline radial growth rings which have 100–500 nm thickness. The amorphous rings consist of amylose and amylopectin in a disordered conformation, whereas the semi-crystalline rings are formed by the lamellar structure of alternating crystalline and amorphous regions.

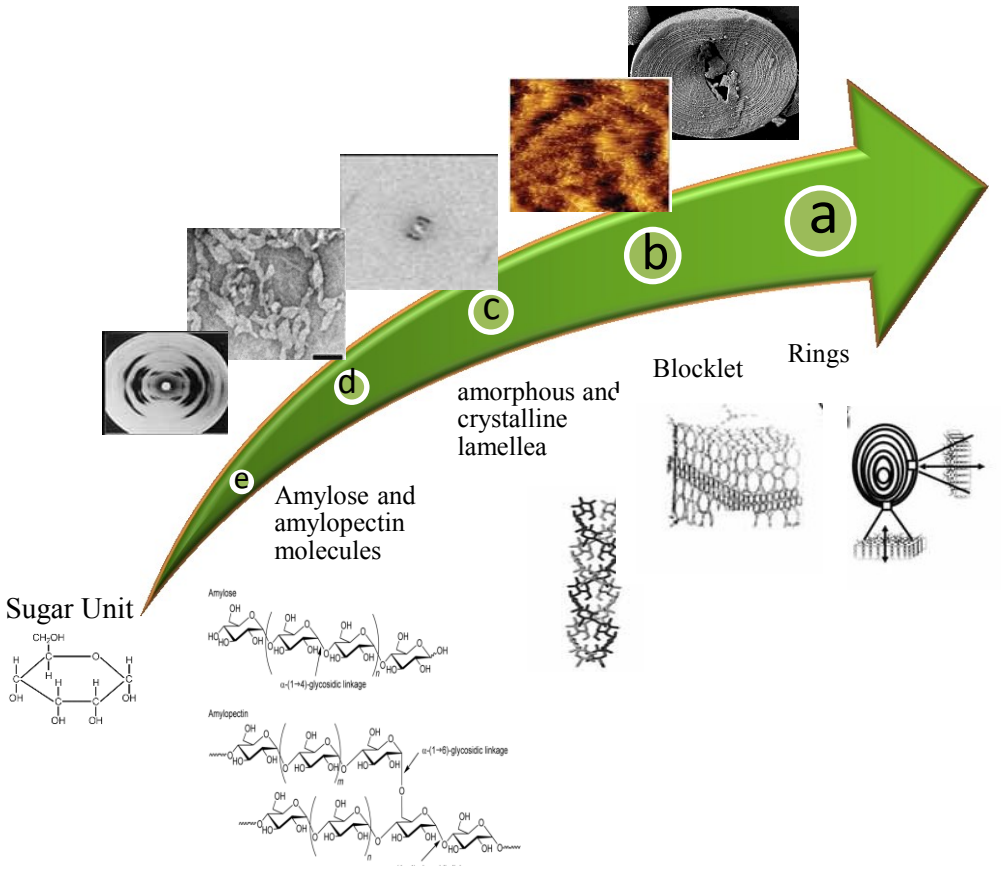

Figure 2.6. Schematic of the starch granules a) the granules (2-100 μm), b) amorphous and semicrystalline rings (120-500 nm), c) blocklets (20–50 nm), d) amorphous and crystalline lamella (9-19 nm) and finally e) amylose and amylopectin chains (0.1-1 nm) [7].

2.2.8. Starch Nanocrystals (SNCs)

Starch nanocrystals (SNCs) are crystallite phase of starch particles and their morphology, crystalline type and size depend on the botanic origin and/or relative proportion amylose to amylopectin of starch granules. SNCs is one of the most brilliant nanomaterials due to their renewability, biocompatibility, biodegradability, non-toxicity. In addition, the high degree of crystallinity, special platelet-like morphology, high surface area, and remarkable physical properties of SNCs make them as an interesting reinforcing agent in a wide variety of polymers nanocomposites resulted in good mechanical, thermal and barrier properties [7,47,48].

SNCs are synthesized in different ways such as acid hydrolysis, enzymatic treatment, physical treatment, combination of acid hydrolysis and ultrasonication [34,47,48]. Among these different modifications, acid hydrolysis has been widely used for preparation of SNCs, due to it is simple, easy to control and its wide industrial applications. Acid hydrolysis procedure involves hydrolysis of the amorphous regions and enhancing the relative proportion of crystalline regions and double helices regions. Generally, SNCs were obtained by mixing native starch granules with dilute sulfuric acid (H_2SO_4) or hydrochloric acid (HCl) at 30°C–60°C for different time periods. It has been shown that, acid hydrolysis can effect on the molecular structure, crystalline structure and morphology of SNCs depending on the acid hydrolysis conditions and procedures. Table 2.2 summarizes the effects of different extraction methods and starch sources on SNCs size and Figure 2.7 shows TEM images of SNCs after acid treatment from different resources [49].

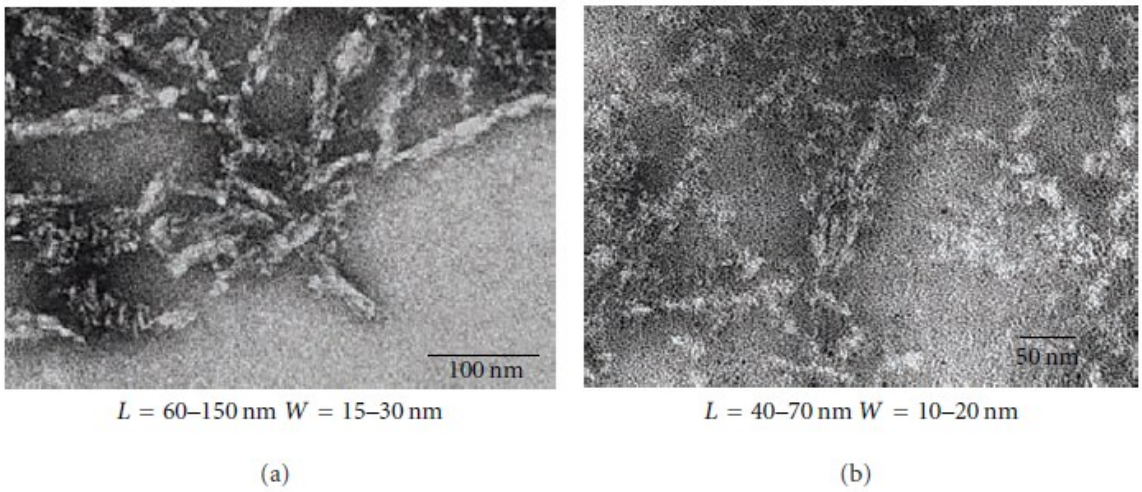

Figure 2.7. TEM image of SNCs from different resources a) pea starch and b) potato starch [49].

Table 2.2: The effects of different extraction methods and starch sources on SNCs size.

Starch resources	reaction Time (days)	Size (nm)	Yield (%)	Morphology	Refrences
Waxy maize	5	>50	-	platelet	[32]
Waxy maze	5	L[1]: 20–40, W [2]:15–30	-	platelet	[46]
Waxy maze	5	5-7	-	platelet	[7]
Pea starch	5	L:60–150, W:15–30	-	-	[9]
Potato starch	5	L: 40–70, W :10–20	-	-	[48,50]
Corn starch	7	L:50	-	spherical	[51]
Waxy maze	5	20-40	15.7	platelet	[52]
Cassava	5	46-146	30.0	spherical	[53]
Waxy maize	5	50-100	15.0	platelet	[54]

L[1]: length and W[2]: wide

2.2.9. PLA/Starch Blends, Composites and Copolymers

PLA/starch polymer blend is one of the most promising polymer blend with benefits of being complete biodegradable, biobased and having desirable properties for packaging applications. However, the difference in surface polarity of PLA and starch leads to an incompatibility between two polymer materials and poor dispersity of starch in PLA matrix. Since PLA is hydrophobic in nature, whereas; starch is hydrophilic in nature and blending of them leads to a poor interfacial adhesion. In order to realize it, various chemical modifications of starch, PLA and both PLA and starch have been realized in the past [55–57]. Among various chemical modifications of starch, surface esterification is the most common rout, during which a number of hydroxyl groups (OH) of the starch are replaced by carboxylic groups (COOH) and form ester functional groups on the starch surface [55–57]. It has been shown that this replacement not only significantly enhances hydrophobicity of starch but also enhances the barrier, crystallinity and mechanical properties of PLA/starch final products [58,59]. Esterification of cassava starch with long-chain fatty acid chlorides in aqueous media at 4 ℃ is carried out by Thitisomboon et al. [57]. They showed that esterified starch enhances the thermal stability and young modulus of PLA/starch blend. In another effort, Zue et al., prepared starch/PLA composites by using dry method and studied the mechanical properties of starch/PLA composite [46]. They found that, the tensile strength and bending strength of esterified starch/PLA were stronger than neat starch/PLA composite. Similarly, Ojobo et al., incorporated lauric acid and replaced of the OH functional groups of the starch chains by using a one-step homogeneous process. They enhanced mechanical, thermal and compatibly of PLA/starch blend [60].

In addition, several studies have been carried out by the combination of the two polymer materials (PLA and starch) and adding different type low molecular weight of compatibilizer such as

methylenediphenyl diisocyanate (MDI) and malic anhydride (MA) and plasticizer such as glycerol, sorbitol and triethyl citrate [64-69]. The MDI is one the mostly reported compatibilizer that can enhance the compatibility between PLA and starch polymer materials. MDI is a small molecule, composed of isocyanate groups, which are highly reactive with both hydroxyl and carboxyl groups to form urethane linkages, thus being an effective compatibilizer for these two immiscible materials. Acioli-Moura and Sun reported thermal stability of PLA/starch blend, with or without MDI and they showed that the thermal endurance of PLA/starch blend enhances considerably by adding MDI [61]. Morover, Wang et al., added 5 wt% of MDI into PLA/starch composites and they showed that the tensile strength improved from 62.8 to 68 MPa and elongation at break increased from 2.7 to 4.2%. In addition, malic anhydride (MA) has also used to improve the interfacial adhesion between PLA and starch by grafting on either starch and/or neat PLA [59]. Zuo et al., esterified starch with 1 wt% of MA and they showed that the introduction of a hydrophobic ester bond in starch chains increased the interfacial compatibility between PLA and starch and led to an increase the water resistance and tensile properties PLA/starch blend [62]. However, Orozco et al., grafted MA on the PLA molecular chains using dicumyl peroxide (DCP) as an initiator [63]. They obtained PLA/starch copolymers by reactive blending, varying the starch composition from 0 to 60%. They demonstrated that MA can play as a plasticizer and it enhances not only the compatibility between PLA and starch polymer materials and but also the young modulus. Hwang et al., showed that the esterification of starch with MA can enhance the melt flow of the PLA/starch composite material as well [64]. They grafted MA on both polymers in the presence of DCP in a one-step reactive compatibilization process. They showed that the tensile properties of PLA/starch (80:20) with 2 wt% of MA and 0.1 wt% of DCP enhanced significantly. In addition, Xiong et al., demonstrated that the tung oil anhydride (TOA) as a bio-based reactive plasticizer can increase not only compatibility but also the elongation at break of PLA-starch blends [65]. In addition, PLA-grafted-starch with various lengths and numbers of graft starch chains were synthesized using a trimethylsilyl protection method. The graft-copolymer films exhibited a lower melting temperature, degree of crystallinity, T_g and higher viscosity properties compared to PLA films. For example, Ohya et al., prepared PLA-grafted amyloses by ring-opening anionic polymerization of lactide using the polymeric alkoxide as initiators and subsequent removal of the TMS groups [66]. In another study, Gong et al., prepared copolymers of starch grafted with PLA by in situ polymerization reaction of corn starch with lactic acid in aqueous

media in the presence of stannous 2-ethyl hexanoate [Sn $(Oct)_2$] [67]. The procedure of the graft reaction was elucidated, based on the HPLC analysis, as the ring-opening polymerization (ROP) from starch surface. Bolay et al., ball milled PLA and starch without adding any compatibilizer or plasticizer and they showed that the mechanical properties of the blends were improved due to the better interface between the matrix and the filler which is improved by ball milling process [68]. The PLA/starch blends without compatibilizer were studied by Wokadala et al., as well [69]. They chemically modified waxy and high amylose starch particles to increase their hydrophobicity and compatibility with PLA. Although the polymer thermal stability decreased, the modified blend exhibited an improved mechanical performance, while SEM micrographs showed a more homogeneous structure with this starch modification (Figure 2.8). Additionally, this study demonstrated that the amylose/amylopectin content of starch plays an important role in the tensile properties of the starch-PLA blend films. At higher starch levels, composites with butyl-etherified high amylose starch gave a lower elongation at break and tensile strength, as compared to those with butyl-etherified waxy starch, due to the tendency of amylose to self-aggregate.

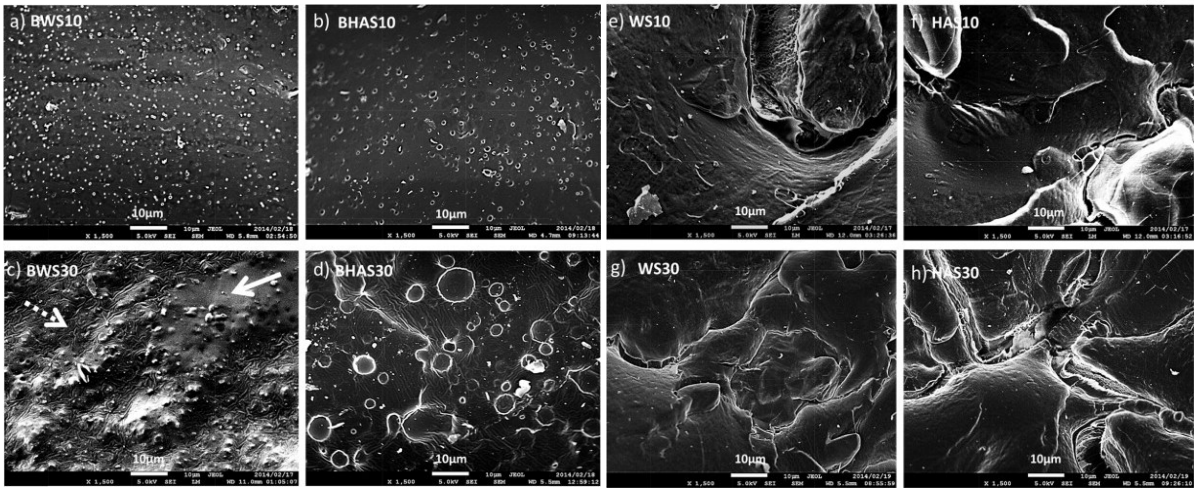

Figure 2.8. Morphology of PLA/starch composites with added butyl-etherified waxy (BWS) and high amylose starch (BHAS), non-butyl-etherified waxy (WS) and high amylose starch (HAS) at 10% w/w and 30%w/w starch addition levels [74].

2.2.10. Crystallization of PLA/Starch Blend

Starch has a great effect on the crystallization of PLA by increasing nucleation density and decreasing the crystallization half-time ($t_{1/2}$). For example Sun et al., have studied the effect of

dry starch (1-40 wt%) on crystallization of PLA [45]. They reported that the $\boldsymbol{t_{1/2}}$ of PLA/starch blend decreases from 14 min to 3.2 min. However, effect of starch becoming more significant when it is in thermoplastic state [75–77]. For the first time, Martin and Averous were investigated the crystallinity of PLA/TPS blends [71]. They found that TPS has an effect on the crystallization of PLA. They attributed the higher crystallinity of PLA/starch blend to the higher miscibility between PLA in TPS matrix and/or due to the migration effect of glycerol from the TPS to the PLA phase. Similarly, Jang et al., believed that plasticizer migration is a responsible for crystallization of TPS/PLA blend [72]. They obtained 25% crystalline content upon heating at low rate of crystallization for PLA/dray starch (30 wt%) composites and around 35% crystalline content for PLA/TPS (30 wt%) blend. Another factor to consider in the crystallization of compatibilized PLA/TPS blends is the potential reduction in free energy barrier at the blends interphase. In the case of the PLA/TPS system for example, MA grafted PLA reacts with starch macromolecules to produce graft copolymer of PLA and amylose or amylopectin chains. The PLA segment that is attached to the starch macromolecules would be expected to decrease free barrier energy and thus its crystallization rate can be enhanced. This effect was observed in PLA/starch (55/45) composites where MDI was used as a coupling agent [83]. Similar effect has been investigated for the PLA/TPS blends by Huneault et al., [70]. They studied the effect of interfacial area by compatibilizing the blend using maleic anhydride grafted PLA. They reported that, the crystallization half-time of PLA was decreased significantly (75 s) in presence of the TPS phase and this effect was strengthened by the blends interfacial modification. However, Hwang et al., showed that in the case of PLLA/starch blends, PLA grafted maleic anhydride (MA) reacted with starch showed lower crystallinity as the starch content increased to 30 wt% [64]. In another study, Park et al., gelatinized starch with various content of glycerol and they investigated in terms of the effect of the glycerol addition on crystallinity characteristics of PLA [73]. They found that starch played a role as a nucleating agent and glycerol as plasticizer contributed to an improvement in crystallinity in PLA blends. In addition, Kang et al., studied the effect of chemically modified thermoplastic starch (CMPS) on isothermal crystallization kinetics of PLA [74]. They showed that, in the presence of CMPS the $t_{1/2}$ decreases from 24.7 to 3.2 min. In addition, the overall crystallization rate (K) and the Avrami exponent (n) of PLA/CMPS increases and decreases respectively compared to neat PLA which shows higher nucleation rate. Similarly, the thermoplastic starch/poly (lactic acid) (TPS/PLA) composites were prepared using PLA melt

blending with glycerol plasticized-starch [75]. They showed that TPS acts as a nucleating agent and it can improve the crystallinity of PLA.

2.2.11. Barrier Properties of PLA

Commercial PLA presences a relatively low gas barrier performance which is limiting it's usages in food packaging applications. Figure 2.9 comperes barrier properties of PLA with other common synthetic polymer materials such as polyethylene terephthalate (PET) at 30 ℃ [76,77]. As can be seen from Figure 2.8, the O_2, N_2 , CH_4 and CO_2 permeability of PLA is considerably higher than PET but slightly lower than the rest of conventional oil-based polymer materials. Finding a solution to overcome poor barrier properties of PLA is very important for the chemical, physical and microbiological safety of the stored polymer materials and allowing a broader applications of PLA in the packaging industry.

The permeability characteristics of a polymer can be controlled in many ways. The physical properties of polymers are the most responsible for controlling the permeability properties of polymers such as glass transition temperature (T_g), chain symmetry, chain stiffness, chain packing, intermolecular interaction, polarity, molecular weight and molecular orientation and presence of lateral chains [81-82]. For example, polymers with high free volume fraction result in higher diffusivity and permeability. In addition, external factors such the nature of the penetrant (size, type, number and polarity), temperature and humidity are another important factors can control the permeability of polymer materials [76,77]. For example, permeability of gases such as O_2 and H_2 is largely governed by diffusion due to the little degree of interaction of O_2 and H_2 with the hydrophobic polymer materials. Whereas, permeability of gases such as CO_2 and water vapour interact very largely with polymer matrix and permeability is largely governed by solubility [90]. In addition kinetic diameter of different gases can control the gas permeability of polymer materials (Figure 2.10). Finally, the presence of additives such as plasticizers and compatibilizer, crosslinking and nucleating agents can engineer permeability of polymer as well. The effect of these additives is extensively discussed in the section 2.10.

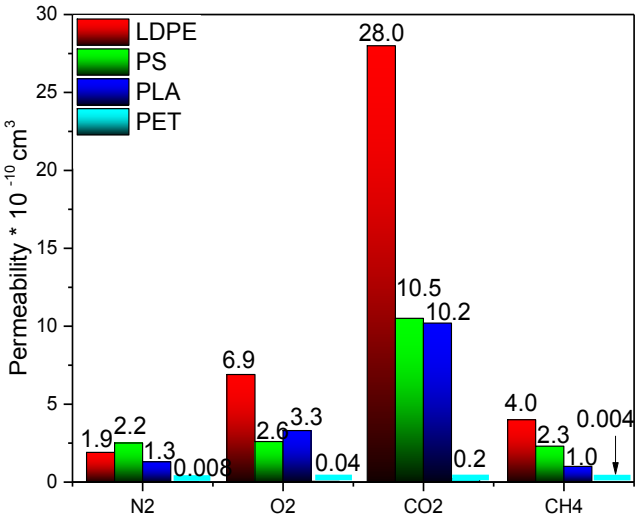

Figure 2.9. Barrier properties of PLA in comparison to other common polymers, Low-density polyethylene (LDPE), polyethylene terephthalate(PET) and polystyrene (PS) at 30 °C [81-82].

Recently, there is a growing interest in correlation of inner microstructures and gas permeability of PLA polymer materials. Generally, semicrystalline polymers such as PLA are containing two regions, a crystalline region with long-range order and a noncrystalline or amorphous region with a short-range order and/or no order. The crystalline region is considered as an impermeable region whereas, it is widely accepted that the amorphous region is the most permeable one. Furthermore, the creation of crystalline structures decreases the amount of amorphous phase which is available for penetrating gas molecules. The relation between the crystallinity and gas barrier properties of PLLA has been widely studied in the past [90-96]. Knehashi et al., have extensively studied the relation between degree of crystallinity (X_c) and gas permeability of many semicrystalline polymers [78]. They reported that, in most of the polymers the gas solubility, diffusivity and permeability decreases with increasing X_c whereas, some polymers revealed almost constant or slightly increased values of permeability and diffusivity at higher X_c values. However, Bao et al., observed that the gas solubility increases with increasing crystallinity, while, gas diffusivity decreases. They investigated the gas permeability of amorphous PLA by estimating the gas diffusivity and solubility using a time-lag method [79]. Morover, Sawada et al. have reported the increased crystallinity reduced the oxygen permeability of PLA because of the lower continuous

space around crystalline regions [80]. However, Colomines et al., observed that the oxygen permeability of PLA increases with increasing degree of crystallinity [81]. Drieskens et al., controlled the morphology of PLA by subjecting PLA samples to cold crystallization at different temperatures and time [82]. They showed that barrier properties of PLA decreased by decreasing the amorphous chain density but not in linear portion. It seems there is no linier relationship between crystallinity and gas permeability (diffusivity and solubility) of PLA and gas permeability is controlled by other factors as well. To find the other factors, the morphological parameters of the crystallized PLA are studied in detail in the past. For example, Guinault et al., determined the effect of the crystalline polymorphism (α and α') and crystalline morphology on barrier properties of PLA [34]. They showed that recrystallization leads to an important decrease of the elongation at break and gas permeability of PLLA. In addition, the effect of crystalline polymorphisms quantity on the barrier and mechanical properties of compression-molded PLLA is studied by Cooca and his coworkers [83]. They showed that the amount of highly ordered $\alpha-$ crystal structure is enhanced above 130℃ crystallization temperature. It enhances water vapour barrier properties and decreases the Young's modulus of PLLA. The correlation between the inner crystal structures and morphological parameters of compression-molded PDLLA (4:96%) and variation in oxygen transport characteristics (permeability, diffusivity and solubility) has been reported as well [84]. Sato et al., have investigated the relationship between amorphous structure and gas permeability of PLA. They found that not only the crystallite size and crystallinity effect on gas permeability of PLA but also the high-density and low mobility of the rigid-amorphous phase restricted the gas diffusion and permeation in the PLA films [85]. The relation between rigid-amorphous fraction (RAF) and oxygen permeability of PLLA is investigated further by Sangroniz et al.,[86]. They observed that as the annealing time increases, the crystallinity fraction and RAF increases and the permeability to water vapor, oxygen, and carbon dioxide decreased considerably. This result is also confirmed by Frrnandes et al., [87]. They showed that the rigid amorphous fraction is the factor that plays a major role in the oxygen diffusion coefficient while the solubility is more affected by the crystallinity level. In addition, the effect of processing techniques and conditions (i.e. temperature, pressure and relative humidity) on the gas permeability of PLA is studied. For example, Oliveila et al., studied the gas solubility of carbon dioxide in PLA films under high-pressure conditions at various annealing temperatures and L to D ratio [88]. They found that the solubility strongly depended on the L to D ratio. In another study, Shogren et al., studied

the effect of environment temperature (6, 25, and 49 ℃) on the water vapor transmission rate (WVTR) of crystalline and amorphous PLA. They found that the WVTR of the amorphous PLA is around 54, 172, and 1100 g/m^2 per day which is reduced to 27, 82, and 333 g/m^2per day for crystalline PLA [89]. The effect of the D-lactide content, degree of crystallinity and M_w on the WVTR of PLA films studied in detail by Tusji and his coworkers [90]. They observed that WVPT of PLA decreases with increasing crystallinity up to 20%, however, it decreases with further increasing of the crystallinity (up to 30 %). They supposed that this changes is due to the higher resistance of restricted amorphous regions to water vapor permeation compared with that of the free amorphous regions. They also showed that variation of M_w in the range of 9×10^4 to 5×10^5 g/mol and D-lactide unit content in the range of 0% to 50% have insignificant effects on WVTR values of PLA. There are various mathematical models available in literature that relate permeability of the PLA to the permeant molecules. For example, Duan and Thomas have modified the Nielsen equation to predict the water vapour permeability of PLA films and they showed that water vapor permeability of PLA is well fitted with Nielsen model [95].

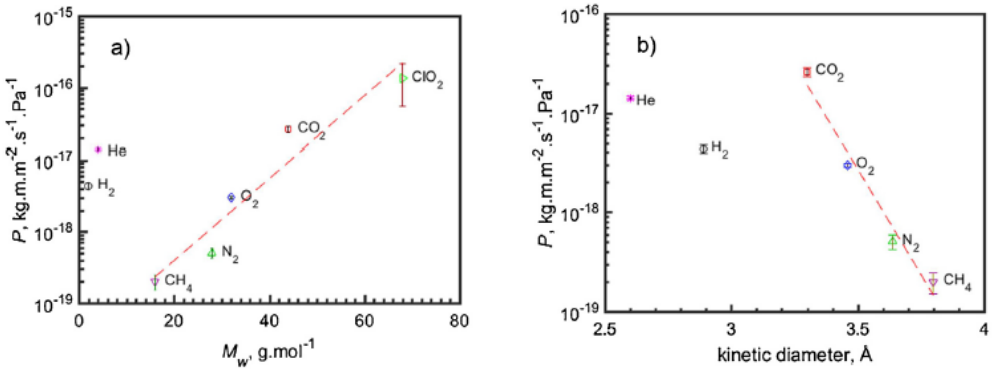

Figure 2.10: Average permeability as a function of M_w and kinetic diameter of different gases [91].

2.2.12. Barrier Properties PLA Nanocomposites

Until now, several approaches have been explored to decrease the level of the gas permeability of PLA. Addition of nanosized nucleating agents (NNAs) is an efficient, unique and versatile approach to improve not only the nucleation density and overall crystallization rate, but also to enhance gas barrier properties of PLA nanocomposites. Addition of NNAs creates physical obstacle to the passage of the gas molecules, thus it can be a unique option to engineer the barrier

properties of the PLA nanocomposites. Many kinds of NNAs have been successfully incorporated into PLA matrix. Henceforth, the effect of these NNAs on the gas permeability of the PLA will be reviewed in the following sections.

Nanoclay is the most promising NNAs for PLA due to their commercial availability, simple proccessability and low cost. Nanoclay is crystalline materials consisting octahedral sheets of alumina packed in between two tetrahedral sheets of silica. The length of individual sheets is ranged from 10-30 nm depending on the silicate layer. Two main possibilities arise upon melt blending of nanoclay with a polymer: a) melt intercalation, for which the clay is mixed with a polymer in the molten state and b) in situ intercalative polymerization, where the clay is dispersed in the monomer, which is then polymerized. Depending on the preparation conditions and on the type of the nanoclay, these two approaches result in either to intercalated or exfoliated morphologies or to a coexistence of the two morphologies. The intercalated or exfoliated morphologies nanoclay offer a unique opportunity to control physical properties such as barrier properties of polymer materials. It is well documented that the gas barrier properties of polymer materials can be significantly enhances by the intercalated clay nanoparticles [89-100]. This is due to the extended tortuous travelling pathway for diffusion gas molecules (Figure 2.11). Moreover, the addition of nanoclay enhances degree of crystallinity and level of crystalline phase consequently provides lower available amorphous phase for diffusing gas molecules and changes the solubility parameters [89,97]. Therefore, synergic effect of nanoclay as an effective nucleating agent and an impermeable crystalline regions which is blocking gas molecules diffusion and increasing tortuosity, greatly reducing gas permeation rate of PLA. During past few years, many diffrent clay nanoparticles with different surface characteristics were tested to enhance barrier properties of PLA. For examples, Rhim et al., examined the effect of different type of nanoclays, such as Cloisite Na^+, Cloisite 30B and Cloisite 20A on the WVP, tensile test and elongation at break of PLA [92]. They reported that, among the PLA/clay composite films tested, only PLA/Cloisite 30B showed a significant decrease in WVP (33% reduction) of PLA composite due to the higher effective diffusion path length. However, Thellen et al., shown that the plasticized poly (L-lactide) (PLLA)/montmorillonite layered silicate (MLS) nanocomposites shows a higher reduction in both water vapour permeability (up to 50%) and in oxygen permeability (up to 48%) of PLA nanocomposite [93]. Similarly, Courgneau et al., showed that the formulation of PLA with both talc and acetyl tributyl citrate (ATBC) is a good way to increase the crystallization rate and

improvement of the barrier properties of PLA [94]. They showed that the addition of 5 wt% Cloisite 25A and acetyltriethyl citrate ester as plasticizer decreases the oxygen and water vapor permeability of blown films to 48% and 50%, respectively. Montmorillonite nanoparticles with different surface modifications also represent as a good candidates for decreasing barrier properties of PLA. Şengül and Dilszi investigated the effect of different surface modified montmorillonite on the oxygen barrier properties of PLA [95]. They showed that surface modified montmorillonite increases oxygen barrier properties of PLA, however, the amount of enhancement is depend on the exfoliated and intercalated level controlled by the surface modifier. Chang et al., examined PLA nanomaterials with different organoclays content and compare the influences of the clay loading, the dispersion, the intercalation states and oxygen permeability of PLA nanocomposites [84]. The results showed that, a decrease by more than half is observed for all different nanoclays. They believed that, a reduction in oxygen permeability is due to an increase in the lengths of the tortuous paths followed by the gas molecules and to the interaction between the oxygen molecules and the alkyl moiety in the organoclays. Similarly, Maio et al., found 60 % decrease in the oxygen permeability of PLA/Cloisite 30B (6 wt%) flat film which is prepared by extrusion [96]. The combined effect of crystallinity and clay minerals itself (montmorillonite) on the gas barrier properties of both amorphous and annealed PLA nanocomposites is reported by Picard et al. [97]. A reduction of 60% in oxygen permeability in an annealed PLA nanocomposite sample was shown to result from the respective contribution of the montmorillonite and the crystalline phase.

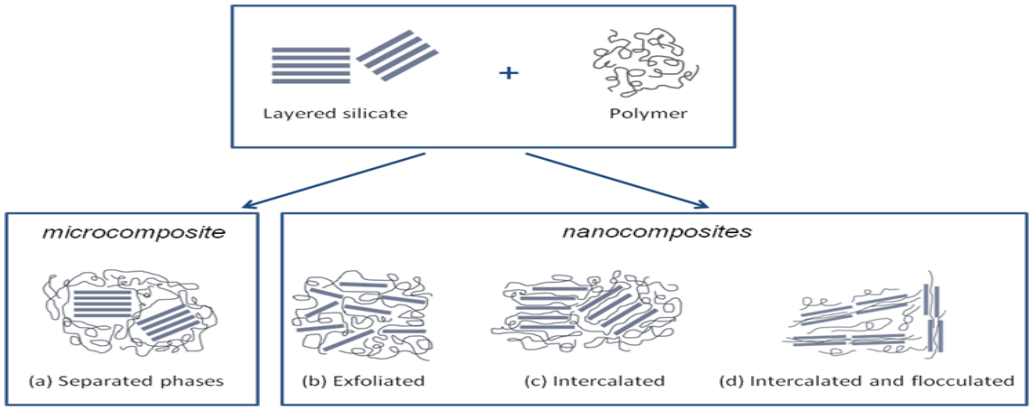

Figure 2.11. The structure of the polymer and clay nanocomposite [97].

As mentioned before talc is another efficient nucleating agent which decreases considerably the crystallization half-time and spherulite size of PLA [98,99]. Therefore, PLA crystallinity can be significantly improved. The addition of talc is providing high resistivity and lower gas permeability as well. Talc is the hydrated magnesium silicate with a chemical composition of $Mg_3Si_4O_{10}\ (OH)_2$). Talc has a plate-like structure which provides oxygen atoms and hydroxyl groups on the planar layers and weak van der waals forces hold these planar layers together [105, 106]. Therefore, talc can be delaminated at low shearing stress making it easy to disperse in polymer matrix and increases the lengths of the tortuous paths [102]. Sekelik et al., [108] and Murthy et al., [103] studied the oxygen and water vapor barrier properties respectively, by addition of talc. They showed that talc enhances the crystallinity and improves gas the barrier properties of the polymer matrix. This is because of the fact that crystalline phase is impermeable to permeant gas molecule compared to amorphous phase of polymer matrix. Buzarovska et al., prepared PLA/talc blend with different content of talc ranging from 5 to 15 wt% by solvent casting and study gas barrier properties of the PLA/talc blends [95]. They demonstrated up to 55% enhancement in the barrier properties of PLA/talc blend (5 wt%) against water vapor which represent good potential of these materials for their possible applications in packaging. Jain et al., also studied gas barrier properties of PLA composite films and they showed that the addition of 3wt% talc has a considerable effect on the oxygen (33% reduction) and water vapor (25% reduction) barrier properties of PLA [99].

In addition, several studies have been conducted on the nanocomposites of PLA obtained using natural nano fillers such as cellulose nanocrystals (CNCs). PLA/CNCs nanocomposite is the most outstanding system to study gas transport properties, because CNCs have interesting chemical and physical features including a large surface area to volume ratio, high reactive area and flexibility in surface modifications[100]. Additionally, CNCs can act as nucleating agents to increase crystallinity and to improve the barrier properties of PLA/CNC nanocomposites due to the decrease in free volume [101]. However, it has been shown that adding unmodified CNCs has almost no effect on the gas barrier properties of PLA due to high hydrophobicity, low distribution and less tortuous path of CNCs. PLA nano-biocomposites containing 5 wt% of unmodified CNCs nanocrystals exhibited 17.4 ± 1.4 cm^3mm/m^2 day, while that for modified CNCs with an acid phosphate ester was reduced to 15.8 ± 0.6 cm^3mm/m^2 day [104]. Addition of 1 wt% of silver nanoparticles to these modified PLA/CNCs nanocomposites further decreased the OTR to

12.6±0.1 cm^3mm/m^2 day [101]. Similarly Siro et al., demonstrated that the combination of 5 wt% of CNCs and 1 wt% Ag nanoparticles reduced 60% of oxygen permeability of PLA[105]. This is explained by the ability of the CNCs to enhance the crystallization of PLA and to decrease the PLA permeability. In another study, Fortunati and his coworkers reported a reduction of 34% in water vapor permeability of PLA when 1% modified CNCs with an acid phosphate ester of ethoxylated nonylphenol was added into PLA [104]. The reduction in WVP of PLA nanocomposites is attribute to the nucleation effect of modified CNCs. The oxygen transmission rate (OTR) of ternary systems consisting of PLA, PHB (poly hydroxybutyrate) and 5 wt% unmodified CNCs was 15.3 cm^3mm/m^2 day, while; that for modified CNCs with an acid phosphate ester was 13 cm^3mm/m^2 day. [102]. This results were due to high hydrophobicity and the presence of sulphate groups with low polarity on the surface of CNCs which is increased the surface hydrophobicity of CNCs. The incorporation of 3 wt% or even 1 wt% loading of CNCs bring about a reduction in an oxygen permeability of the bio-nanocomposites, between 10-30% and 50-55% respectively. Since, lower amount of CNWs have a better effect on the crystallization. Prez et al., showed that incorporation of cellulose nanowhiskers (CNW) which are grafted by n-octadecyl-isocyanate (CNW-ICN) decreased the water vapor permeability (WVP) because of PLA because hydrophobic nature graft surface and improved compatibility could lessen the effect of inclusion of hydrophilic structures in a matrix on water vapor transport [106]. In addition, Trifol et al., demonstrated that combination of clay and nanocellulose clearly resulted in synergistic behaviour in terms of the oxygen transmission rate (OTR) through a reduction of up to 90% in OTR and a further reduction in the water vapour transmission rate of up to 76% [107].

Chitosan (CH) is an another intersing polysaccharide obtained from deacetylation of chitin. Besides its biodegradibility and biocompatibility chitosan is reported as an effective nano bio-filler on barrier properties of PLA. Fan et al., were prepared Water dispersions of TEMPO-oxidized α-chitin nanowhisker (TOChN), partially deacety lated α-chitin nano whisker/nanofiber mixture (DEChN), HCl-hydrolyzed chitin nanowhisker (HHChN) and squid-pen β-chitin nanofiber (SQChN) were prepared by casting methods. They showed that, all chitin nanowhisker/nanofiber films had similar oxygen permeabilities of ∼1 mL μm m^{-2} day^{-1} kPa^{-1}, which was clearly lower than that (184 mL μm m^{-2} day^{-1} kPa^{-1}) of a poly (lactic acid) film [108].

2.2.13. Barrier Properties of PLA/SNCs Nanocomposite

PLA/SNCs nanocomposite is one of the most attractive nanocomposite for food packaging applications. However, very few researches investigated barrier properties to oxygen and water vapor due to the hydrophilic nature of SNCs. Angelier et al., found a continuous decrease in permeability upon SNCs addition [109], whereas, Kristo et al., reported that there is no changes in WVP between the neat film and those containing up to 20 wt % nanocrystals [55]. However, by increasing SNCs concentrations up to 40 wt%, the WVP decreases considerably. Nevertheless, Garcia et al., observed that by decreasing SNCs concentrations up to 2.5 wt% the WVP of thermoplastic starch (TPS) decreases by 40% [110]. An explanation for this difference could also be found in the way SNCs are dispersed and it is considered as an impermeable nanocrystalline particles to create a tortuous pathway for water vapor and oxygen molecules to pass through (Figure 2.12). Inclusion of the SNCs into the hydrophobic polymer can be a challenging issue due to the hydrophilic nature of SNCs. Therefore, SNCs presents a poor dispersity into polymer matrix. To overcome these shortcomings, many diffrent modifications have been proposed in the past few years (section 2.8). The effect of these different modifications on the WVP of the PLA/SNCs films has also investigated in the past. Yin et al., found that hydrophobic cross-linked starch nanocrystals (CSNs)/PLA nanocomposite has a better water vapor barrier properties than neat PLA [111]. They attributed this phenomena to the higher degree of crystallinity of PLA nanocomposites which makes difficult for the water molecule to penetrate through it. In another study, Muller et al., prepared PLA/thermoplastic starch (TPS) film by extrusion and thermo pressing method [112]. They showed that water vapor barrier properties of the PLA/TPS blends were enhanced due to the decrease in the number of free hydroxyl groups present in the cross-linked starch chains which then hindered the diffusion of water molecules through the film matrix. Overall, the incorporation of PLA into sugar palm starch (SPS) films improves the mechanical properties (tensile strength and tensile modulus) and water barrier properties of SPS-based films which enhance their suitability for food packaging. There are a few works on the barrier properties of PLA/starch bilayer composites, with the objective to optimize the functional properties of biodegradable packaging materials. Sanyang et al., managed to improve the water vapor properties of PLA by adding sugar palm starch (SPS) bilayer cast films with different PLA concentrations (20-50 wt%) [113]. They showed that the water vapour permeability of PLA/SPS (50 wt%) reduced significantly due to PLA hydrophobic resistance perpendicular to the transfer of water molecules.

The film microstructure revealed a lack of strong interfacial adhesion between the starch and PLA cast layers. However, cast amorphous PLA and thermo processed cassava starch with good interfacial adhesion were obtained by Muller et al [114]. They found that starch layers improve in tensile and water vapor barrier properties despite the lower ratio of PLA sheet in the bilayer assembly. In addition, Ortega et al. [115] were obtained Starch-PCL bilayer films by compression molding. Neat starch and starch/PCL (5 wt%) layers were plasticized by ascorbic acid or potassium sorbate . Before compression, starch layers (neat starch and starch with 5% PCL) were plasticized by spraying aqueous solutions of ascorbic acid or potassium sorbate, for the purposes of favoring the starch-PCL adhesion. The results showed that all bilayers enhanced barrier properties to water vapor and oxygen, as compared to neat starch and PCL films up to 96% and 99% respectively. The effect of the starch on the oxygen permeability of the PLA was further studied by Battegazzore et al., whose prepared the of maize starch/PLA blend by using a co-rotating twin screw micro extruder [116]. They showed that it was difficult for the oxygen molecule to penetrate in Starch/PLA composites due to the formation of clusters of starch that modify the intermolecular forces between the chains of the polymer and decreases the free volume. Bher et al., blended PLA with thermoplastic cassava starch (TPCS) and functionalized with commercial graphene (GRH) nanoplatelets in a twin-screw extruder, and films were produced by cast-film extrusion [117]. They found that PLA-GRH and PLA-*g*-TPCS-GRH showed a reduction of the oxygen permeability coefficient with respect to PLA of around 35% and 50%, respectively.

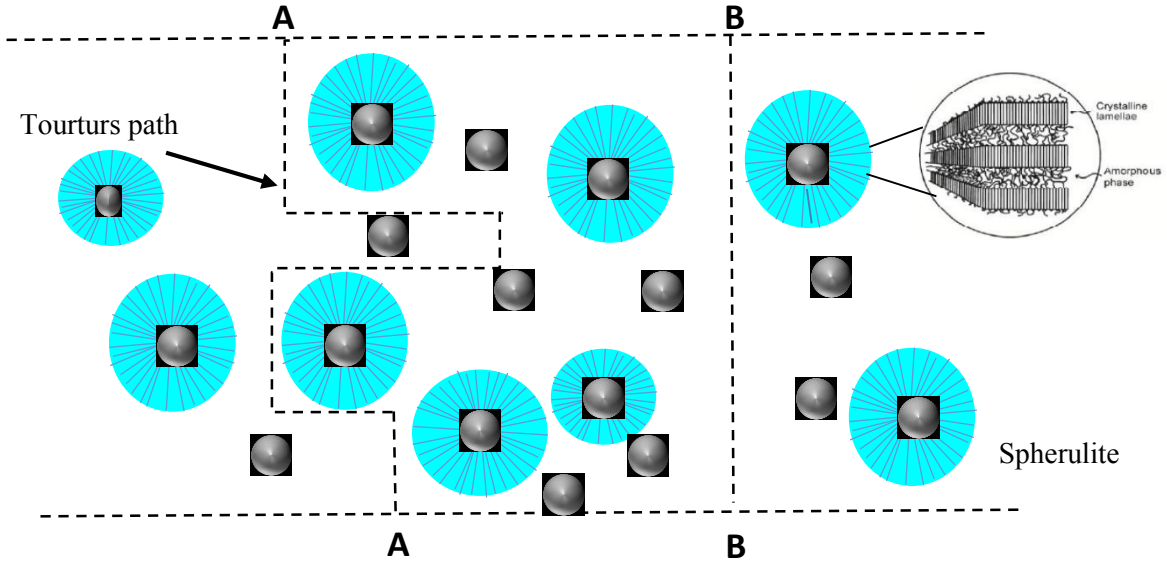

Figure 2.12. Schematic illustration of tortuosity for diffusion penetrant.

2.2.14. Degradation of PLA and PLA/Starch Composite

PLA is fully biodegradable polymer however, the rate of degration of PLA is very low due to the low susceptibility to microbial attack in natural environment. PLA naturally degraded in soil or compost. The degradation of PLA in soil occurs in three stages, in the first stage water molecules diffuse into PLA material and it hydrolysis of ester bonds and lowering molecular weight then followed by assimilation by microorganisms (such as fungi or bacteria) into non-toxic, harmless substances such as carbon dioxide, water, methane, natural substances and biomass. The biodegradation of PLA can be enhance by increasing temperature above 58 ℃ or by enhancing moisture content [118–120]. In addition, the rate of degration of PLA can be catalyzed by increasing free carboxyl groups of the hydrolyzed PLA terminal groups. The degradation of PLA is also influenced by its impurity, residual monomer, molecular weight, chemical structures and environment conditions such as temperature, humidity, and microorganism. Many studies have been focused on the soil burial degradation of PLA [118–120]. Ho et al., buried PLA films with average soil moisture of 80% and temperature of 27 ℃ in outdoor environment in Costa Rican soil. They found that the average degradation rate of PLA films in the soil of banana field was 7675 M_w (M_w/week) [118]. The degradation of PLLA films in south Finland soil for two years was also investigated by Gallet and his coworkers [119]. They reported that during the first year the PLLA films undergoes just hydrolysis and in the second year microorganisms assimilate the small products of degradation. Calmon et al., found that weight losses of PLA varying from 0 to 100% after soil burial for 24 months depending on PLA type and location. However, Urayama et al., found opposite results, molecular weight of PLA (L-rich) plates is reduced only 20% after 20 months in soil [121].

Blending of PLA with natural products such as starch is considered as an effective technique to accelerate the biodegradation rate of PLA. It has been demonstrated that starch is more susceptible to biological attack under an environmental condition after use, hence; it enhances the degradation rate of PLA. The crystallinity, thermal and mechanical properties of PLA/starch blend with different chemical and physical modifications have been extensively studied. However, there are a few reports considering the effect of mentioned modifications on the biodegradation of PLA/starch blend specifically in soil and compost conditions. Shogren et al., [122] reported that the addition of pure starch (up to 60% by weight) to PLA does not significantly accelerate the degradation (weight loss) of PLA and PLA/pure starch composites required many years to

biodegrade. Phetwarotai et al., found that adding compatibilizer such as MDI enhances the biodegradation rate of PLA/ gelatinized starches (GS) blend [123]. In addition, Shi et al., prepared ternary blend of PLA, thermoplastic starch (TPS) and glycidyl methacrylate grafted poly (ethylene octane) (GPOE) and the indicated that the compatibilizer of GPOE can accelerated PLA/TPS biodegradation rate due to the radicals formed in the biodegradation of GPOE [124]. Inconstant, Zuo et al., showed that the degradation rate and degree of the starch/PLA composites were attenuated due to the improved compatibility between PLA and starch esterified by dry method [58]. Similar results about the influence of compatibility on PLA/starch blend biodegradation were also reported by Iovino and his coworkers. They reported that the compatibilized PLA/starch blend revealed a lower biodegradation level due to the improved interface interaction [125]. The soil degradation mechanism of the esterified starch with MA/PLA composites is investigated by Zuo et al., and his coworkers [126]. They showed that the degradation of PLA/Starch composites took place at the carbonyl group linkage in starch structure and provide energy source for the microorganism to degrade the PLA matrix. In the other study Shogren et al., prepared injected moulded tensile bars composed of native starch (0-70%), poly (D,L-lactic acid) (95% L) and poly(hydroxyester-ether) (PHEE, 0–27%) and determined the soil burial degration behaviours of the composites. They showed that, rates of weight loss increased in the order starch/PHEE/PLA (4–50%) > starch/PLA (0–15%)> neat PLA (0%) and increased with increasing starch and PHEE contents [122].

Chapter 3

3. Chemical Compatibility of Lactic Acid grafted Starch Nanocrystals (SNC) with Polylactic acid (PLA)

Somayeh Sharafi Zamir[1,2,3], Mohammad Reza Frouzanmehr[2], Abdellah Ajji[3], Mathieu Robert[2] and Said Elkoun[2]
[1]Department of Chemical and Biotechnological Engineering, University of Sherbrooke, Sherbrooke, Qc, J1K 2R1, Canada.
[2]Center for Innovation in Technological and Ecodesign (CITE), University of Sherbrooke, Sherbrooke, Qc, J1K 2R1, Canada.
[2]3SPack, CREPEC, Polytechnique Montreal, Chemical Engineering Department, Montreal, Qc, H3C 3A7, Canada.

3.1. Résumé

Dans ce travail, des nanocristaux d'amidon (SNCs) ont été greffés chimiquement par réaction d'estérification et leur compatibilité avec les matrices de PLA a été étudiée. Initialement, SNCs pur et greffée a été caractérisée pour comprendre les propriétés cristallines, fonctionnelles et morphologiques au moyen de la diffusion des rayons X à grand angle (WAXS), de la spectroscopie infrarouge à transformée de Fourier (FT-IR), de la spectroscopie photoélectronique par rayons X (XPS) et de la microscopie électronique en transmission(TEM) respectivement. Les résultats confirment que la surface des SNCs a été modifiée avec succès avec LA. Ensuite, des SNCs greffées avec de l'acide lactique (SNCs-g-LA) ont été incorporées avec du poly (acide lactique) (PLA) avec un contenu de charge différent variant de 5 à 30% en poids par le procédé de coulée en solution. L'influence des concentrations de nanoparticules de SNCs-g-LA sur les propriétés thermiques, mécaniques et morphologiques des nanocomposites de PLA obtenus a été déterminée par calorimétrie à balayage différentiel (DSC), analyse thermogravimétrique (TGA), analyse mécanique dynamique (DMA) et microscopie électronique à balayage (SEM) respectivement. Les résultats ont démontré que l'adhérence interfaciale et la compatibilité entre les SNCs et la matrice de PLA étaient considérablement améliorées après le greffage. Grâce à une bonne compatibilité le degré de cristallinité des composites de PLA résultants a été amélioré de manière significative de 1,1% à 15,7% par rapport au PLA pur.

Mots clés: Nanocristaux d'amidon, greffage chimique, adhérence interfaciale, nanocomposites de PLA, Cristallinité.

3.2. Abstract

In this work starch nanocrystals (SNCs) was chemically grafted by esterification reaction and their compatibility with PLA matrices studied. Initially, neat and grafted SNCs was characterized to understand crystalline, functional, and morphological properties by means of Wide Angle X-ray Scattering (WAXS), Fourier Transform Infrared (FT-IR), X-ray Photoelectron Spectroscopy (XPS) and Transmission Electron Microscopy (TEM) respectively. The results confirm that the surface of SNCs was successfully modified with LA. Subsequently, grafted SNCs with lactic acid (SNCs-g-LA) were incorporated with poly (lactic acid) (PLA) by different filler content varying from 5-30 wt% by solvent casting process. The influence of the SNCs-g-LA nanoparticles concentrations on thermal, mechanical and morphological properties of resulting PLA nanocomposites were determined by Differential Scanning Calorimetry (DSC), Thermogravimetry Analysis (TGA), Dynamic mechanical analysis (DMA) and Scanning Electron Microscopy (SEM) respectively. The results revealed that the interfacial adhesion and compatibility between SNCs and PLA matrix were substantially improved after grafting. As a result of good compatibility the degree of crystallinity of the ensued PLA composites was improved significantly from 1.1% to 15.7% compared to neat PLA.

Keywords: Starch nanocrystals, chemical grafting, Interfacial adhesion, PLA nanocomposites, Crystallinity.

3.3. Introduction

During the last decades, environmental pollution due to the excessive consumption of petroleum-based synthetic polymers has been a major concern. Hence, these petroleum-based polymers need to be replaced by biopolymers derived from renewable resources [2,2,127,128]. Among the biopolymers family, poly (lactic acid) (PLA) has attracted a particular attention due to good mechanical (high strength and high modulus), optical and physical properties as compared to petroleum based polymers such as polystyrene (PS) and polyethylene terephthalate (PET) [129]. Until the 2000s, PLA was predominantly used for high-value-added applications like medical implant devices [130]. PLA is the most used commercial bioplastic in the world [1]. By 2020, the production of PLA is expected to grow by a factor of four to reach ~ 800,000 ton per year. However, PLA applications are still limited due to its low thermal stability, poor barrier properties (mainly oxygen and water vapor) and low degree of crystallinity [77,82-153]. Hence, numerous approaches to improving its properties were reported [71,131–135]. Blending PLA with organic materials such as N,N-ethylenebis (12-hydroxystearamide) [84] and 1,3,5-benzene tricarboxyamide (BTA) [136] and inorganic materials such as clay [137] and silicate [39] was regarded as an easy and cost-effective approach to overcoming PLA shortcoming. However, those fillers are generally non-biodegradable and not recyclable. Polysaccharides materials such as cellulose, chitosan and starch have attracted attention of researchers during the last few years [138,139]. Polysaccharides were seen as good candidates for food packaging, implant materials and drag carriers due to their light weight, low cost, biocompatibility and non-toxicity [72,140]. It was shown that these abundant, renewable and recyclable materials have a potential to act as reinforcing fillers and nucleating agents for PLA. Generally, polysaccharides can be found in both amorphous and crystalline phase. The crystalline phase can be extracted by acid hydrolysis using concentrated sulfuric acid (H_2SO_4) and hydrochloric acid (HCl) [59]. Among the nanocrystals, starch nanocrystals (SNCs) were considered as a potential candidate for improving PLA properties [56,59,141]. Surface modification of SNCs is relatively easy due to the presence of hydroxyl groups and have a large surface area [56,59,141]. However, the poor interfacial adhesion between PLA and SNCs limits the processing of the PLA/SNCs nanocomposites [141]. Several studies showed that an enhancement of the interfacial adhesion between SNCs and PLA matrix led to significant improvement in thermal resistance and mechanical properties of the PLA/SNCs composite [56,142]. The interfacial adhesion was improved by grafting on SNCs surface small

molecules or hydrophobic polymer chains such as methylene diphenyl diisocyanate (MDI), fatty acid, isocyanate group, fatty acid in organic solvent, halides or vinyl ester, poly (ethylene glycol) methyl ether (PEGME), stearic chloride, poly (tetrahydrofuran) (PTHF) or poly (propylene glycol monobutyl ether) (PPGBE) [56,126,143–147]. Researchers also reported that the interfacial adhesion was improved by copolymerization of the starch with various biopolymers such as PLA, poly 1 3 Polymer Bulletin (ε-caprolactone) (PCL) or poly (3-hydroxy butyrate) (PHB) [49,148,149]. For instance, Chen et al., used in situ ring-opening polymerization (ROP) of ε-caprolactone [150] to graft polymer chains at starch surface using SnO_2 as a catalyst. However, this ROP polymerization is time-consuming, is water sensitive and requires sometimes highly toxic metal-based initiators [188]. Therefore, a viable, feasible and non-toxic process is still necessary to improve the compatibilization between starch and PLA. In this aspect, grafting of SNCs with monomers such as lactic acid (LA) seems to result in hydrophobic SNCs which can increase the interfacial adhesion between SNCs and PLA. LA is an organic acid with secondary alcohol functional groups that can form covalent bonds through esterification with SNCs. In addition, LA is also the monomeric unit of PLA. Therefore, grafting LA on the SNCs surface was regarded as an interesting way to obtain fully bio-based composite [49,149]. In this work, SNCs were prepared by acid hydrolysis from corn starch according to a previously reported method [141]. Subsequently, lactic acid monomers (LA) were grafted on the SNCs surface by simple esterification reaction. Then, chemically modified SNCs, referred to as SNCs-g-LA, were characterized and, subsequently, PLA/SNCs-g-LA nanocomposite films were prepared at different concentrations using solvent casting method. The effect of LA grafting on the thermal and mechanical properties of PLA-based nanocomposites was investigated and compared with ungrafted SNCs.

3.4. Experimental

3.4.1. Materials

Commercial PLA (4032D) pellets, having a semi-crystalline grade (2% D-LA), were supplied by Nature Works LLC (Minnesota, USA). The measured average molecular weight (M_w) and polydispersity index (M_w/M_n) of PLA pellets was found to be $109\ kg/mol$ and 1.57 respectively. Corn starch and LA was purchased from Sigma-Aldrich, Canada. Corn starch majorly contained pure amylopectin.

3.4.2. Extraction of Starch Nanocrystals (SNCs)

Starch nanocrystals (SNCs) were prepared by acid hydrolysis of corn starch as previously reported [174]. Briefly, 147g corn starch granules was dispersed into 500 mL of 3.16 M aqueous sulfuric acid (H_2SO_4). The suspension was then kept under 400 rpm mechanical stirring at 40 ℃. Subsequently, the resulting solution was washed in distilled water at 11 ℃ by successive centrifugation (Centrifuge 6K-15C, Sigma) at 10,000 rpm until a neutral pH to establish. Finally, the suspension was freeze-dried using a Heto Power Dry PL6000 apparatus from Thermo Scientific. After freeze-drying, few drops of chloroform was added to the SNCs powder to avoid the bacterial activity and then SNCs were kept in the cold environment.

3.4.3. Surface Modifications of SNCs by LA

Surface modification of SNCs by LA was carried out as follows; starch nanoparticles (30 g) was first dispersed into 100 ml of Tetrahydrofuran (THF). Then LA was added slowly to the stirring solution. The resulting suspension was heated up to 60 ℃ for 30 mins under argon atmosphere. After THF evaporation, 150 ml toluene was added to the reaction and the mixture was heated up to 85 ℃ for 24 hrs. After washing the resulting reaction mixture with THF and ethyl acetate, the final product was dried under vacuum at 45 ℃. Figure 3.1 shows the reaction scheme of the chemical grafting of LA on SNCs.

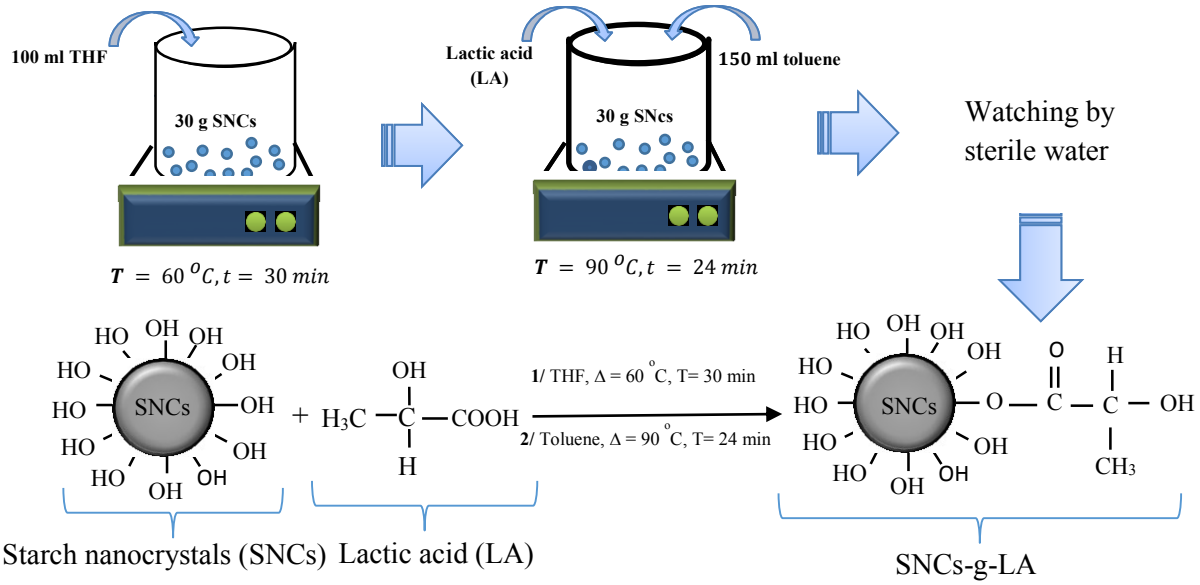

Figure 3.1. Reaction schematic of the chemical modification of SNCs with LA.

3.4.4. Preparation of PLA Nanocomposites

The PLA/SNCs-g-LA nanocomposites were prepared by adding the desired amount of SNCs-g-LA nanoparticles and PLA pellets together in dichloromethane (CH_2Cl_2). Then, the mixture was stirred at 70 ℃ for 24 hrs. Subsequently, the CH_2Cl_2 solvent was evaporated by keeping it at room temperature for 24 hrs. Finally, the prepared films were vacuum dried overnight. The PLA/SNCs-g-LA nanocomposites were named as: PLA/SNCs-g-LA nanocomposites (5 wt%), PLA/SNCs-g-LA nanocomposites (10 wt%), PLA/SNCs-g-LA nanocomposites (20 wt%), PLA/SNCs-g-LA nanocomposites (30 wt%); where 5, 10, 20 and 30 wt. % represents the weight percent of SNCs-g-LA nanoparticles in the PLA nanocomposites. In addition, a PLA film was also prepared according to the above-mentioned process without adding SNCs-g-LA particles and named as neat PLA.

3.4.5. Characterizations

3.4.5.1. Fourier-Transform Infrared (FT-IR)

Fourier Transform Infrared (FT-IR) analysis was performed to determine the different functional groups present on the SNCs surfaces before and after grafting by LA by using JASCO-4600 FT-IT Spectrometer (Japan) equipped with attenuated total reflectance (ATR) PRO ONE reflection accessories method in the range of $4000 - 600\ cm^{-1}$ with resolution of $4\ cm^{-1}$.

3.4.5.2. Wide Angle X-ray Scattering (WAXS)

Wide Angle X-ray Scattering (WAXS) analysis was used to determine the crystalline structure of SNCs before and after grafting by LA, neat PLA and PLA nanocomposites. WAXS measurements of the samples were performed using Philips X'Pert diffractometer. The diffractometer was equipped with a general area detector diffraction system. The diffractometer emits Cu K_α radiation ($\lambda = 0.1542$ nm), while operating at 50 kV and 40 mA. The experiments were performed in the angular range (2θ) between 5 and 40°, with a step size of 0.02°.

3.4.5.3. X-ray Photoelectron Spectroscopy (XPS)

X-ray Photoelectron Spectroscopy (XPS) measurements were performed to confirm the formation of new functional groups on the SNCs surfaces after grafting by LA. XPS on a KRATOS Axis Ultra electron energy analyzer operating with an Al K_α monochromatic source. The over viewing spectra were taken between 0 and 1400 eV with an energy step of 1 eV, while the details of the

peaks of interest (C1s and O1s) were recorded with energy step of 0.05 eV. Casa XPS version (2.3.16 Pre-rel 1, 4) was used for curve-fitting software. The overlapping peaks were resolved by the peak synthesis method, applying Gaussian-Lorentzian peak components after Shirley type background subtraction.

3.4.5.4. Transmission Electron Microscopy (TEM)

Morphologies of SNCs and SNCs-g-LA nanoparticles and PLA nanocomposites were analyzed by an H-7500 Transmission Electron Microscopy (TEM) analysis (Hitachi, Japan). SNCs and SNCs-g-LA nanoparticles were dispersed in ethanol, dried at 25℃ on a copper grid and observed with 80 kV acceleration voltage.

3.4.5.5. Scanning Electron Microscopy (SEM)

The cross-sectional image of neat PLA and PLA nanocomposites were analyzed by an S-7500 Scanning Electron Microscopy (SEM) (Hitachi, Japan). All samples were cut in liquid nitrogen, coated with a thin layer of Pd-Au, using vapor deposit process before SEM characterization.

3.4.5.6. Differential Scanning Calorimetry (DSC)

Thermal properties of neat PLA and PLA nanocomposites were characterized using Differential Scanning Calorimetry (DSC) (Q2000, TA instrument).

Samples of approximately 5-10 mg in weight were sealed in a closed aluminum pan. Two heating scans were performed. During the first heating scan, the samples were heated from 25 to 200 ℃ in the presence of nitrogen atmosphere. Thereafter, the samples were quickly brought back to room temperature to eliminate any thermal history. Subsequently, a second heating scan was performed raising the temperature of the samples up to 200 ℃. The samples were maintained at 200 ℃ for 5 min and then cooled to 25 ℃ at the rate of $5\ ℃.\min^{-1}$. Corresponding melting temperature (T_m) , cold crystallization temperature (T_{cc}), heat of fusion (ΔH_m) and degree of the crystallinity ($X(x)$) of neat PLA and PLA/SNCs-g-LA nanocomposites were recorded after the second heating scan. The crystallinity degree of PLA and PLA/SNCs-g-LA nanocomposites was calculated by using following formulation;

$$X(x) = \frac{\Delta H_m}{(1-w)\,\Delta H_0} \times 100\% \qquad (3\text{-}1)$$

where w is the weight fraction of starch, ΔH_0 is the enthalpy of melting for fully crystalline PLA (93 J/g) [182].

3.4.5.7. Dynamic Mechanical Analysis (DMA)

Dynamic Mechanical Analysis (DMA) was carried out on a DMA (Q800, Perkin Elmer instrument, USA) using dual cantilever device at a fixed frequency of 1 Hz. Samples ($64 \times 12 \times 3$ mm) with a thickness of ca. 0.2 mm were tested in the temperature range of -25 to 120 ℃ at a heating rate of 3℃. min^{-1}.

3.4.5.8. Thermogravimetric Analysis (TGA)

Thermogravimetric Analysis (TGA) was performed using TGA-SETARMAN instrument under argon flow. Samples (10 mg) were heated from 25 to 700 ℃, at the rate of 10 ℃/min. Then, the corresponding loss of mass was noted.

3.4.5.9. Dynamic Contact Angle Measurement (DCA)

The contact angle of SNCs before and after grafting by LA was obtained by the Wilhelmy method using a Dynamic Contact Angle Tensiometer (DCA-100F) with distilled water as the probe liquid. Contact angle measurements were performed at room temperature. Smooth surface pellets were obtained by compacting the dried SNCs and SNCs-g-LA nanoparticles under a pressure of 5 ton at 50 ℃. Both samples were dried under vacuum for 24h before DCA measurements.

3.5. Results and Discussion

3.5.1. FT-IR Analysis of SNCs and SNCs-g-LA Nanoparticles

The FTIR spectra of neat SNCs and SNCs-g-LA nanoparticles are shown in Figure 3.2. The FTIR spectra of neat SNCs show characteristic peaks of stretching and bending vibrations of −OH groups at wavenumbers of 1650 cm^{-1} and 3300 cm^{-1} [56]. Moreover, the stretching vibrations of C–O bonding in C–O–H and C–O–C groups of neat SNCs appear at wavenumbers of 1150, 1077 and 990 cm^{-1}, respectively [56]. After grafting SNCs by LA, FTIR spectrum shows an additional sharp peak at 1730 cm^{-1}. This peak is attributed to the ester carbonyl stretching groups (=CO) which is present in lactic acid. In addition, two new peaks at 1250 and 1055 cm^{-1} were observed and can be attributed to C–O vibration in ester groups. Moreover, after grafting LA on SNCs 3300 cm^{-1} is observed. Those results indicate that LA monomers were successfully grafted on the

surface, a decrease in the peak intensity of –OH functions around wavenumbers of 1650 cm^{-1} and SNCs surface.

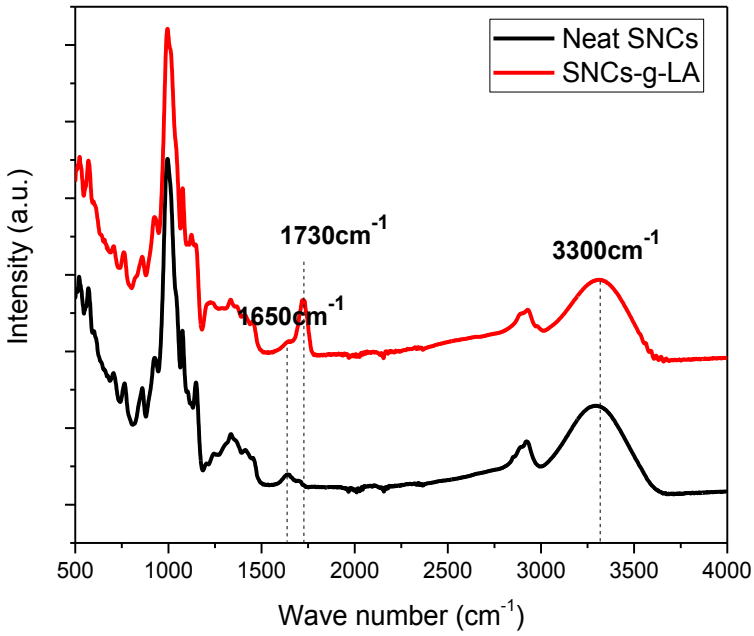

Figure 3.2. FTIR analysis of the neat SNCs and SNCs-g-LA nanoparticles.

3.5.2. XPS Analysis of SNCs and SNCs-g-LA Nanoparticles

The XPS characterization is a semi quantitative elemental analysis technique that provides additional quantitative information about the chemical surface modification of materials. It is an appropriate tool to determine the chemical composition resulting from the surface down to about 8–10 nm depth. Figure 3.3a and b shows the XPS spectra of neat SNCs and SNCs-g-LA nanoparticles, respectively. The relative atomic percentages of oxygen and carbon elements, oxygen-to-carbon ratio (O/C) and atomic concentrations of various peaks are given in Table 3.1. The XPS spectra of both neat SNCs and SNCs-g-LA nanoparticles were deconvoluted into four peaks at different binding energies: 284.8 eV, 286.5 eV, 287.7 eV and 289.0 eV which correspond to C–C and/or C–H group, C–O group, C=O and O–C–O/C=O groups [49]. However, the SNCs-g-LA nanoparticle spectrum shows higher intensity at 289.0eV and lower intensity at 284.8eV as compared to neat SNCs. In addition, the atomic concentration of the O–C–O/C=O groups is increased from 1.36 to 2.35% and the atomic concentration of C–H is decreased from 13.2 to 4.2%

after grafting LA on SNCs (Table 3.1). Hence, the increase in the −COO bond portion and the decrease in −CH bond level can be attributed to the larger carboxylic groups on the grafted SNCs surface than the neat SNCs. Although the penetration depth of FTIR spectroscopy is greater than XPS, this increase in COO concentration after grafting is in good agreement with the FTIR results.

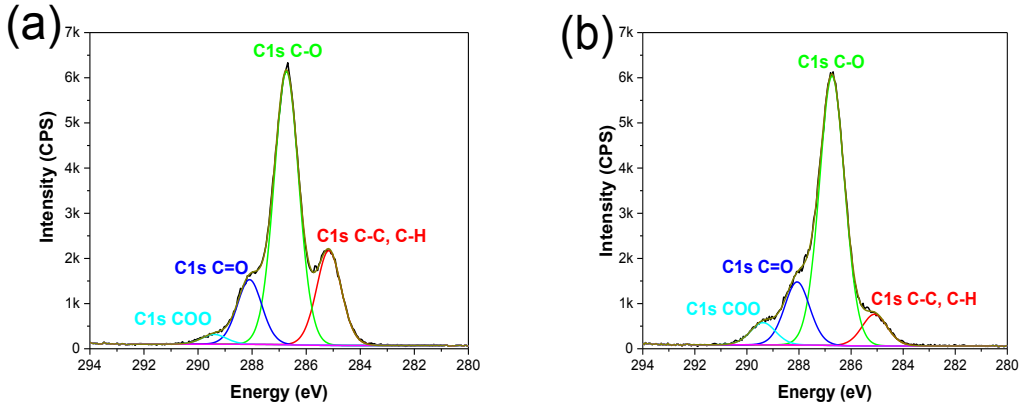

Figure 3.3. XPS spectra of a) SNCs and b) SNCs-g-LA nanoparticles.

Table 3.1 Relative atomic percentages of oxygen and carbon, O/C ratio and atomic concentrations of different peaks obtained by XPS on SNCs and SNCs-g-LA nanoparticles.

Name		SNCs	SNCs-g-LA
O%		45.45	49.32
C%		54.55	48.91
O/C		0.83	1.01
Peaks	Binding Energy	Atomic Concentrations (at%)	
C − C/C − H	284.8	13.29	4.81
C − O	286.5	38.28	41.42
O − C − O/C = O	287.7	9.05	9.86
COO	289.0	1.36	2.35
O		38.02	42.56

3.5.3. XRD Analysis of SNCs and SNCs-g-LA Nanoparticles

The crystallinity of neat SNCs and SNCs-g-LA nanoparticles was determined using XRD analysis (Figure 3.4). This method allows to quantify any crystallinity change that may occur during the chemical surface modification by LA. Neat SNCs display a typical crystalline structure of corn starch nanoparticles with two small diffraction peaks located at 2θ=10.1° and 11.5°, as well as a sharp peak at 15.3° [178]. Additionally a double peak at 17.1° and 18.2° and a strong peak at 23.2° are observed. These peaks are related to the (002), (112), (103), (110) and (213) planes of neat

SNCs, respectively [178]. Grafted SNCs show similar XRD scattering pattern as compared to non-grafted SNCs. Consequently, the crystallinity of the SNCs was not affected by grafting. Moreover, the ungrafted and grafted SNCs show the typical A-type crystalline structure, which indicates that the grafting did not affect the crystalline structure of SNCs [141].

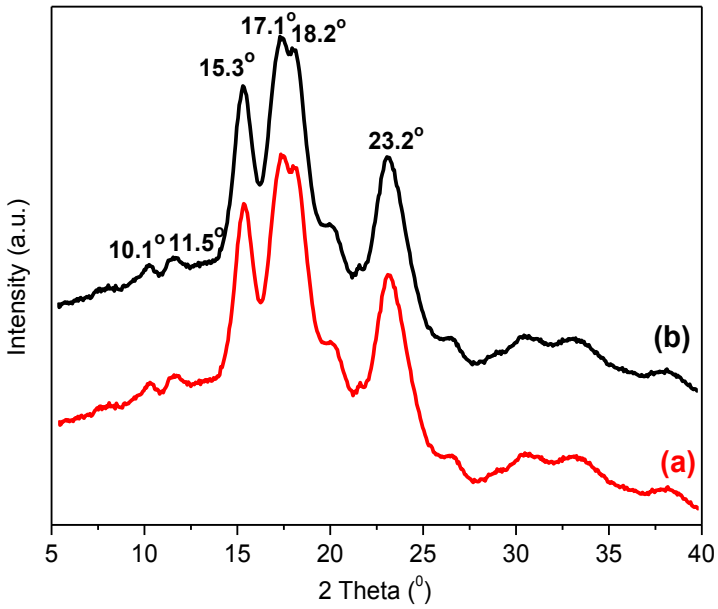

Figure 3.4. WAXS patterns of a) SNCs and b) SNCs-g-LA nanoparticles.

3.5.4. Morphology of SNCs and SNCs-g-LA Nanoparticles

Figure 3.5 shows TEM micrographs of SNCs surfaces before and after chemical modification by LA. The surfaces of SNCs look smooth, whereas grafted SNCs exhibit rough and bumpy surface. As a result, grafting seems to alter the surface morphology of SNCs by creating new functional groups. Moreover, as can be seen in the TEM image, the average size of SNCs-g-LA is higher (~80 nm) than the unmodified SNCs one (~60 nm). This increase is probably due to the new functional groups on the surface of grafted SNCs.

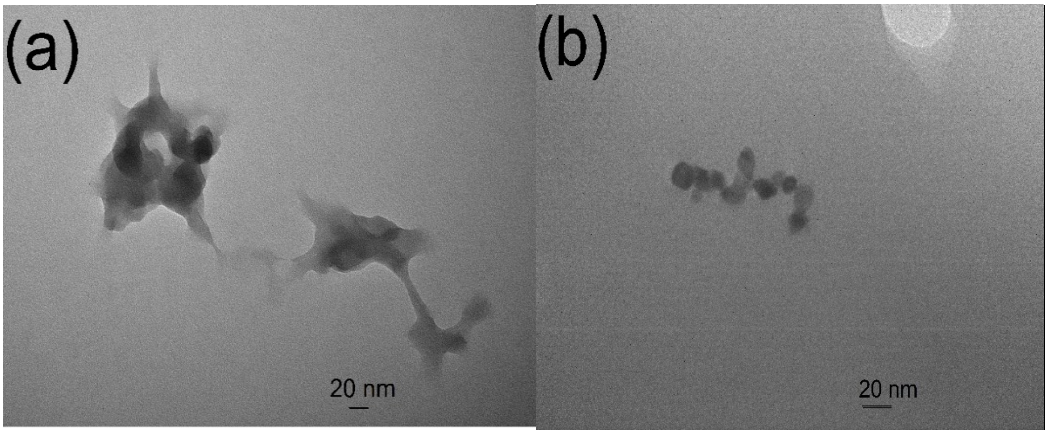

Figure 3.5. TEM micrographs of SNCs and SNCs-g-LA nanoparticles.

3.5.5. Thermogravimetric Analysis

The thermal stability of the SNCs before and after grafting was investigated using TGA. Figure 3.6a and b show the TGA thermograms of neat SNCs and SNCs-g-LA nanoparticles respectively. As shown in Figure 3.6a, the TGA curve of neat SNCs exhibits two sharp weight loss. The initial weight loss of is about 17 wt% (between 30 ℃ and 100 ℃) is followed by a larger weight loss of about 74 wt% (between 100 °C and 700 °C). The first weight loss can be related to the evaporation of moisture present in the neat SNCs, while the second one is to degradation of the neat SNCs. However, the TGA thermogram of grafted SNCs is quite dissimilar and exhibits three moderate weight losses between 30–150 ℃, 150–275 ℃ and 275–700 ℃. As shown in Figure 3.6b, the initial weight loss of SNCs-g-LA, located between 30 and 150 ℃ is about 4 wt%, much lower than the neat SNCs (37 wt%) that can be attributed to the partial hydrophobic behavior of the SNCs after grafting and the formation of ester bonds. In addition, the second weight loss, between 150 and 275 ℃, is likely due to the degradation of LA monomers on the surface of SNCs. Eventually the last weight loss, located between 275 and 700 ℃, can be ascribed to the degradation of the SNCs-g-LA nanoparticles. The TGA results clearly show that the LA grafting increases thermal stability of SNCs. Degradation temperature is shifted from 300 ℃ to 345℃.

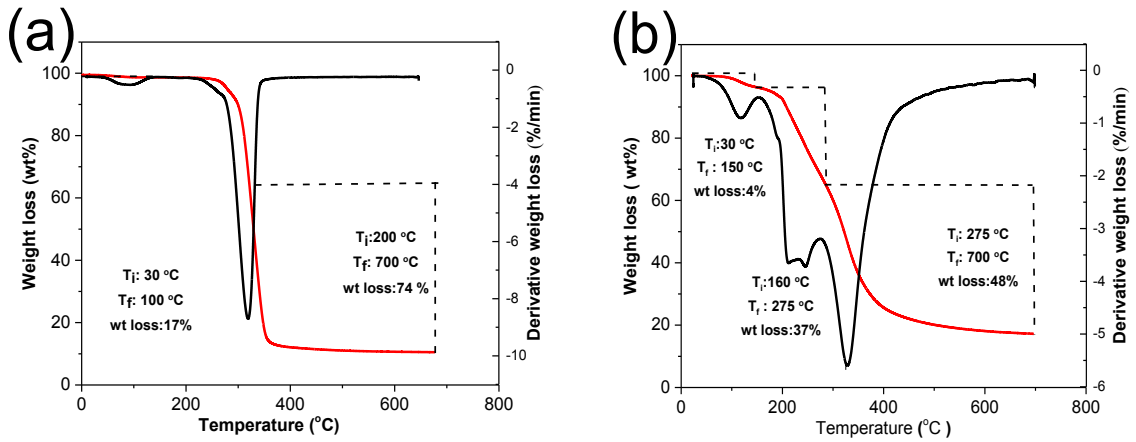

Figure 3.6. TGA and DTA thermograms of a) SNCs and b) SNCs-g-LA nanoparticles.

3.5.6. Contact Angle Measurement

The contact angle measurements were taken to understand the hydrophilic/hydrophobic behavior of neat and grafted SNCs. As expected, the contact angle of neat SNCs (44.3°) is significantly lower than the one of grafted SNCs (59.5°). The hydrophilic behavior of hydroxyl groups present at the surface of the SNCs can react with water to create hydrogen bonds, whereas for grafted SNCs, the formation of ester bonds at the surface of SNCs reduces the interactions with water and leads to an increase in the contact angle.

3.5.7. Wettability of SNCs and SNCs-g-LA Nanoparticles

In addition to the contact angle measurements, wettability of neat and grafted SNCs was checked in a solvent mixture made of dichloromethane and water. The lower phase is dichloromethane (DCM) and upper one is water since the density of DCM is higher (1.3 g/L) than the one of water (1.02 g/L). Same amount of the neat and grafted SNCs were mixed with the solvent mixture. Results are shown in Figure 3.7a (neat SNCs) and 3.7b (grafted SNCs). As expected, the neat SNCs were dispersed only in water due to their hydrophilic behavior (Figure 3.7a). However, grafted SNCs were well dispersed in DCM solvent (Figure 3.7b). This phenomenon can be attributed to the hydrophobic nature of the grafted SNCs. This result shows that the neat SNCs have higher affinity for polar solvent such as water, whereas grafted SNCs with LA show lower polar nature due to their migration toward dichloromethane.

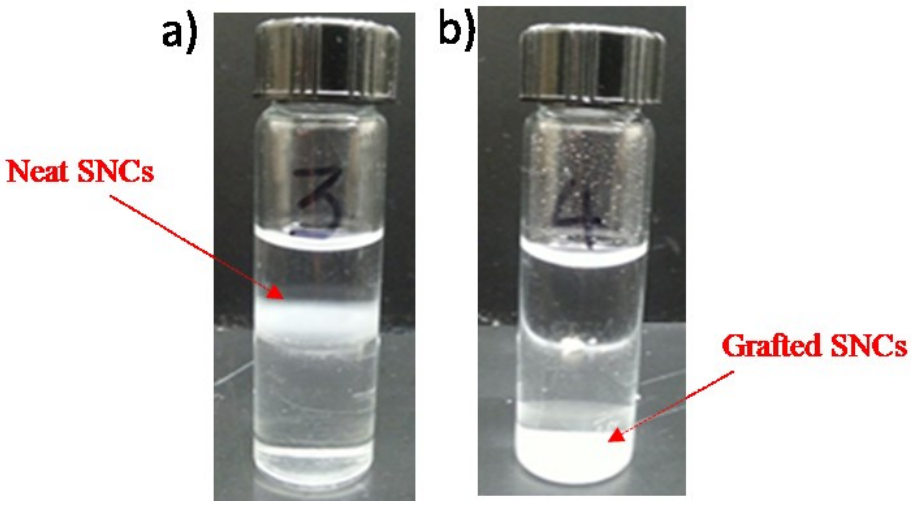

Figure 3.7. Wettability of a) Neat SNCs b) Grafted SNCs in a mixture of solvents lower phase (dichloromethane) and upper phase (water).

3.5.8. Morphology of Neat PLA and PLA Nanocomposites

The microstructure of neat PLA, PLA/SNCs and PLA/SNCs-g-LA nanocomposites was characterized using SEM (Figure 3.8). After fracture, the surface of PLA/SNCs-g-LA nanocomposites was smooth, whereas the fractured surface of PLA/SNCs nanocomposite exhibited a relatively rough surface with cavities at the interfaces. The two phases can clearly be seen in the fracture surfaces of PLA/SNCs nanocomposite where neat SNCs particles were pulled out from the matrix due to poor interfacial adhesion between neat SNCs and PLA. However, the fractured surfaces of PLA/ SNCs-g-LA nanocomposites revealed that the grafted SNCs were well embedded into PLA matrix leading to a better interfacial adhesion between grafted SNCs and PLA as compared to ungrafted ones. In addition, the grafted SNCs were dispersed homogeneously at lower concentrations (i.e., 5 wt%), while nanocomposites with high concentrations of grafted SNCs (i.e., 30 wt%) showed agglomeration. This can be due to the threshold limit of the filler content and the irreversible agglomeration of the SNCs during the freeze-drying.

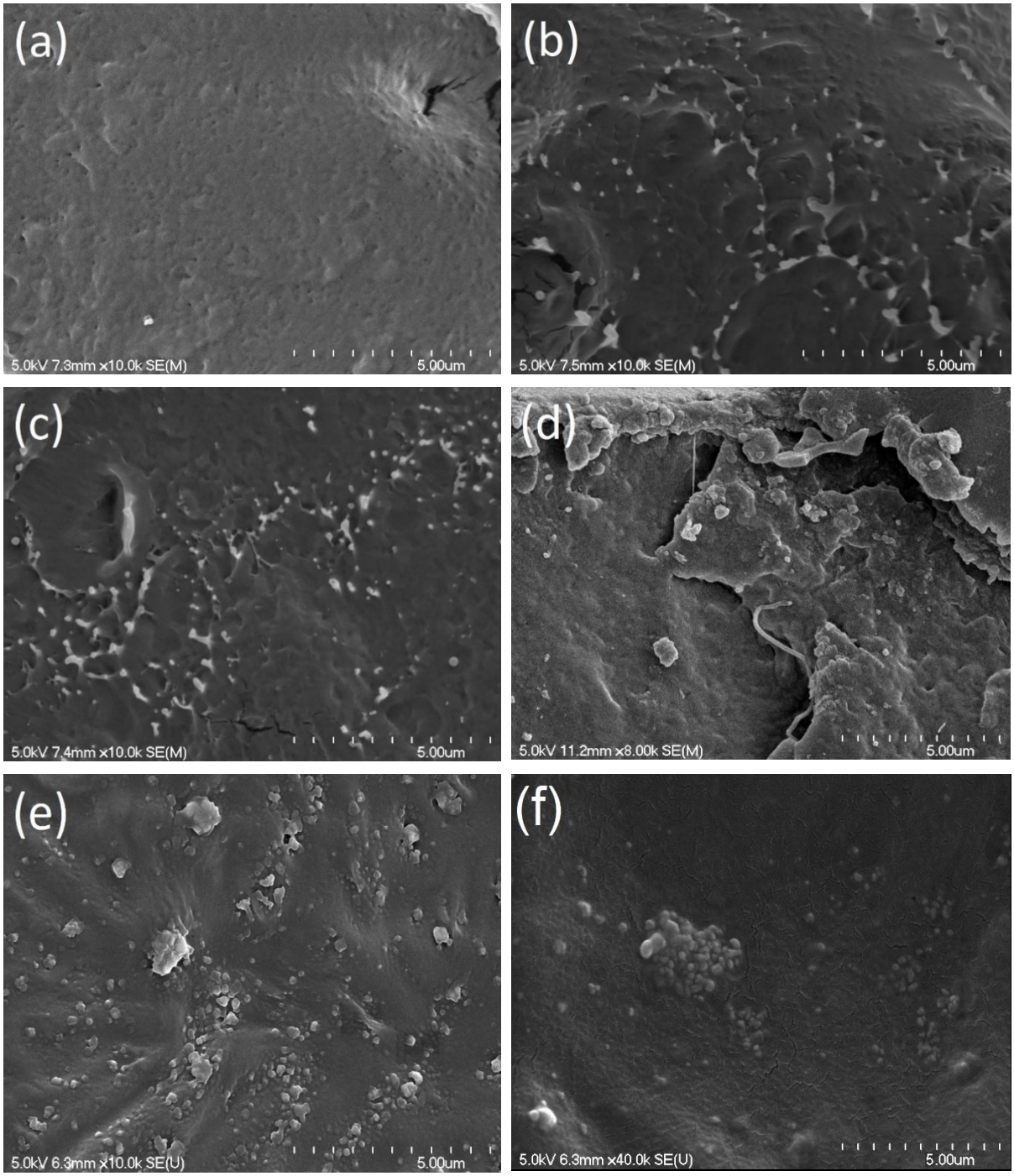

Figure 3.8. SEM micrographs of; (a) Neat PLA, b) PLA/SNCs-g-LA (5 wt%), (c) PLA/SNCs-g-LA (10 wt%), (d) PLA/SNCs-g-LA (20 wt%), (e) PLA/SNCs-g-LA (30 wt%) and (f) PLA/neat SNCs (5 wt%) nanocomposite

3.5.9. Thermal Behaviour

Figure 3.9a and b show the DSC thermograms of neat PLA and grafted and ungrafted SNCs-reinforced PLA nanocomposites during the second heating and cooling cycle respectively. The corresponding thermal data of all samples are summarized in Table 3.2. The glass transition temperature (T_g) of neat PLA is at about 62 °C, and a broad cold crystallization peak is observed around 125 °C. However, the T_g of PLA nanocomposites has no significant change and the cold crystallization temperature (T_{cc}) shifted to lower temperature when SNCs-g-LA nanoparticles are added. As given in Table 3.2, the minimum T_{cc} was observed for PLA/SNCs-g-LA (5 wt%) at around 108 °C. In addition and as compared to neat PLA, the degree of crystallinity ($X(t)$) for the PLA nanocomposites is significantly higher than neat PLA. The $X(t)$ decreases when grafted SNCs content was decreased to 5 wt%. These results suggest that SNCs-g-LA nanoparticles act as effective heterogeneous nucleating agents at low concentrations. Similar results were found during second cooling cycle. As shown in Figure 3.9b, a sharp crystallization peak is observed during cooling by adding 5 wt% SNCs-g-LA nanoparticles into PLA. In the case of higher concentrations of SNCs-g-LA nanocomposites (i.e., 30 wt%), the crystallization is low. Crystallization seems to be hindered by the addition of 30 wt% SNCs-g-LA nanoparticles [149,150]. Furthermore, neat PLA and ungrafted SNCs-reinforced PLA nanocomposite did not show any crystallization peak upon cooling, which indicates that crystallization kinetic of PLA is still low.

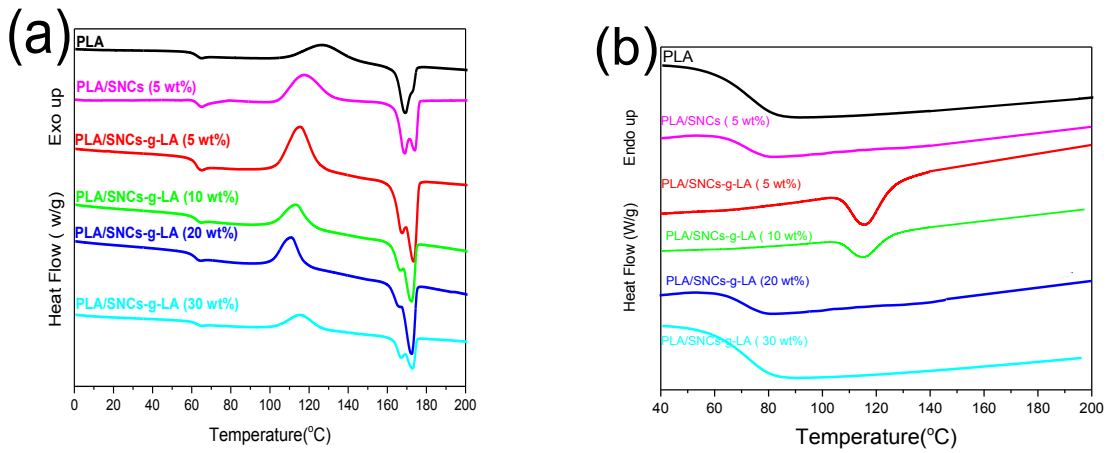

Figure 3.9. DSC thermograms of neat PLA, PLA/SNCs and PLA/SNCs-g-LA nanocomposites with different concentrations of SNCs-g-LA nanoparticles at the (a) second heating and (b) cooling scan.

Table 3.2. Thermal properties of neat PLA and PLA/SNCs-g-LA nanocomposites.

Samples	T_g (°C)	T_{m1} (°C)	T_{m2} (°C)	T_{cc}(°C)	$\Delta H_m (J/g)$	$\chi(x)\%$
PLA	62.0	165.5	168.0	124.4	29.3	1.1
PLA/SNCs (5 wt%)	61.9	165.2	168.5	125.1	27.1	2.1
PLA/SNCs-g-LA (5 wt%)	61.4	163.1	169.9	108.8	31.7	15.7
PLA/SNCs-g-LA (10 wt%)	61.8	164.5	169.5	110.9	28.0	7.5
PLA/SNCs-g-LA (20 wt%)	61.4	164.9	169.4	113.0	25.7	6.6
PLA/SNCs-g-LA (30 wt%)	61.4	164.9	169.6	113.2	23.7	1.2

3.5.10. Dynamic Mechanical Properties

The mechanical properties of the neat PLA and ungrafted and grafted reinforced PLA nanocomposites were investigated by DMA. The storage modulus (E′) and damping factor (tan δ) as a function of temperature are shown in Figure 3.10a and b respectively. The storage modulus of the SNCs-g-LA nanoparticles-reinforced PLA composites was enhanced as compared to the neat SNCs-reinforced PLA composites. However, for 20 and 30 wt% SNCs-g-LA-reinforced composites, storage modulus is lower than the 5 and 10 wt%. This might be due to the threshold limit of the filler content which was achieved between 5 and 10 wt% SNCs-g-LA/PLA composites. Moreover, this phenomenon can be attributed to the good compatibility between the matrix and filler. These results are in agreement with DSC (crystallization) and SEM (homogeneous dispersion) results. Irrespective of the samples, tan δ shows a sharp peak corresponding to the glass transition temperature (T_g) around 60–61°C.

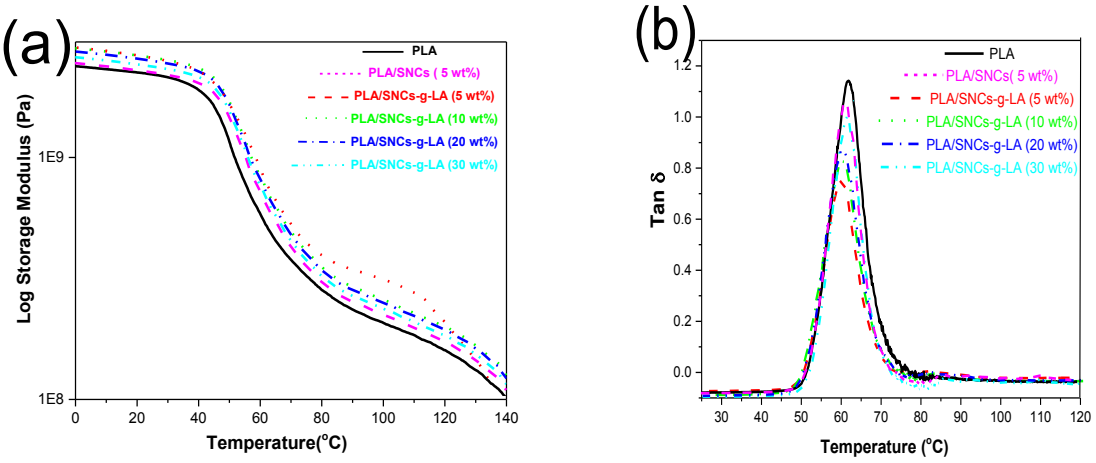

Figure 3.10. DMA analysis of neat PLA, PLA/SNCs (5 wt%) and PLA nanocomposites with diffrent concentrations of SNCs-g-LA concentrations, (a) Storage modulus and (b) damping factor ($tan\delta$)

3.6. Conclusion

In this work, Lactic acid (LA) molecules were successfully grafted onto SNCs through a simple esterification reaction. After grafting SNCs with LA molecules, SNCs-g-LA nanoparticles incorporated into the PLA and then the PLA nanocomposites were fabricated with varying SNCs-g-LA contents. The results reveal that the interfacial adhesion between PLA and SNCs-g-LA nanoparticles increases considerably after chemical modification of SNCs. Besides that, results indicate that the SNCs-g-LA nanoparticles act as a nucleating agent and provide a better nucleation sites for crystal growth. This enhanced crystallization at low SNCs-g-LA nanoparticles concentration levels, while on the other hand, thwarted crystallization at higher concentrations. The 5 wt% of SNCs-g-LA nanoparticles loading increased the degree of crystallinity (15.7%) and decreased the T_{cc} (108.8℃) significantly. In addition, 5 wt% of SNCs-g-LA nanoparticles loading showed a sharp crystallization peak upon cooling. Furthermore the E' in glassy state decreased with a 5 wt% of SNCs-g-LA nanoparticles loading to 1.75 GPa, which is lower than that of neat PLA and all other PLA nanocomposites. This means that the 5 wt% of SNCs-g-LA nanoparticles can act as a plasticizer in glassy state. However, the highest concentration of SNCs-g-LA nanoparticles (30 wt%) acts as a reinforcing agent.

Chapter 4

4. Phase Transition and Crystallization Behaviour of grafted Starch Nanocrystals/PLA Nanocomposites

Somayeh Sharafi Zamir[1], Abdellah Ajji[2], Mathieu Robert[1] and Said Elkoun[1*,]

[1]Center for Innovation in Technological and Eco-design (CITE), University of Sherbrooke, 730 Rue Bernard, Granby, Qc, J2J 0H6, Canada.
[2]Chemical Engineering Department, Polytechnique Montreal, Montreal, Qc, H3C 3A7, Canada.

4.1. Résumé

L'Acide polylactique (PLA) est un bioplastique principalement utilisé, produit à partir de matériaux biosourcés renouvelables dans le monde. Le PLA a deux structures cristallines différentes, à savoir α et α' à l'état fondu. Cependant, la forme α (hautement ordonné cristallin) du PLA a montré une amélioration significative de la barrière et des propriétés mécaniques pour les applications d'emballages alimentaires. Dans ce cadre, des nanocristaux d'amidon greffés d'acide lactique (SNCs-g-LA) ont été renforcés avec du PLA à différentes concentrations par un procédé de coulée. De plus, les nanocomposites de PLA ont été caractérisés par diffusion de rayons X à grand angle (WAXS) et calorimétrie à balayage différentiel (DSC) pour comprendre le comportement de la transition de phase et de la cristallisation à différentes températures de cristallisation isotherme (T_c =80-130 ℃). Les résultats indiquent qu'à un faible contenu en charge, la température de transition de phase était diminuée par rapport au PLA pur. Finalement, ce comportement promeut le degré de transition cristalline pour donner l'α-PLA hautement ordonné cristallin. En outre, la cristallisation à mi-temps ($t_{1/2}$) des composites de PLA a été calculée par l'équation d'Avrami. ($t_{1/2}$) de PLA a diminué en diminuant la concentration de nanoparticules de SNCs-g-LA. ($t_{1/2}$) de PLA était minimale en ajoutant 5% en poids de nanoparticules de SNCs-g-LA et diminuait à partir de 10,4 min. à 3,9 min. Le taux de croissance de la morphologie de sphérulite dans les composites de PLA a été observé en utilisant une microscopie optique et les résultats ont montré une amélioration significative de la structure cristalline des nanocomposites de PLA par rapport à PLA pur.

Mot clé: transition de phase, Cristallisation, Acide polylactique (PLA), Nanocomposites et Greffage, Nanocristaux d'amidon.

4.2. Abstract

In this paper, the effect of starch nanocrystals grafted lactic acid (SNCs-g-LA) nanoparticles on the crystal structures (α′and α), crystallization mechanism and crystallization behaviour of PLA were studied. For this purpose, different concentrations of SNCs-g-LA (3, 5 and 7 wt%) were added into the PLA in order to obtain PLA/SNCs-g-LA nanocomposites. It was found that, the formation of **α**-structure in PLA nanocomposites is more likely than **α′**-structure and the rate of α′-to-α crystalline phase transition in a melt-recrystallization process of PLA nanocomposites was higher than neat PLA. This phenomenon is more prominent in PLA nanocomposite with 5 wt% SNCs-g-LA nanoparticles. Moreover, spherulite growth rate observations revealed that PLA spherulites of α −structure were accelerated by the presence of SNCs-g-LA nanoparticles. The spherulite growth rate where just α −structure was formed showed that the size of spherulite was minimum in PLA/SNCs-g-LA (5 wt%) nanocomposite compared to the other PLA nanocomposites. Furthermore, the half-time of crystallization ($t_{1/2}$) of PLA decreases by addition of SNCs-g-LA nanoparticles. Interestingly, the $t_{1/2}$ of PLA was decreased nearly 4-fold by adding 5 wt% SNCs-g-LA nanoparticles.

Keyword: Phase transition, Crystallization, Poly lactic acid (PLA), Nanocomposites and Grafting, starch nanocrystals.

4.3. Introduction

Development of bio-based and biodegradable polymers is an important step towards replacement of traditional synthetic plastics materials with natural resources [1]. Among the different bio-based polymers, Poly (lactic acid) (PLA) has been a subject of many previous investigations due to its biodegradability and various applications in different domains such as medical, food packaging film and automotive industry [1,5,92,151]. In 2016, about 14% of the total food packaging materials was manufactured by using PLA [6]. This figure is likely to be double by 2026 [6]. PLA has high impact and tensile strength, good optical and physical properties compared to the most common type of petroleum-based polymers such as Polystyrene (PS) and Polyethylene terephthalate (PET) [152,153]. However, PLA has some shortcomings such as slow rate of crystallisation and poor gas barrier properties that do not fulfill all the prerequisites of the food packaging industry [83,155]. Hence, many researchers are working towards finding more efficient ways to enhance the PLA crystallization kinetics and to increase its degree of crystallinity and gas barrier properties at the same time. Two well-documented approaches to increasing the crystallinity of PLA have been reported in the past, a) by controlling of configurational isomers of PLA which is consisting of different ratios of enantiomeric L-and D-lactic acid units [156] and molecular weight [157] and b) by adding nucleating agents [158], plasticizer [159] and/or both nucleating agents and plasticizer together [160] in practical processing conditions.

Adding nucleating agents is an effective way to speed up the rate of crystallization through a reduction of surface free energy barrier for nucleation. Therefore, they are applied to accelerate the nucleation rate and the growth of spherulites that will result in to decrease the processing time [161–168]. In addition, the amount, size and surface morphology of nucleating agents can determine not only the rate of crystallinity but also the size and morphology of spherulites of semicrystalline polymers [161–168]. Besides, adding nucleating agents can improve other properties such as thermal resistance, impact strength, transparency and gas barrier properties of polymer materials [161–168]. The nucleating agents are also used to control the crystalline structures of polymorphic polymers such as PLA. PLA exhibits two different crystalline structures namely $\boldsymbol{\alpha}$ and $\boldsymbol{\alpha'}$. The α structure of PLA is highly ordered crystalline structure compared to $\boldsymbol{\alpha'}$ structure of PLA (a slightly altered crystal structure) [171-172]. It has been shown that, this changes in crystal structure of $\boldsymbol{\alpha'}$ and $\boldsymbol{\alpha}$ structure can effect on the gas permeability and mechanical

properties of PLA [171-172]. It was shown that $\boldsymbol{\alpha}-$ structure due to the more packed crystal structure has lower water vapor and oxygen permeability than $\boldsymbol{\alpha'}-$ structure, which is very important for food packaging applications [170]. This compact arrangement also effect on the mechanical properties such as young modulus and elongation at break [83]. However, only limited nucleating agents have been developed for PLA to control crystalline structures and to enhance the kinetics of crystallization of PLA at the same time including; graphene nanosheet (GNSs) [170], dibenzylidene-D-sorbitol (DBS) [171] and uracil [172]. Li et al., demonstrated that the presence of graphene nanosheet (GNSs) resulted in more α' −structure in PLLA nanocomposite than $\alpha-$ structure [170]. They also showed that the phase transition temperature of PLLA/GNSs shifted to higher temperature compared to neat PLLA. In addition, Lai et al., investigated the effect of 1-4 wt% of dibenzylidene-D-sorbitol (DBS) on thermal and crystalline behaviour of PLLA [171]. They found that the ordered and stable form ($\alpha-$form) is favored in PLLA/DBS nanocomposites and phase transition temperature shifted to lower temperature as more DBS content was added. Nevertheless, most of these nucleating agents are not bio-resourceable and biodegradable therefore, the composition of them with PLA are not desirable in utilization of final product. Therefore, there is an increasing interest in bio-based and natural nanofillers such as cellulose nano whiskers, chitosan nano particles and starch nano crystals that can allows making 100% bio-based and biodegradable polymer nanocomposites [173-174].

Among different bio-based nano size nucleating agents, starch nanocrystals (SNCs) have attracted widespread attention due to high availability, renewability and biodegradability than most of the nucleating agents tested [173,174]. SNCs are the crystalline phase of native starch granules that are mainly produced by acid hydrolysis of amorphous phase of native starch [32, 33]. SNCs have also a large surface area and higher reactivity compared to native starch [32-33]. In addition, it has been demonstrated that, the incorporation of SNCs in PLA matrix has several other secondary benefits such as higher mechanical strength, better mechanical behaviour and lower gas permeability [72]. Therefore, SNCs can be a versatile and multipurpose nucleating agent for PLA based materials. However, poor interfacial adhesion and chemical affinity between hydrophilic SNCs and hydrophobic PLA are major disadvantages of PLA/SNCs nanocomposite. Moreover, the lack of adhesion between the SNCs and PLA leads to the formation of strongly bonded SNCs aggregates during the nanocomposite preparation, thus many studies had been conducted to improve the interface adhesion between the SNCs and PLA. Generally, the surface of SNCs can

be modified either a) via physical interactions or adsorption of small molecules or oligomers onto SNCs surface or b) through chemical approach to achieve covalent bonds between SNCs and the grafting agent. It has been proposed that the introduction of modified SNCs into the PLA matrix can effect on the permeability and mechanical properties of PLA more than native starch [72]. For example, Xiong et al., showed that in the presence of epoxidized soy-bean (ESO) the impact strength and elongation at break of the PLA/starch blends improved up to 42 kJ/m^2 and 140%, respectively [46]. However, only a few studies have been investigated the potential of SNCs as a nucleating agent for PLA [176]. To best of our knowledge, there have been no reported study on the effect of grafted SNCs on the trans-crystallization of PLA. In addition, the effect of SNCs on the crystalline structures and crystallization behaviour of PLA were not fully understood. The aim of this work is to determine the effect of SNCs-g-LA nanoparticles on the formation of different polymorphic crystal structures and on the kinetic of crystallization of PLA. In this regard, LA molecules grafted onto the surfaces of SNCs through simple esterification reaction based on the protocol which is developed in the previous work [39]. Then, the effect of SNCs-g-LA nanoparticles content on the crystallization kinetic parameters and crystallization behaviour including nucleation and spherulitic growth rate of PLA were investigated by Differential Scanning Calorimetry (DSC), Wide Angle X-ray Diffraction (WAXD) and Polarized Optical Microscopy (POM). In addition, the effect of SNCs-g-LA nanoparticles content on the on the crystalline structures ($\alpha'$and α) and solid-state transition (from α' to α) were studied by DSC and WAXD.

4.4. Experimental

4.4.1. Materials

Semi-crystalline commercial grade PLA (4032D) pellets, were purchased from Nature Works LLC (Minnesota, USA) and has 2% of D-lactide units. The average molecular weight (M_w) and polydispersity index (M_w/M_n) of PLA pellets was about 109 kg/mol and 1.57 respectively. Corn starch and LA were purchased from Sigma-Aldrich, Canada.

4.4.2. Extraction of Starch Nanocrystals (SNCs)

Starch nanocrystals (SNCs) were prepared by acid hydrolysis of corn starch according to previously reported method [174]. Briefly, 147g of raw corn starch were dispersed into 500 mL of 3.16 M aqueous sulfuric acid (H_2SO_4). The suspension was then kept under 400 rpm

mechanical stirring at 40 ℃ for 5 days. Subsequently, the resulting solution was washed in distilled water at 11 ℃ by successive centrifugation (Centrifuge 6K-15C, Sigma) at 10,000 rpm until a neutral pH was obtained. Finally, the suspension was freeze-dried using a Heto Power Dry PL6000 apparatus from Thermo Scientific. After freeze-drying, few drops of chloroform were added to the SNCs powder to avoid the bacterial activity and then SNCs were kept at ~4℃.

4.4.3. Chemical Modification of SNCs

Surface modification of SNCs by lactic acid (LA) was carried through simple esterification reaction based on the protocol which is described in our last work [174]. Briefly, SNCs (30 g) was first dispersed into 100 ml of Tetrahydrofuran (THF). Then LA monomers were added slowly to the reaction mixture. The resulting suspension was heated up to 60 ℃ and kept for 30 mins under argon atmosphere. During the evaporation of THF, 150 ml toluene was slowly added to the reaction mixture and the mixture was heated to 85 ℃ for 24 hrs. The resulted reaction mixture was centrifuged to remove the toluene. After the resulting reaction mixture was washed with THF and ethyl acetate and, the final product was dried under vacuum at 45 ℃.

4.4.4. Preparation of PLA/SNCs-g-LA Nanocomposites

The PLA/SNCs-g-LA nanocomposites were prepared by the solvent casting process. Firstly, both PLA and SNCs-g-LA nanoparticles were dried in a vacuum oven at 45 ℃ for 24 hrs. Subsequently, 0.12, 0.20 and 0.28 g of SNCs-g-LA nanoparticles and 3.88, 3.80 and 3.72 g of PLA were dissolved in the 40 ml of dichloromethane as a solvent respectively. Then, the mixture was stirred for 24 hr. to obtain a desired solution. The solution of PLA/SNCs-g-LA nanocomposite was cast by pouring the 40 mL of the solution onto glass Petri dishes (internal diameter 60 mm) and dried at room temperature for two days. Finally, the prepared films were vacuum dried overnight in order to remove the dichloromethane solvent.

4.4.5. Characterization

4.4.5.1. Differential Scanning Calorimetry (DSC)

The isothermal crystallization behaviour of neat PLA and PLA/SNCs-g-LA nanocomposites were studied by a Differential Scanning Calorimetry (DSC), Q2000, TA instrument equipped with nitrogen cooling system. Prior to the measurements, the temperature and heat flow were calibrated using Indium as a standard material. Samples of 5-10 mg were sealed in a closed aluminum pan.

Afterward, samples were heated from room temperature to 200 ℃ at 10 ℃/min and then kept at this temperature for 5 min to erase thermal history. Then samples were quenched to the selected crystallization temperatures ($T_c = 80 - 130$ ℃) and held for 2 hr. to obtain the isothermal crystallization curve. After isothermal crystallization, the samples were heated to 200 ℃ at 10 ℃/min to determine the melting behaviour after crystallization process.

4.4.5.2. Wide Angle X-ray Diffraction (WAXD)

The crystalline structures of neat PLA and PLA/SNCs-g-LA nanocomposites were analyzed after isothermal crystallization at the different crystallization temperatures (T_c) by Wide Angle X-ray Diffraction (WAXD), D-8, Bruker. The samples were exposed to an X-ray beam with the X-ray generators running at 40 kV and 40 mA. The copper $K\alpha$ radiation (k = 1.542 Å) was selected, and the scanning was carried out at 0.03°/s in the angular region (2θ) of 5–40°.

4.4.5.3. Polarized Optical Microscopy (POM)

The crystalline growth rate of neat PLA and PLA nanocomposites were investigated by means of Polarized Optical Microscopy (POM), Nicon 249171, and the hot-stage (Mettler Toledo FP82HT). Samples were prepared by cutting small pieces from prepared films. Then the sample was placed between two microscopy slides and pressed gently to form a thin film (~20−50 μm). Then, heated up to 200 ℃ and hold for 3 min before starting the crystallization. After that, the sample was quenched to different isothermal crystallization temperature (T_c = 80-135 ℃) and kept for one hour. The hot stage is calibrated using melting point standard to ±0.2 ℃ accuracy prior to any of samples. The crystalline morphology of the samples was recorded using the CCD camera.

4.4.5.4. Small Angle X-ray Scattering (SAXS)

Small Angle X-ray Scattering (SAXS) patterns were collected with a Bruker SAXS Nanostar system, equipped with a Microfocus Copper Anode at 45 kV / 0.65 mA, MONTAL OPTICS and a VANTEC 2000 2D detector. The distance from the detector to the sample were calibrated with a Silver Behenate standard prior the measurements. The scattering intensities were integrated from 0.1° to 2.8°. Collection exposure times were 500 seconds.

4.4.5.5. Oxygen Permeability (OP)

Oxygen Transmission Rate (OTR) of samples were measured according to the ASTM standard D3985 using Mocon Oxtran 2/21 Oxygen Permeability Tester. The OTR measurements were carried out at 23℃ on circular having an area 50 cm^2 at 0% relative humidity using oxygen high purity gas (>99.99%). The samples were conditinated in diffusion cell by purging nitrogen gas (>99.99% purity) for a minimum of 24 hr., under equilibrium humidity. During test, pure oxygen at pressure 0.5 bar and rate of 20 ml/min was introduced into the upper half of the sample chamber while nitrogen gas was injected into the lower half of the chamber. The test was performed for at least 4h so as to reach steady state. The OP was calculated from OTR values as follows:

$$OP = \frac{OTR \times l}{\Delta p} \qquad (5\text{-}1)$$

Where l is the thickness, Δp is difference in partial pressure of oxygen through the sample.

4.5. Results and Discussion

4.5.1. Effect of SNCs-g-LA Nanoparticles on the Crystalline Structures of PLA

In order to investigate the effect of SNCs-g-LA nanoparticles on the crystalline structures (α and α') and phase transition temperature (T_{trans}) of neat PLA and PLA nanocomposites WAXS analysis was performed after crystallization at different T_c. Figure 4.1 shows the WAXS patterns of isothermally crystallized neat PLA and PLA/SNCs-g-LA nanocomposites respectively as a function of T_c. As can be seen, distinct diffraction peaks were observed for isothermally crystallized neat PLA samples at different isothermal crystallization temperatures (80-130℃). At T_c above 120 ℃ five diffraction peaks are observed at $2\theta = 12.1^{\circ}, 14.5^{\circ}, 16.5^{\circ}, 19.5^{\circ}$ and 22.5°. These diffraction peaks can be attributed to the (103)/(004), (010), (110)/(200), (203)/(113) and (210) planes respectively [200-201-238]. The presence of these diffraction peaks displays the characteristics of $\alpha -$ structure in PLA [200-201]. In contrast, at T_c below 110 ℃ the diffraction peaks for (103)/(004), (010) and (210) planes disappeared. Moreover, the 2θ value of diffraction peaks for 16.5° and 19.5° which is related to the (110)/(200), (203)/(113) planes shifted to smaller 2θ value (evidenced in the enlarged WAXD patterns). These

changes in the WAXD profile of neat PLA indicate that the obtained crystal structure at lower T_c (below 110 ℃) is different than the one at higher T_c (above 120 ℃)[200-201-238]. It can be seen, three small peaks appear at $2\theta = 12.1^{\circ}. 14.5\ and\ 22.5$ as well as a shifting in 2θ values for the two main peaks ($2\theta = 16.5^{\circ}$and 19.5°) to lower 2θ values. These are related to the presence of the both α and α′ crystal formation [200-201-238]. However, the 2θ value of two main peaks at $16.5^{\circ}$and 19.5°shifted to lower values when T_c is decreased to 80 ℃. Which means that by further decreasing T_c only α′ −structure is present [83,154,155]. Similarly, Figure 4b, c and d show the WAXD patterns of PLA/SNCs-g-LA nanocomposites with 3, 5 and 7 wt% of SNCs-g-LA nanoparticles respectively. In contrast to neat PLA, in the WAXD profile of PLA nanocomposites, the 2θ value of diffraction peaks for (110)/(200) and (203)/(113) planes shifted to higher value with increasing T_c to 130 ℃ (Figure 4b). In addition, with increasing T_c the diffraction peaks for (103)/(004), (010) and (210) planes enhances further compared to neat PLA. These changes in 2θ value which can indicate that the transformation of α′ − to α − structure is started at lower temperature in PLA nanocomposites (100 ℃) compared to neat PLA (110 ℃). Interestingly, the PLA/SNCs-g-LA (5 w%) exhibits the lowest of α′ to α crystal structure transition temperature. This means that the addition of 5 wt% SNCs-g-LA nanoparticles were more favor to form the most stable crystal structure (α structure) in PLA matrix. Therefore, it can be concluded that the addition of SNCs-g-LA nanoparticles act as a α − nucleating agent at lower isothermal crystallization temperature. Figure 4.2 shows the variation of lattice spacing of the (110)/(200) diffractions ($d_{110/200}$) derived from the Braggs law for neat PLA and PLA nanocomposites. As can be seen, the $d_{110/200}$ values of α′-structure of all PLA nanocomposites are obviously smaller than the $d_{110/200}$ values of α′-structure of neat PLA. Intestingly, the $d_{110/200}$ for PLA nanocomposites is lower than neat PLA, however the $d_{110/200}$ decreses further with the decresaeing SNCs-g-LA concentrations. This means that SNCs-g-LA affect on the $d_{110/200}$ value of both $\alpha' -$ and $\alpha -$ crysytal structures. This phenomena were more predominant in PLA/SNCs-g-LA (5 wt%) nanocomposites and reduse the phase transition from $\boldsymbol{\alpha'}$- to $\boldsymbol{\alpha}$ crystal structure by 10 ℃.

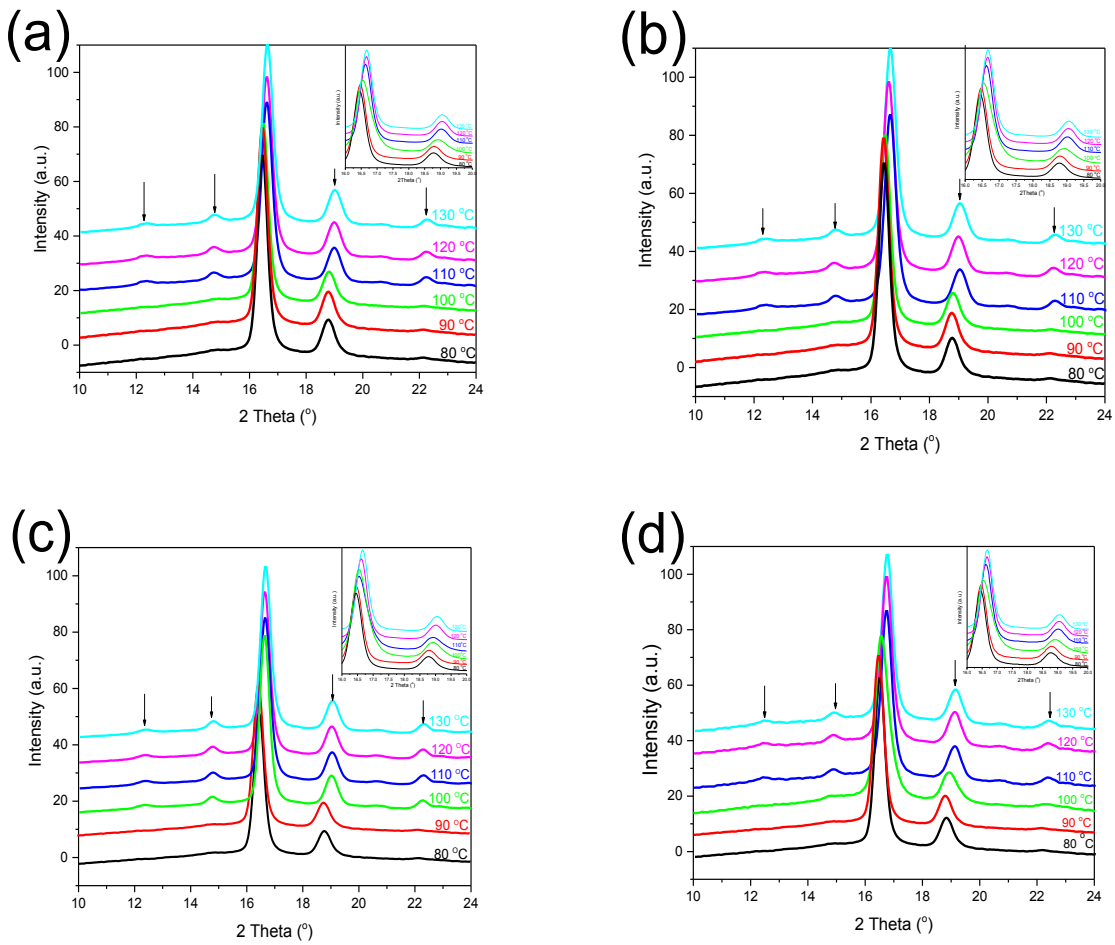

Figure 4.1. WAXD patterns of a) neat PLA, b) PLA/SNCs-g-LA (3 wt%), c) PLA/SNCs-g-LA (5 wt%) and d) PLA/SNCs-g-LA (7 wt%) nanocompsoites.

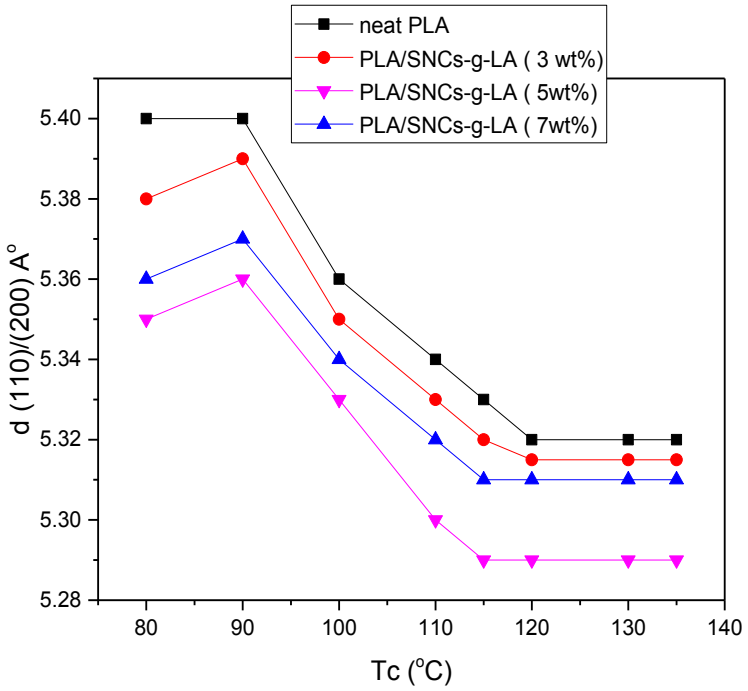

Figure 4.2. Lattice spacing of the (110)/(200) diffractions ($d_{110/200}$) of neat PLA and PLA nanocompsoites with different concentrations.

4.5.2. Effect of SNCs-g-LA Nanoparticles on the Melting behaviour of PLA

It has been shown, there is a close relation between crystal stucture and melting behavior of semicrystalline polymers [24,31]. Therefore, the melting behavior of both PLA and PLA nanocomposites were investigated by using DSC analysis. Figure 4.3 shows the melting behavior of isothermally crystallized neat PLA and PLA/SNCs-g-LA nanocomposites. Three different melting behaviors were observed in the DSC thermograms irrespective of the sample: i) single endothermic melting peak above 120 ℃ , ii) two endothermic melting peaks appear between 100 ℃ −120 ℃ and iii) below 100 ℃ an additional small exothermic peak appears. As mentioned previously in WAXD results, neat PLA shows an $\alpha' -$ to $\alpha -$ phase transition between 110 ℃ $< T_c <$120 ℃. Furthermore, for neat PLA sample crystallized below 110 ℃ or above 130 ℃ only $\alpha' -$structure or $\alpha -$structure were observed respectively. Since $\alpha' -$structure is less ordered than $\alpha -$structure, thus the melting point of $\alpha' -$ is lower than $\alpha -$structure of PLA. As can be seen in Figure 4.3a, the neat PLA isothermally crystallized at 80 ℃, exhibites lower melting temperature (166.0 ℃) as compared to that one which is isothermally crystallized at 130 ℃ (168.8 ℃). This means that the crystal structure of a sample which is isothermally

crystallized at 80 ℃ and 130 ℃ are different. Acording to the melt recrystallization theory [17,85], although the higher melting temperature (168.8 ℃) can be solely attributed to the melting of $\alpha-$crystal structure, the lower melting temperature (166.0 ℃) cannot be uniquely attributed to the $\alpha'-$crystal structure. The exothermic peak which appears before the main endothermic peak of the PLA sample is isothermally crystallized at 80 ℃ can be related to the transition of $\alpha'-$ to $\alpha-$ crystal structure [30-33]. For neat PLA samples crystallized above 100 ℃ those two endothermic peaks are well seprated and a double melting peak is observed in the DSC thermograms (Figure 4.3a). However, at T_c above 120 ℃ the two melting peaks collapse and a single sharp endothermic peak is observed. In the case of PLA nanocomposites, a very similar T_c dependent DSC thermograms were observed. However, a small exothermic peak is starts to dispeare at a lower T_c (90 ℃) compared to neat PLA (100 ℃). Furthermore, the melting temperature of PLA nanocomposite samples isothermally crystallized at 130 ℃ is higher than neat PLA sample isothermally crystallized at same T_c. Indicating that the more $\alpha-$ crystal structure is present in PLA nanocompsoite compared to neat PLA especially when 5 wt% of SNCs-g-LA is added into the PLA matrix. This indicates that the addition of SNCs-g-LA nanoparticles encourages the PLA molecular chains to arrange themselves in more ordered form ($\boldsymbol{\alpha}-$ crystal structure) at lower temperature. This results are consitent with WAXD results as well.

The equilibrium melting temperature (T_m^0) of the both neat and PLA nanocomposites were calculated by Hoffman-Weeks theory [177]. The T_m^0 was measured based on the extrapolation of the linear part of the T_m above 110 ℃, since at above this temperature, the measures T_m is related to the melting point of the α phase. Figure 4.4 shows the T_m^0 as a function of T_c of neat PLA and PLA nanocomposites containing 3, 5 and 7 wt% SNCs-g-LA nanoparticles. Neat PLA exhibits T_m^0 at 187.5℃ which is consistent with reported value by Zhang et al, as well [154]. For PLA nanocomposites, regradless of the different amount of grafted SNCs present, the T_m^0 is smaller than neat PLA. Indeed, the addition of 3, 5 and 7 wt% of SNCs-g-LA nanoparticles decreases the T_m^0 to 185.4, 183.7 and 185.9 ℃ respectively. This decrease indicates the formation of the more ordered crystalline structure at lower under cooling. As can be seen, PLA/SNCs-g-LA (5 wt%) showed the minimum of the T_m^0 value while, increasing the concentrtion of grafted SNCs were unfavoralbe and induced higher T_m^0. Therfore the phase transition temperature is lowered with decreasing SNCs-g-LA nanoparticles concentrations till 5 wt%.

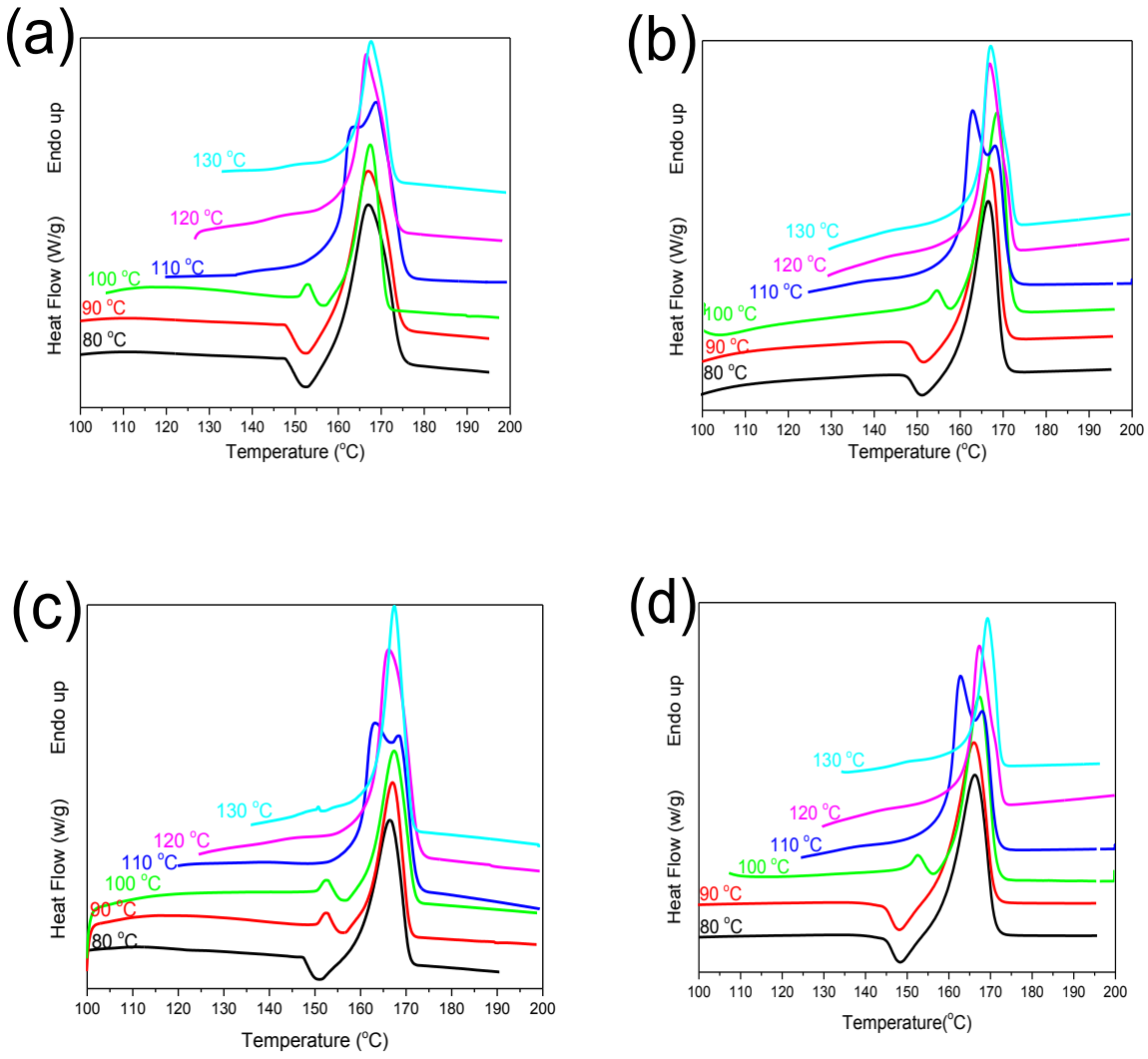

Figure 4.3. Melting behaviour of a) neat PLA, b) PLA/SNCs-g-LA (3 wt%), c) PLA/SNCs-g-LA (5 wt%) and d) PLA/SNCs-g-LA (7 wt%) nanocompsoites.

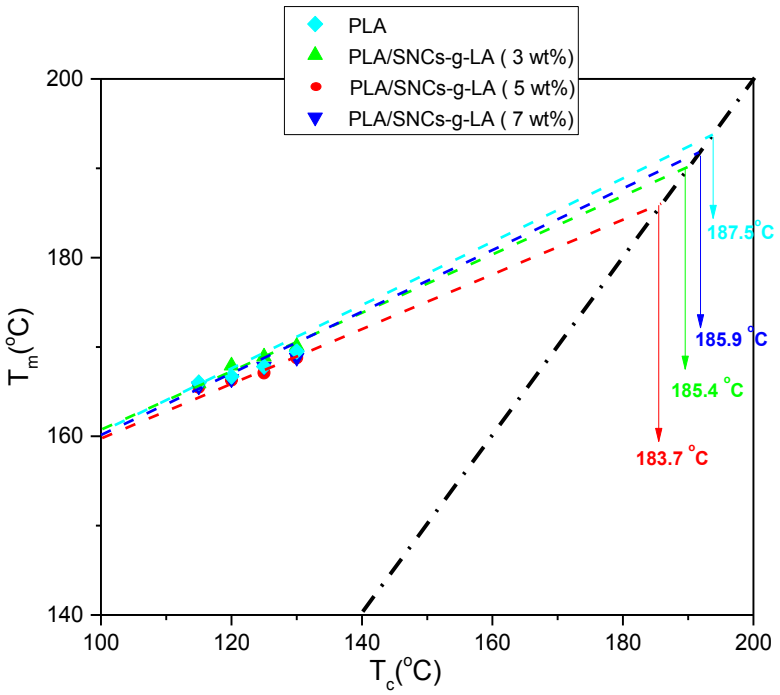

Figure 4.4. Equlibrium melting point of neat PLA and PLA nanocompsoites with different concentrations.

4.5.3. Effect of SNCs-g-LA Nanoparticles on the Nucleation Rate of PLA

The influence of SNCs-g-LA nanoparticles concentrations (3, 5 and 7 wt%) on the overall isothermal crystallization behaviour and kinetics of PLA were studied by using DSC. Then, the relative degree of crystallinity (X(t)) was quantified theoretically by Avrami equation at different T_c using the equation (4-1) [178]:

$$X(t) = 1 - \exp(-kt^n) \qquad (4\text{-}1)$$

where k is the crystallization rate constant and n is the Avrami exponent which depends on the nucleation and growth mechanisms of crystallites.

The Avrami parameters (n and k) can be calculated using the following relation:

$$\ln(-\ln[1 - X(t)]) = n\ln(t) + \ln k \qquad (4\text{-}2)$$

Figure 4.5 shows the plot of $\ln[-\ln(1 - X(t)]$ versus $\ln(t)$ of neat and PLA nanocomposites at different T_c. In all samples, Avrami plots were found to be linear demonstrating the accuracy of the procedure as shown in Figure 4.5a – d. The slope of line in the plot of $\ln[-\ln(1 - X(t)]$

versus $\ln(t)$ gives the value of n. Subsequently the crystallization rate constant (k) can be obtained using the following equation;

$$k = \frac{\ln 2}{t_{1/2}^{n}} \qquad (4\text{-}3)$$

The $t_{1/2}$ is the half-time of crystallization which is defined as a time when X(t) is reaches to the half of the crystallization. Table 4.1 summarizes the effect of SNCs-g-LA concentrations on the n and k values and $t_{1/2}$. Avrami exponent (n) for polymer crystallization is usually between 2 and 4 and it is related that the type of nucleation and geometry of crystal growth [179]. As shown in Table 4.1 the value of n decreases and then increases with increasing T_c or with decreasing undercooling. The depletion of n value is related to the heterogeneous mechanism of nucleating agents (i.e. dimensional of nuclei) and spherulite parameters (i.e. spherulite morphology). Furthermore, in both neat PLA and PLA nanocomposites the value of k decreases with increasing T_c revealing that the nucleation is controlled the crystallization process because of the low undercoolings degree present in the current experimental temperatures. However, the crystallization constant k of PLA nanocomposites is greater than that of the neat PLA at the equivalent temperature, which indicates that the crystallization rate of PLA nanocomposites is higher than that of the neat PLA. The value of k increases with increasing SNCs-g-LA nanoparticles concentrations till 5 wt%.

As can be seen from Table 4.1, the crystallization constant k increases with increasing SNCs-g-LA nanoparticles concentrations till 5 wt%. By addition, 5 wt% SNCs-g-LA nanoparticles into PLA induced more crystallization rate. Nevertheless, the value of k decreases with increasing grafted SNCs concentrations (7 wt%), indicating that the addition of more grafted SNCs causes hindrance in the diffusion of the PLA molecules, which results in lower crystallization rate. Further, the effectiveness of SNCs-g-LA nanoparticles as a heterogeneous nucleating agent is studied by looking at the evolution of the $t_{1/2}$ as a function of T_c (see Figure 4.6). The $t_{1/2}$ for both neat PLA and PLA nanocomposites starts to decrease with increasing T_c, but increases further increases of T_c. The minimum $t_{1/2}$ for neat PLA was found to be 10.4 min. at T_c=110 ℃. However, the addition of SNCs-g-LA nanoparticles decreases the minimum $t_{1/2}$ in all PLA nanocomposites irrespective of the concentrations level. This implies that adding SNCs-g-LA nanoparticles not only significantly increases the kinetics of crystallization of PLA but also it decreases the

minimum T_c. Furthermore, T_c of the all PLA nanoparticles are lower than neat PLA. Interestingly, between different concentrations, 5 wt% of SNCs-g-LA nanoparticles content was found to have the lowest value of $t_{1/2}$ (3.9 min.). Further, increasing the amount of SNCs-g-LA nanoparticles again increases the $t_{1/2}$ due to the decrees in the barrier free energy.

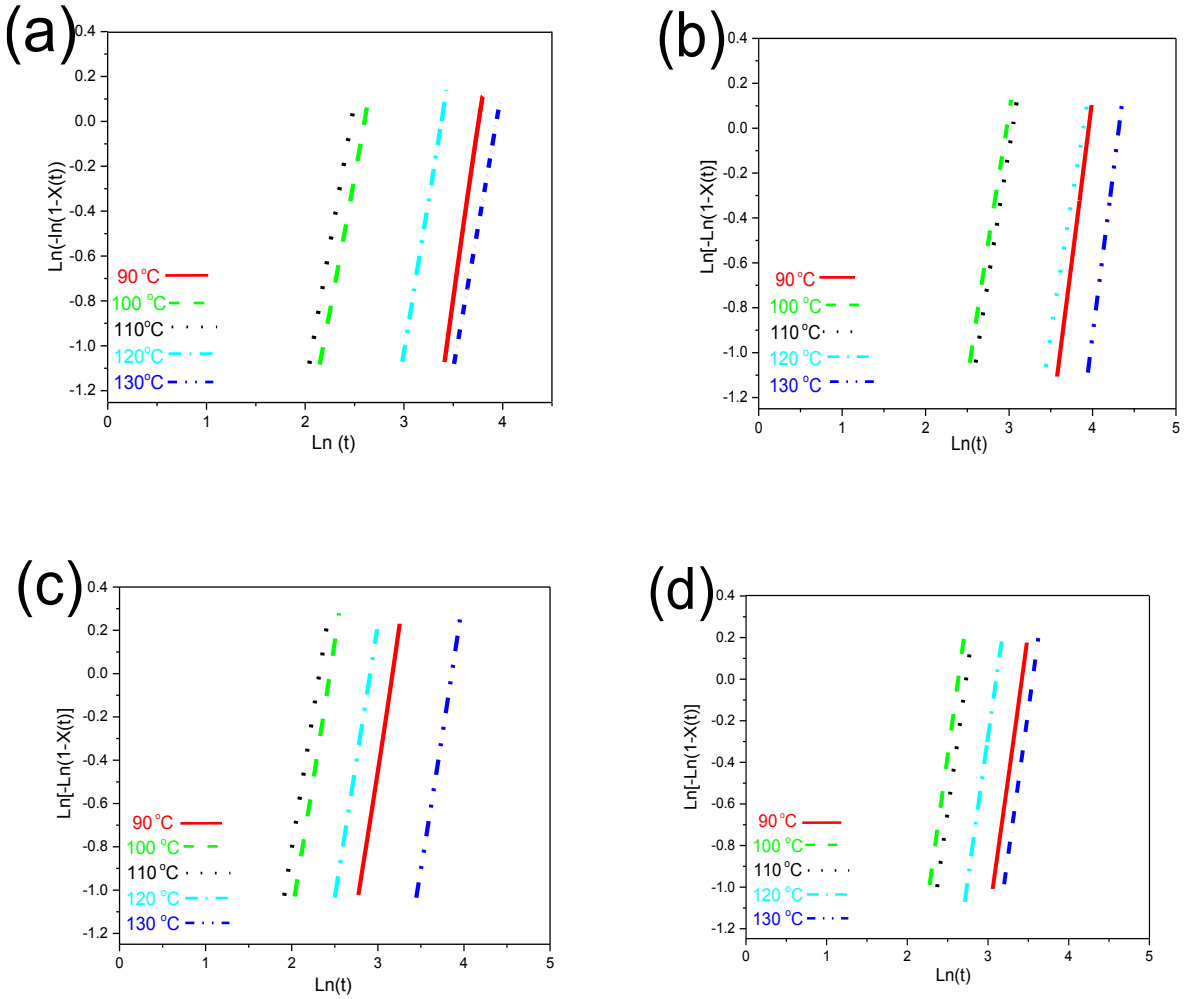

Figure 4.5. Plot of ln $[-\ln(1 - X(t)]$ versus lnt of neat PLA and PLA nanocompsoites with different concentrations. a) neat PLA, b) PLA/SNCs-g-LA (3 wt%), c) PLA/SNCs-g-LA (5 wt%) and d) PLA/SNCs-g-LA (7 wt%).

Table 4.1. The effect of SNCs-g-LA nanoparticles concentrations on n and k values of PLA.

Samples	PLA			PLA/SNCs-g-LA (3 wt%)			PLA/SNCs-g-LA (5 wt%)			PLA/SNCs-g-LA (7 wt%)		
T_C (°C)	$t_{1/2}$ (min)	n	k (min^{-n})	$t_{1/2}$ (min)	n	k (min^{-n})	$t_{1/2}$ (min)	n	k (min^{-n})	$t_{1/2}$ (min)	n	k (min^{-n})
80	43.0	3.3	$2.8208*10^{-5}$	23.0	2.5	$2.7321*10^{-4}$	12.0	2.5	$1.3895*10^{-3}$	15.0	3.0	$2.0537*10^{-4}$
90	22.0	3.3	$2.5753*10^{-5}$	18.6	2.5	$4.6456*10^{-4}$	10.8	2.4	$2.2940*10^{-3}$	12.5	3.0	$3.5489*10^{-4}$
100	13.5	2.5	$1.0351*10^{-3}$	10.3	2.6	$1.6123*10^{-3}$	3.9	2.4	0.02283	5.5	2.8	$5.858*10^{-3}$
110	10.4	2.5	$1.9872*10^{-3}$	12.0	2.6	$1.0838*10^{-4}$	5.1	2.4	0.01388	7.2	2.8	$2.283*10^{-3}$
120	16.6	2.8	$2.6578*10^{-4}$	15.0	2.8	$3.5299*10^{-4}$	7.8	2.6	$7.7484*10^{-3}$	12.7	2.8	$5.6256*10^{-4}$
130	23.0	2.7	$1.4593*10^{-4}$	21.1	2.7	$1.8418*10^{-4}$	14.5	2.6	$6.9964*10^{-4}$	19.9	3.0	$8.7956*10^{-5}$

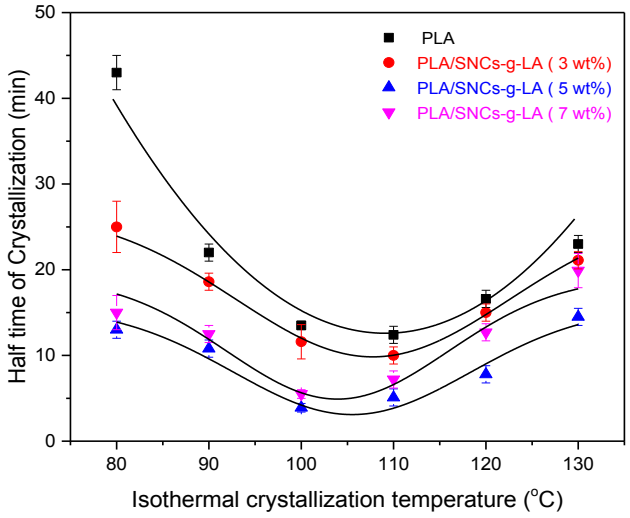

Figure 4.6. The $\mathbf{t_{1/2}}$ of neat PLA and PLA/SNCs-g-LA nanocomposites with different concentrations of SNCs-g-LA nanoparticles.

4.5.4. The Effect of SNCs-g-LA Nanoparticles on the Spherulite growth rate of PLA

In order to understand the effect of adding SNCs-g-LA nanoparticles on spherulite growth rate (SGR) of PLA nanocomposites the SGR of PLA/SNCs-g-LA nanocomposites were obtained at variousT_c. Figure 4.7 shows the SGR as a function of T_c for neat PLA and PLA nanocomposites. The spherulitic growth rate curves show Gaussian-shaped temperature dependence, as reported by many other research groups [171-174].As can be seen from, the SGR of all PLA nanocomposites increases with increasing T_c and after reaching a maximum value, SGR decreases with further increasing T_c. The maximum SGR for both PLA and PLA nanocomposites are around 120 °C.

However, the SGR of PLA enhances by adding of SNCs-g-LA nanoparticles. For example, the SGR at 120 °C for the neat PLA and PLA nanocomposites with 3, 5 and 7 wt% of SNCs-g-LA nanoparticles are measured to be 5.14, 5.40, 5.81 and 5.60 μm respectively. Interestingly, it can be seen that the SGR of PLA in the presence of 5 wt% of SNCs-g-LA nanoparticle are the highest among all PLA nanocomposites samples at each crystallization temperature. This phenomenon can be explained by the competition between thermodynamic and kinetic of crystallization for grafted SNCs as a nucleating agent at lower (3 wt%) and higher (7 wt%) concentrations of SNCs-g-LA nanoparticles. In addition, the spherulite morphology of neat PLA and PLA nanocomposites was observed at T_c=130 ℃ where just α −crystal structure was obtained and the results were shown in Figure 4.8. The results show that regardless of the sample, the presence of the spherulites with maltase extinction crosses can be seen for both neat PLA and PLA nanocomposites. However, the number and size of spherulites in neat PLA were lower and bigger respectively compared to the SNCs-g-LA reinforced PLA nanocomposites. This is also attributed to the nucleation effect of SNCs-g-LA nanoparticles. Interestingly, the maximum number of spherulites was found in the presence of 5 wt% of SNCs-g-LA nanoparticle. This is due to the higher α −nucleation density in PLA/SNCs-g-LA (5 wt%) nanocomposites which is confirmed by kinetic of crystallization as well. It is worth to note that the morphology of spherulite is less compact and more irregular in neat PLA. However, a compact and regular structure were observed for PLA/SNCs-g-LA nanocomposites.

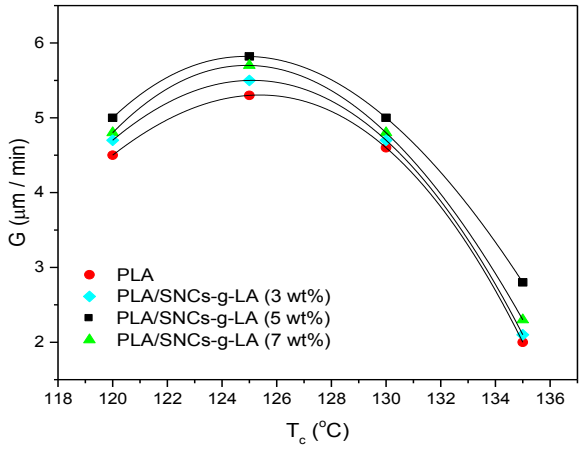

Figure 4.7. Spherulite growth rate of neat PLA and PLA nanocomposites measured at different isothermal crystallization temperatures.

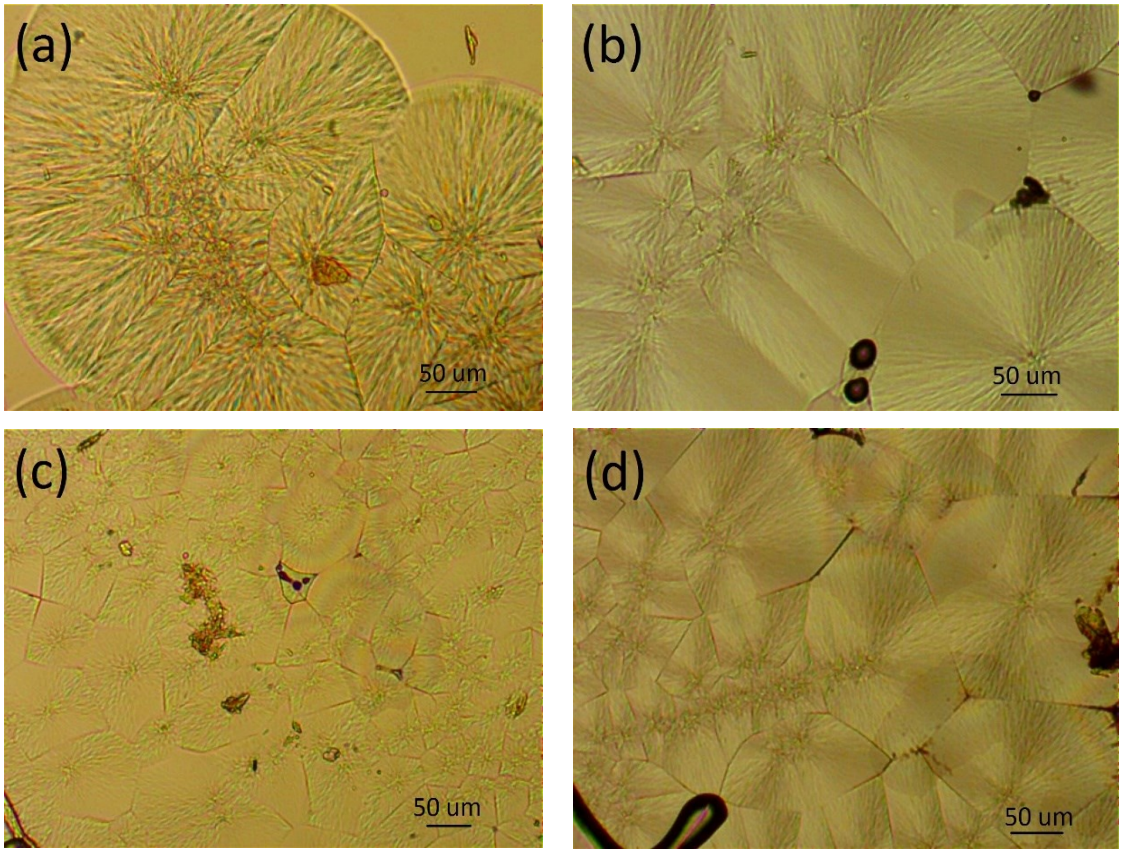

Figure 4.8. Spherulite morphology of a) neat PLA, b) PLA/SNCs-g-LA (3 wt%), c) PLA/SNCs-g-LA (5wt%) and d) PLA/SNCs-g-LA (7 wt%) nanocomposites which measured at T_c=130 ℃.

4.5.5. Effect of SNCs-g-LA on the long period (L_{ac}) of PLA

The SAXS technique is performed to observe the effect of the SNCs-g-LA nanoparticles on the long period (L_{ac}) of PLA. Figure 4.10, shows the Lorentz-corrected SAXS profiles of PLA and PLA nanocomposites that are crystallized at diffrent T_c. The SAXS patterns of the all samples depend on the T_c and by increasing T_c a noticeable change in the SAXS correlation function plots was observed. At $T_c = 80$ ℃, neither a peak no shoulder is observed in the SAXS scattering pattern of PLA. However, when T_c is increased from 80 ℃ to 100 ℃, the SAXS peak began to visible and its intensity increased with further increasing of T_c. At T_c=100 ℃, a small shoulder appears at the maximum scattering vector (q_{max}) equal to 0.31 nm is corresponding to the L_{ac} of 18.5 nm. By increasing temperature from 100 up to 130 ℃, q_{max} value is shifted to lower value (0.28 nm) and it becomes sharper. This is indicating that the L_{ac} increases by increasing the T_c and higher and lower thickness distribution of the lamellae in crystalline and amorphous regions can be observed respectively. The higher L_{ac} at 130 ℃ is probably due to the formation of secondary

lamellae in the amorphous region which decreases the size of the amorphous region. The PLA nanocomposite shows similar SAXS profile. However, the SAXS peak is started to appear at lower T_c and the position of scattering peak at all T_c is shifted to smaller q_{max} compare to neat PLA. This decrement is clearly affected on the morphological parameters of PLA nanocomposites. For example, adding 5 wt % SNCs-g-LA nanoparticles resulted in the maximum increment in the L_{ac}. Furthermore, at 90 ℃, a small peak is observed in the SAXS scattering pattern of PLA/SNCs-g-LA (5 wt%) nanocomposites which is shifted to higher q_{max} (0.32 nm) by increasing T_c. These results reveal that the grafted SNCs nanoparticles promote crystalline chain packing of PLA, which leads to an increase in crystal layer thickness and a decrease in the amorphous layer thickness.

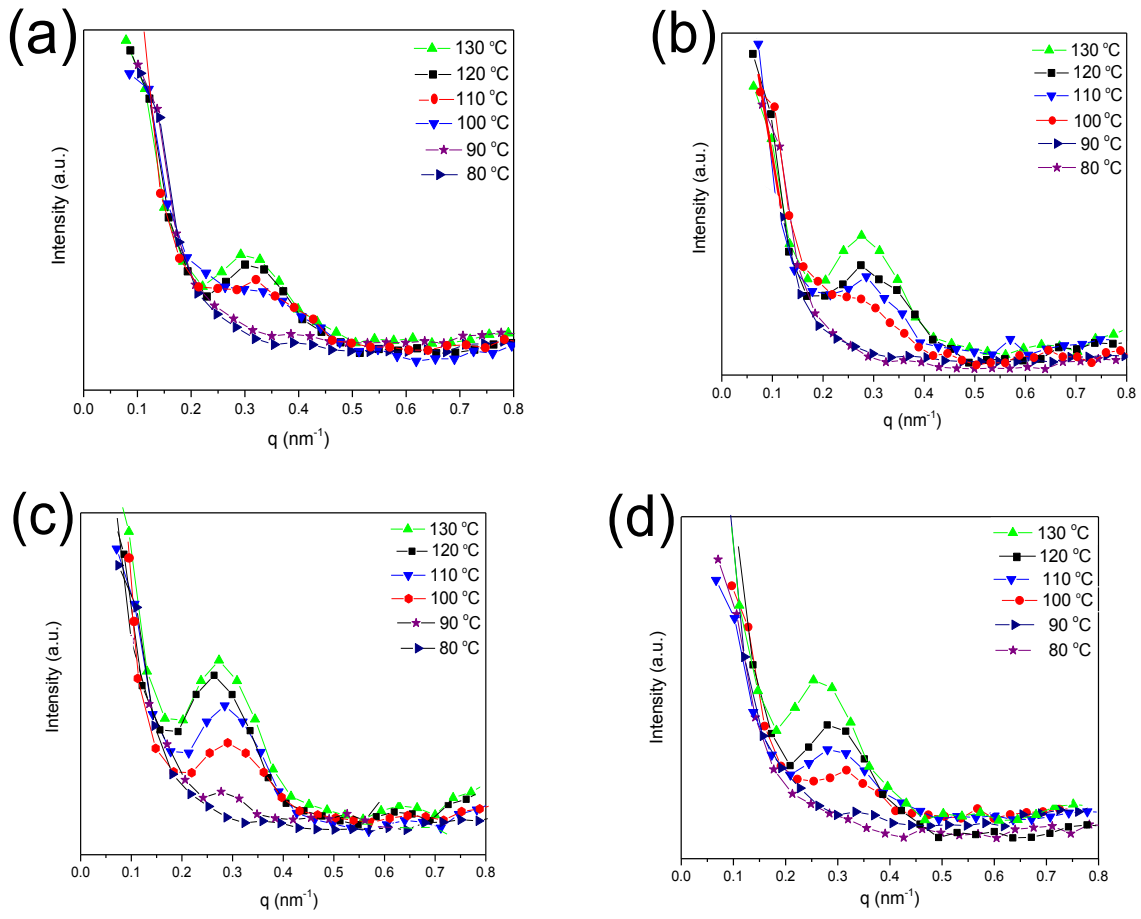

Figure 4.10. SAXS patterns of a) neat PLA, b) PLA/SNCs-g-LA (3 wt%), c) PLA/SNCs-g-LA (5 wt%) and d) PLA/SNCs-g-LA (7 wt%) nanocomposite which is crystallized at different isothermal crystallization temperatures.

4.5.6. Effect of SNCs-g-LA on the Oxygen Permeability of PLA

The oxygen permeability (OP) of neat PLA and PLA nanocomposites as a function of the degree of crystallinity (X_c) are plotted in Figure 4.11. As can be seen, the OP of neat PLA has the maximum value ($16\ cm^3mm/m^2.day$) at low X_c where just α' structure is appeared. Subsequently, it rapidly decreases with very small variation in X_c, based on the WAXS analysis this range of crystallinity corresponded to the both α and α' −crystalline structures. Finally, the OP has the minimum value ($4.9\times\ cm^3mm/m^2.day$) where just α-structure is observed. Although, the OP curves of all PLA nanocomposite samples follow the same trend as OP curve of neat PLA, it is considerably lower than that of neat PLA. For example OP of PLA/SNCs-g-LA (5 wt%) is around 12.2 and 2.1 $cm^3mm/m^2.day$ at low (26%) and high (42%) X_c respectively. Up until now, many research articles studied the effect of crystallinity and thermal history on the gas permeability of PLA. However, there are a handful articles that investigated the effect of varying crystalline conformations on the gas permeability of PLA. Generally, an increase in crystal fraction limits gas permeability of semicrystalline polymers. For PLA, the trend is largely non-linear (Figure 4.11), therefore the influence of the crystallinity on barrier properties of PLA needs to be discussed in the presence of the two different crystalline conformations. The chain packing in α' and α crystal structures is quite dissimilar. As the α' structure has slightly larger lattice dimensions than α crystal structure [83] therefore, the molecular packing within the unit cell of α' structure PLA is looser and more disordered than α counterpart. It has also shown that, the conformational disorder of $\boldsymbol{\alpha}$ structure can reduce the rigid amorphous fraction (RAF) [169]. Therefore, the reduction of gas permeability in PLA nanocomposites could be due to the enhancement of the crystallinity and more specifically in enhancement of transition from $\boldsymbol{\alpha'}$ to $\boldsymbol{\alpha}$ crystalline structure.

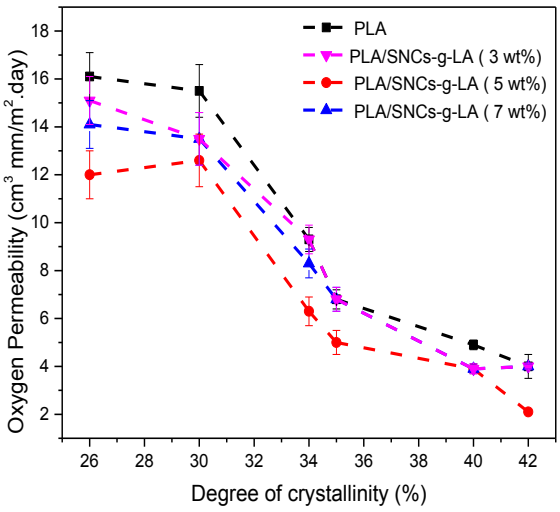

Figure 4.11. Oxygen permeability (OP) of PLA and PLA nanocomposite crystallized at different crystallization temperatures.

4.6. Conclusion

In this work, the isothermal crystallization kinetic of the neat PLA and PLA/SNCs-g-LA nanocomposites have been performed by DSC at different T_c. It was found that the crystallization characteristics of PLA nanocomposites are affected by incorporation of SNCs-g-LA nanocomposites. The Avrami crystallization exponent (n) of PLA nanocomposites is slightly larger than that of neat PLA at the same T_c and it was in the range of 2.5-3. It is implied that gradual growth of two-dimensional morphology to a three-dimensional morphology with a combination of thermal and athermal nucleation process. The addition of SNCs-g-LA nanoparticles can significantly results in an increase in the crystallization kinetic constant (*k),* suggesting that SNCs-g-LA nanoparticles can act as an effective nucleating agent and can accelerate the crystallization rate of PLA in the composites. After introducing a small amount of SNCs-g-LA nanoparticles, the crystallization half-time values ($t_{1/2}$) are all lower than those of neat PLA. Interestingly, the $t_{1/2}$ of PLA was minimum by adding 5 wt% SNCs-g-LA nanoparticles and it decreases from 10.4 min. to 3.9 min. Therefore, it can be concluded that, 5 wt% of SNCs-g-LA is an optimum concentration and it can help both thermodynamically and kinetically to enhance kinetic of crystallization of PLA. In addition, it is found that, the formation of **α**-crystal structure in PLA nanocomposites is more likely than **α′**-crystal structure and the rate of phase transition in PLA nanocomposites was

higher than neat PLA. This phenomenon is more prominent in PLA nanocomposites with 5 wt% SNCs-g-LA nanoparticles. WAXD and DSC results confirmed that by adding 5 wt% of SNCs-g-LA nanoparticles, the T_{trans} shifts to lower temperature and the degree of α-crystal shifts to higher value compared to other SNCs-g-LA nanoparticles concentrations. Moreover, POM observations revealed that PLA spherulites of α −phase were accelerated by the presence of SNCs-g-LA nanoparticles. The SGR where just α −crystal was formed showed that the number of spherulite was higher in PLA/SNCs-g-LA (5 wt%) nanocomposite compared to neat PLA. Therefore, it can be concluded that, 5 wt% SNCs-g-LA is an optimum concentration and it can help both thermodynamically and kinetically to form more α −crystalline structure of PLA.

Chapter 5

5. Crystallinity and Gas Permeability of Poly (lactic acid)/Starch Nanocrystals (SNCs) Nanocomposites

Somayeh Sharafi Zamir[1], Abdellah Ajji[2], Mathieu Robert[1] and Said Elkoun[1*]

[1]Center for Innovation in Technological and Ecodesign (CITE), University of Sherbrooke, Sherbrooke, Qc, J1K 2R1, Canada.
[2]Chemical Engineering Department, Montreal, Polytechnique Montreal, Qc, H3C 3A7, Canada.

5.1. Résumé

Le présent travail cherche à déterminer l'impact de la variation en pourcentage en poids (wt%) de nanoparticules de SNCs-g-LA sur la perméabilité à l'oxygène et à la vapeur d'eau du PLA en raison de la modification de l'épaisseur et de la cristallinité de ses cristaux. Pour cet objectif, les nanoparticules de SNCs-g-LA avec variant wt% (3, 5 et 7 wt%) ont été mélangées avec du PLA par coulée au solvant, puis le comportement de fusion, la structure cristalline, la morphologie de la sphérulite et le long espacement des nanocomposites de PLA ont été déterminés en fonction du temps de cristallisation. Il a été constaté que l'ajout d'un contenu en SNCs-g-LA avec 5% en poids de PLA permettait d'induire une structure cristalline typique à un temps de cristallisation plus court. En outre, il a été constaté que les SNCs-g-LA augmentaient de manière significative la cristallisation de la structure α et l'épaisseur des cristaux de PLA. Cependant, lorsque les concentrations de SNCs-g-LA étaient modifiées, ex : (3 ou 7% en poids), le temps de cristallisation augmentait en raison de la thermodynamique de la barrière de cristallisation. Enfin, la perméabilité à l'oxygène et à la vapeur d'eau du film nanocomposite PLA / SNCs-g-LA (5% en poids) s'est avérée réduite d'environ 70% et 50% respectivement par rapport au film PLA pur.

Mots clés: Acide polylactique, nanocristaux d'amidon greffés (SNCs-g-LA), cristallisation, structures cristallines, les relations de microstructure et de perméabilité.

5.2. Abstract

The present work seeks to determine the impact of varying weight percentage (wt%) of SNCs-g-LA nanoparticles on the oxygen and water vapour permeability of PLA due to modification in its crystal thickness and crystallinity. For this purpose the SNCs-g-LA nanoparticles with varying wt% (3, 5 and 7 wt%) were blended with PLA using solvent casting and subsequently the melting behaviour, crystal structures, spherulite morphologies and long spacing period of PLA nanocomposites were determined as a function of crystallization time. It was found that addition of SNCs-g-LA content with 5 wt% in PLA helped inducing a typical crystalline structure at lower crystallization time. Also, it was found that SNCs-g-LA significantly increases the $\boldsymbol{\alpha}$ −structure crystallization and crystals thickness of PLA. However, when SNCs-g-LA concentrations was altered i.e. (3 or 7 wt%) the crystallization time was found to increase due to thermodynamics of crystallization barrier. Finally, the oxygen and water vapour permeability of PLA/SNCs-g-LA (5 wt%) nanocomposite film were found to be reduced by ∼70% and 50% respectively with respect to neat PLA film.

Keywords: Poly (lactic acid), grafted starch nanocrystals (SNCs-g-LA), crystallization, crystal structures, microstructure and permeability relations

5.3. Introduction

Polymeric materials are widely used in the food packaging industry, because they are lightweight, have relatively low-cost of production and possess good mechanical properties essential for the food packaging industry [180]. However, most of the polymeric materials currently being used are petroleum based polymer, which are inherently non-biodegradable and non-renewable. Therefore, there is a major thrust towards the development of a biodegradable and renewable alternative. Among the various alternative biodegradable polymers known, PLA is the most promising one due to its wide availability, ease in processing, suitable mechanical properties and high transparency [5,181]. However, currently the use of PLA in the food packaging industry is limited due to high gas permeability specifically that of oxygen and water vapour and lower degree of crystallinity [79,182]. This is because of the fact that pure PLA has a higher amorphous to crystalline phase, which is known to facilitate gas permeability [79,182]. Therefore, current research efforts are focused on improving the gas barrier properties by increasing the crystalline phase and thus reducing the amorphous phase present within the PLA [79,182]. In addition of crystalline to amorphous phase ratio, the crystalline structures within the crystalline phase also play an important role in the gas permeability of PLA [183]. The crystalline structures and their morphology within crystalline phase of PLA can be modified by subjecting it to thermal treatment [30,83]. Specifically two different crystal structures of PLA are observed namely α and $\alpha' -$ structure depending upon the thermal crystallization temperature [30, 171,184–186]. The existence of PLA as polymorphic material depending upon thermal treatment is a manifestation of the link between thermal and physical properties as mentioned above. The $\alpha -$ structure of PLA is known to exist above the crystallization melting temperature which is happens above 120 ℃ [30,171,184–186]. Whereas, the $\alpha' -$ structure is observed below the 100 ℃ crystallization melting temperature [30,171,184–186]. A mixture of both crystalline structures (α and α') where found between100-120℃ [30,171,184–186]. The phase transition from α' to $\alpha -$ structure involves rearrangement of the molecular chains to more packing order within a unit cell [30,171,184–186].

It has been shown that the gas barrier properties of semicrystalline polymers such as PLA are highly affected by crystalline polymorphisms. For example, Cooca et al., have shown the effect of crystalline polymorphisms on the barrier and mechanical properties of compression-molded PLLA [83]. They showed that the presence of highly ordered $\alpha -$ crystal structure enhances water vapour barrier properties and decreases the Young's modulus of PLLA, compared to samples

containing just the $\alpha' -$ crystal structure. Guinalt et al., showed that higher concentration of $\alpha -$ crystal structure within PLA improves its oxygen permeability [187].

Direskens et al., have shown correlation between the inner crystal structures and morphological parameters of compression-molded PDLLA (4:96%) and variation in oxygen transport characteristics (permeability, diffusivity and solubility) [82]. They found that the $\alpha -$ crystal structure has a strong impact on gas permeability, in particular on the gas solubility.

Blending with nucleating agents is another way to engineer the crystal structures of PLA. Pan et al. reported that the crystal structure of PLLA is altered with the addition of poly (D, L-lactide) (PDLLA). They showed that the formation of the α-form crystals of PLLA is promoted and incorporation of PDLLA (50 wt%) decreases the phase transition temperature form α'- to α structure [185]. In another study Lai et al., blended 3:2,4- dibenzylidene-D-sorbitol (DBS) with PLLA and showed that the order and regular α-form of PLLA was favored as the DBS component was added. The formation of α- crystal at lower temperatures is facilitated due to the $\pi - \pi$ interaction between DBS and PLA molecules [171]. It was also shown by authors that PDLLA and DBS decreases the crystallization rate of PLLA and PDLLA and DBS can act as a nucleation agent.

Various kind of nanoparticles have been used as a nucleating agents for PLA-based materials. Specifically, the bio-resource nanoparticles has been shown as an efficient way to overcome the low degree of crystallinity of PLA [188–191]. Nanoparticles such as cellulose nano whiskers [134], chitosan nano particles [190] and starch nano crystals [189] can improve the degree of crystallinity of PLA. Among these nanoparticles mentioned Starch Nano Crystals (SNCs) has promising advantages such as a reasonably large reactive surface and strong reinforcing effect [189,189,192–194]. Furthermore, SNCs is known to modify the crystalline properties and thus can alter the gas permeability of PLA. The gas barrier properties of PLA nanocomposites strongly depends on the dispersion of SNCs within the PLA matrix, their inherent properties (i.e., surface area), as well as the interfacial adhesion between SNCs and the PLA matrix. For example, Yin et al., prepared a hydrophobic cross-linked starch nanocrystals (CSNs)/PLA nanocomposite [111]. They showed SNCs/PLA nanocomposite has a better water vapor barrier properties due to the higher degree of crystallinity which makes it difficult for the water molecule to penetrate through it. Muller et al., are also prepared a PLA/thermoplastic starch film by extrusion and thermo pressing method [112]. They showed that water vapor barrier properties of the PLA/thermoplastic starch blends were enhanced due to the decrease in the number of free hydroxyl groups present in

the cross-linked starch chains which then hindered the diffusion of water molecules through the film matrix. The effect of the starch on the oxygen permeability of the PLA was further studied by Battegazzore et al., whose prepared the of maize starch/PLA blend by using a co-rotating twin screw micro extruder [116]. They showed that it was difficult for the oxygen molecule to penetrate in Starch/PLA composites due to the formation of clusters of starch that modify the intermolecular forces between the chains of the polymer and decreases the free volume.

However, to best of our knowledge, no pervious study has used SNCs as a nucleating agent which hence would improve α crystal structure content and thereby improve the gas barrier properties (i.e. oxygen and water vapor permeability) of PLA. Therefore, a comprehensive analysis of SNCs content on the α crystal structure formation and their induced crystalline structure on the barrier performance of PLA is carry out in this work. In a previous study, we showed that the SNCs-g-LA has a considerable effect on the kinetic of crystallization of PLA and reduces the phase transition temperature from $\alpha'$of α crystal structure of PLA [195]. In this work, the effect of the different SNCs-g-LA nanoparticles loading on the crystalline evaluation of the α crystal structure and degree of crystallinity of PLA nanocomposites were carried out. Finally, the oxygen and water vapor permeability of PLA/SNCs-g-LA nanocomposites were evaluated. The obtained results are intended to help our understanding about effect of SNCs-g-LA and its induced crystalline structure on the barrier performance of polymer films.

5.4. Experimental

5.4.1. Materials

The waxy corn starch used in this study contained majorly amylopectin and only trace of the amylose. It was purchased from Sigma-Aldrich Co., Canada. In addition, semi-crystalline commercial grade PLA (4032 D) pellets with an L-lactide to D-lactide ratio of 98:2, were purchased from Nature Works LLC (Minnesota, USA). The average molecular weight ($\mathbf{M_w}$) and polydispersity index ($\mathbf{M_w/M_n}$) of PLA pellets was about e $\mathbf{109\ kg/mol}$ and $\mathbf{1.57}$ respectively.

5.4.2. Preparation of PLA/SNCs-g-LA Nanocomposite

In the previous work starch nanocrystals (SNCs) were chemically grafted with lactic acid (LA) and their properties and compatibility with PLA were studied comprehensively [195]. In this study we used the same protocol which developed in the previous study for fabrication of SNCs-g-LA nanoparticles [195]. Then, PLA/SNCs-g-LA nanocomposites contacting various SNCs-g-LA

loading (3-7 wt%) were prepared by casting process. Initially, PLA was dissolved in dichloromethane and then different concentrations of SNCs-g-LA was added into the PLA solution. The solution was then stirred in a hood at **70** ℃ for 24 hr. Finally, the prepared films were vacuum dried overnight in order to remove the traces of the dichloromethane solvent. For barrier measurement, the resultant nanocomposites were shaped into a diameter of 5 cm and a thickness of 100 $\boldsymbol{mm}$ films by compression molding at 200 ℃ with a pressure of 40 MPa after preheating for 5 min.

5.4.3. Characterization

5.4.3.1. Differential Scanning Calorimetry (DSC)

Differential Scanning Calorimetry (DSC) tests were performed using a TA instrument calorimeter (Q 2000) equipped with liquid nitrogen cooling system. Samples (5-10 mg) were heated from 25 to 200 ℃ with heating rate 5 ℃/min and held for 5 min to completely eliminate any possible crystallinity or residual stress in the samples. Then samples were quenched to $T_c = 130$ ℃ crystallization temperature and were allowed to crystallize for different crystallization time. Subsequently, the temperature was ramped back up to 200 ℃ with a heating rate of 10 ℃/min to probe the melting behaviour after re-crystallization. To investigate the effect of SNCs-g-LA on the degree of crystallinity (X_c) of resulting nanocomposites, cold crystallization enthalpy (ΔH_c), melting enthalpy (ΔH_m) and degree of crystallinity were determined from first heating scan.

5.4.3.2. Wide Angle X-ray Diffraction (WAXD)

Wide Angle X-ray Diffraction (WAXD) measurements were obtained by means of an X-ray diffractometer (D-8, Bruker) to detect the crystal structure of neat PLA and PLA nanocomposites after recrystallization at 130 ℃. Samples were exposed to an X-ray beam with the X-ray generators running at 40 kV and 40 mA. The copper $K\alpha$ radiation (k = 1.542 $A°$) was selected, and the scanning was carried out at $0.03°/s$ in the angular region (2θ) of 5–40°.

5.4.3.3. Small Angle X-ray Scattering (SAXS)

Small Angle X-ray Scattering (SAXS) patterns were collected with a Bruker SAXS Nanostar system, equipped with a Microfocus Copper Anode at 45 kV / 0.65 mA, MONTAL OPTICS and a VANTEC 2000 2D detector. The distance from the detector to the sample were calibrated with a Silver Behenate standard prior the measurements. The scattering intensities were integrated from 0.1° to 2.8°. Collection exposure times were 500 seconds.

5.4.3.4. Polarized Optical Microscopy (OPM)

The morphology of PLA spherulites were observed with a Polarized Optical Microscopy (Nicon 249171) in conjunction with the hot-stage (Mettler Toledo FP82HT) instrument. First, the samples were placed between two microscopy slides and pressed gently to form a thin film (~20−50 μm). Then, the specimens were heated up 200°C on the hot plate and held at that temperature for 3 min to erase the thermal history. After that, sample was quenched to T_c = 130 ℃ and held at that temperatures for 1 hrs. The hot stage is calibrated with a melting point standard to ±0.2 ℃ accuracy. Polarized light is utilized in order to observe the morphology of spherulite as well.

5.4.3.5. Scanning Electron Microscopy (SEM)

The Scanning Electron Microscopy (SEM) images were observed by an S-7500, SEM (Hitachi, Japan). All samples were cut in liquid nitrogen, coated with a thin layer of Pd-Au, using vapor deposit process before SEM characterization.

5.4.3.6. Oxygen Permeability (OP)

Oxygen Transmission Rate (OTR) of samples were measured according to the ASTM standard D3985 using Mocon Oxtran 2/21 Oxygen Permeability Tester. The OTR measurements were carried out at 23℃ on circular having an area 50 cm^2 at 0% relative humidity using oxygen high purity gas (>99.99%). The samples were conditinated in diffusion cell by purging nitrogen gas (>99.99% purity) for a minimum of 24 hr., under equilibrium humidity. During test, pure oxygen at pressure 0.5 bar and rate of 20 ml/min was introduced into the upper half of the sample chamber while nitrogen gas was injected into the lower half of the chamber. The test was performed for at least 4h so as to reach steady state. The OP was calculated from OTR values as follows:

$$OP = \frac{OTR \times l}{\Delta p} \qquad (5\text{-}1)$$

Where l is the thickness, Δp is difference in partial pressure of oxygen through the sample.

5.4.3.7. Water Vapor Permeability (WVP)

Water Vapor Transmission Rate (WVTR) of the samples were measured by a water vapor permeability test machine, PERMATRAN-W model 1 (Mocan USA) following ASTM standard E398-03. The relative humidity (RH) was set to 100% in the wet chamber and 5% in the dry chamber, yielding a driving force of 95% RH. The circular having an area of 50 cm^2 was tested in

the chamber at atmospheric pressure and at a temperature of 25 ℃. Tests were carried out until ten successive readings deviated less than 5% from the average value for each sample, which was then taken as the WVTR value. The obtained WVTR values were normalized by thickness (l) and difference in partial pressure of permeant across the sample (Δp) to calculate the WVP:

$$WVP = \frac{WVTR \times l}{\Delta p} \qquad (5\text{-}2)$$

Where l is the thickness, Δp is difference in partial water vapor pressure on the outside and inside of the test film.

5.5. Results and Discussion

5.5.1. Melting Behavior of PLA/SNCs-g-LA Nanocomposites

The effect of SNCs-g-LA content (3-7 wt%) on the melting behaviour of PLA was studied with the help of DSC measurements. Figure 5.1 shows the DSC thermograms of neat PLA and PLA/SNCs-g-LA nanocomposites which are crystallized at 130 ℃ for diffrent isothermal crystallization time (t_c). As shown in Figure 5.1a, there is no visible melting peak for neat PLA which was crystallized for less than 30 min. However, as crystallization time increases two endothermic melting peak were observed. All PLA nanocomposites also show a dual melting peak except PLA/SNCs-g-LA (5 wt%) nanocomposite. The phenomenon of the dual melting peak has been shown to occur based on the melting of less ordered crystals (i.e. α') formed in the cold crystallization period during heating and followed by simultaneous recrystallization and melting process of more ordered crystal structure (i.e. α) at higher temperature [30,184]. More importantly, between different PLA/SNCs-g-LA nanocomposite samples, the melting temperature of the PLA nanocomposite samples containing 5 wt% of SNCs-g-LA was found to increase considerably till 30 min., and after that it remains constant. This implies that 30 min period is long enough for PLA/ SNCs-g-LA (5 wt%) nanocomposite to arrange its molecular chains in more ordered way. In addition, the value of crystallinity (X_c) is measured based on the equation 1 and the results are listed in Table 5.1. As can be seen from Table 5.1, the X_c of the SNCs-g-LA nanoparticles enhances up to the 5 wt% and then decreases by any further increase in SNCs-g-LA content. This is can be due to the higher concentrations of nano fillers which can then suppress the molecular chain movement of the PLA and therefore decrease the degree of crystallinity. This results indicate

that the crystallization capacity of PLA is relatively poor, while the addition of SNCs-g-LA nanoparticles enhance the crystallization of PLA to varying degrees.

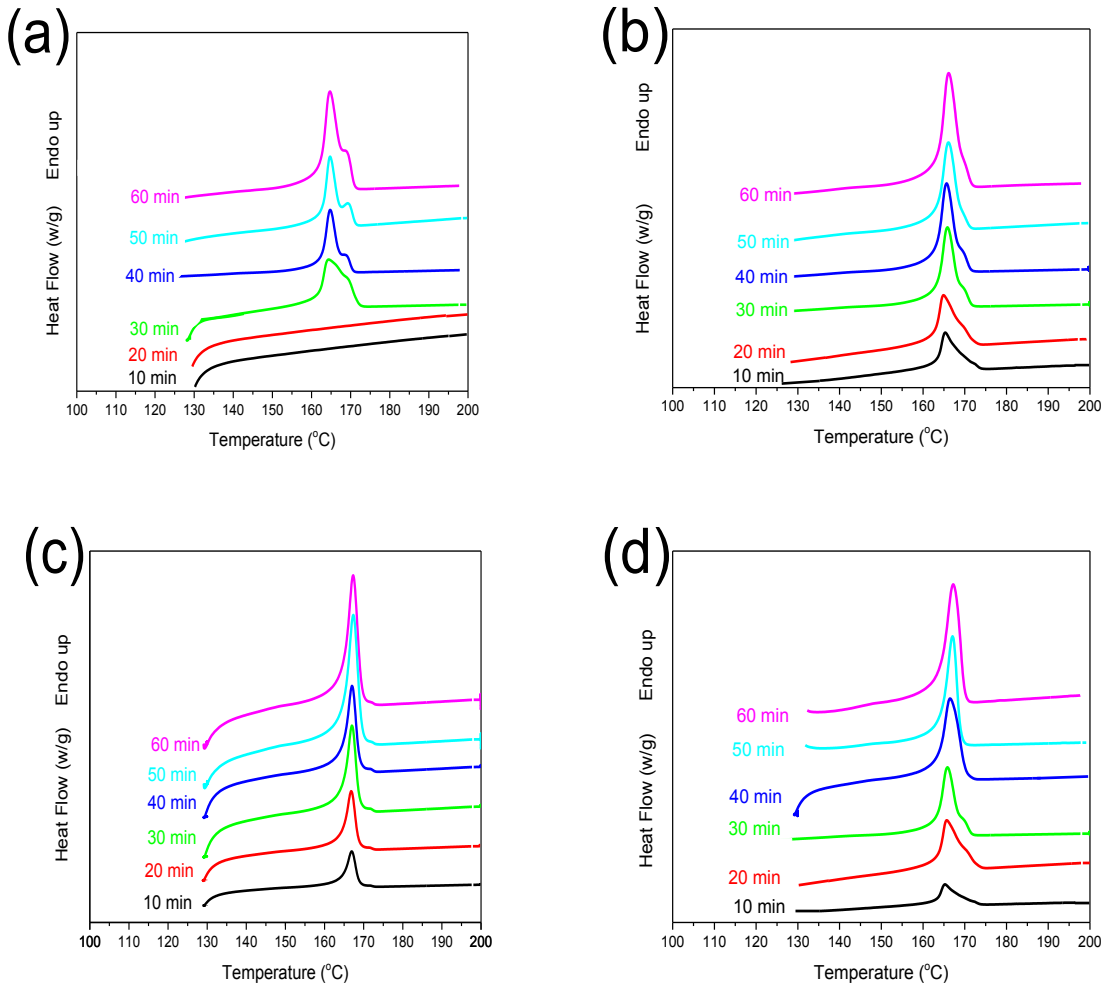

Figure 5.1. The melting behaviour of a) neat PLA, b) PLA/ SNCs-g-LA (3 wt%), c) PLA/ SNCs-g-LA (5wt%), b) PLA/ SNCs-g-LA (7 wt%), nanocomposites which are crystallized at different crystallization time at T_c=130°C.

Table 5.1. DSC and WAXS data of PLA and PLA/ SNCs-g-LA nanocomposite which are crystallized at 130℃ and at various crystallization time.

sample	PLA			PLA/ SNCs-g-LA (3 wt%)			PLA/ SNCs-g-LA (5 wt%)			PLA/ SNCs-g-LA (7 wt%)		
$\boldsymbol{time}$ ($\boldsymbol{min.}$)	T_{m2} (℃)	χ_{WAXS} (%)	χ_{DSC} (%)	T_{m2} (℃)	χ_{WAXS} (%)	χ_{DSC} (%)	T_{m2} (℃)	χ_{WAXS} (%)	χ_{DSC} (%)	T_{m2} (℃)	χ_{WAXS} (%)	χ_{DSC} (%)
10	-	-	-	165.6	-	1.00	166.1	-	4.20	166.5	-	1.20
20	-	-	-	165.8	-	10.3	167.4	24.9	23.3	167.6	-	13.4
30	167.3	-	10.7	168.7	21.9	15.0	168.9	37.5	37.0	167.7	33.9	17.0
40	168.3	-	12.5	168.9	22.7	25.5	169.2	38.9	38.0	168.1	34.7	27.5
50	167.4	-	15.7	168.3	35.5	32.1	169.0	39.0	38.9	168.5	36.5	31.1
60	167.7	35.2	17.1	169.5	36.3	33.4	169.1	41.8	41.1	168.6	37.8	32.4

5.2.2. Crystalline Structures of PLA/SNCs-g-LA Nanocomposites

To determine the effect of SNCs-g-LA content varying from 3 to 7 wt% on the crystalline structures and crystallinity of PLA nanocomposite, the WAXS measurements as a function of the crystallization time were carried out (Figure 5.2). As can be seen, a wide diffraction peak is observed in the case of neat PLA samples which are crystallized for less than 40 min.This is probably due to the fact that 40 min., is not enough for movement of the PLA molecular chain, therefore giving rise to a handful of short range ordered lamellae. When isothermal crystallization time increases beyond 40 min., two strong diffraction peaks appears at $2\theta = 16.5^{\circ}$ and 19.5° which are attributed to the (110)/(200) and (203)/(113) planes respectively. In addition, three small diffraction peaks at $2\theta = 12.1^{\circ}, 14.5^{\circ}$ and 22.5° were observed which were assigned to the (010), (110)/(200) and (015) planes respectively. These five diffraction peaks are characteristics of α crystal structure in neat PLA [186]. Although, all of these diffraction peaks appear in PLA/SNCs-g-LA nanocomposites, the crystallization time decreases considerably as SNCs-g-LA increasers up to 5 wt%. The decreasing of the crystallization time can be related to the nucleation ability of SNCs-g-LA that can promote formation of α −crystalline structure at lower SNCs-g-LA concentrations (5 wt%). Morover, WAXS measurement is also an effective way to determine the X_c (Table 5.1). It is worth mentioning that, the value of crystallinity obtained using WAXS analysis is a little higher than that of the value of crystallinity obtained via DSC analysis. The differences can be attributed to the differences in the measurement techniques. At crystallization time of 0 min, all samples were amorphous due to rapid isothermal crystallization rate (100 ℃/min.). After keeping the samples for 10 min at crystallization temperature of 130 ℃ only a tiny amount of crystals with X_c equal to 1% is obtained in all PLA/SNCs-g-LA

nanocomposites. However, at longer isothermal crystallization time of 20 min., PLA/SNCs-g-LA (5 wt%) exhibits a significant increase in X_c and is about 23.3% higher than that of neat PLA. This can be due to the presence of the highly crystalline SNCs-g-LA nanoparticles which act as an efficient nucleating agent at a relatively lower loading of SNCs-g-LA (5 wt%). Therefore, the crystallization rate of PLA is enhanced radically and more crystals are formed at the same time, when SNCs-g-LA were loaded at 5 wt%. In contrast, a relatively high concentration of SNCs-g-LA (7 wt%) in PLA restricts instead of promoting the formation of the PLA crystals and hence results in decreases the value of X_c to 13.4% . Finally, when PLA nanocomposites kept for 60 min., all samples are completely crystallized, whereas; this time is not enough for PLA crystallization. The X_c of all three PLA/SNCs-g-LA nanocomposites samples are varying in the range of 38.9-45.0 (Table 5.1). This is confirmed by DSC analysis as well.

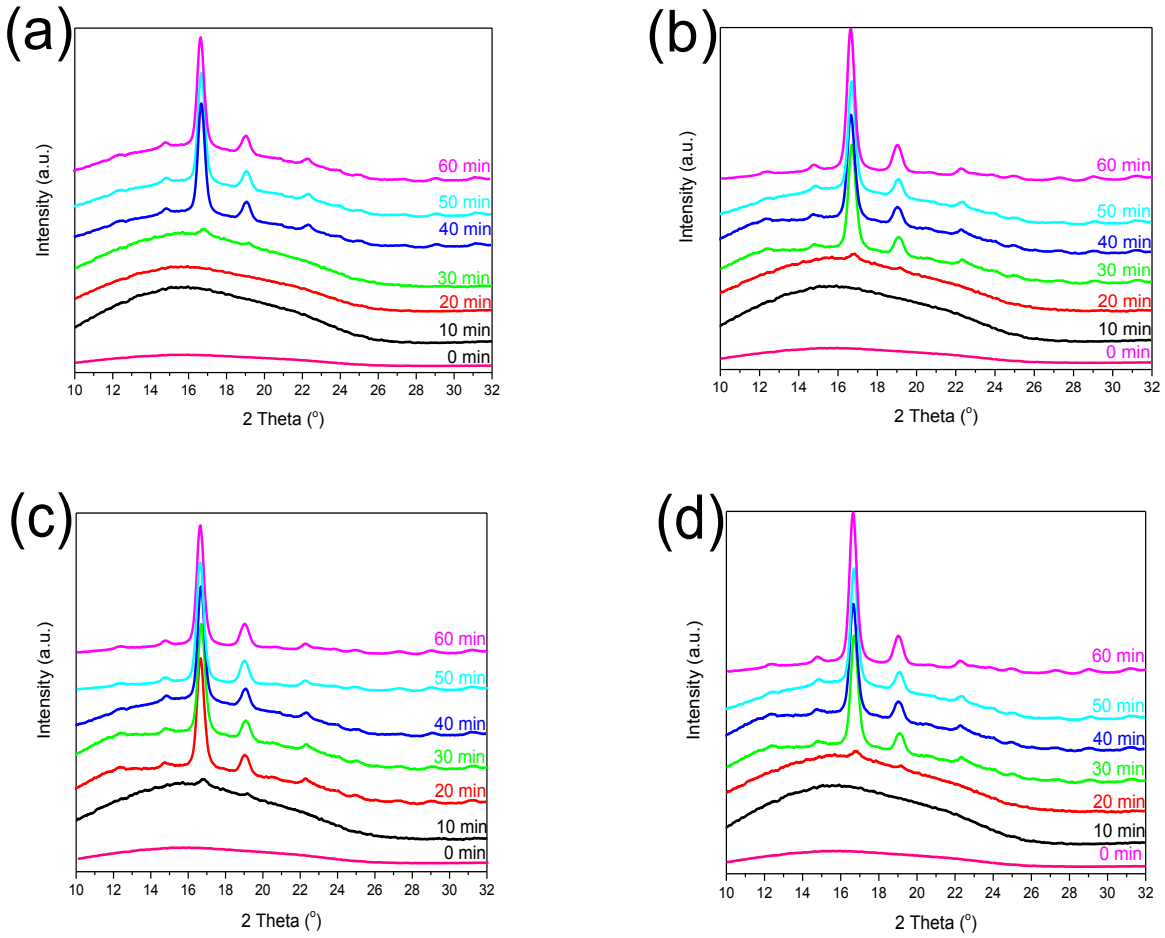

Figure 5.2. The WAXS analysis of a) neat PLA, b) PLA/SNCs-g-LA (3 wt%), c) PLA/SNCs-g-LA (5 wt%), b) PLA/SNCs-g-LA (7 wt%), nanocomposites which are crystallized at different crystallization time at T_c=130℃.

5.5.3. Long Period (L_{ac}) of PLA/SNCs-g-LA Nanocomposites

SAXS is an influential technique that is probing the morphological changes of semi-crystalline polymers such as PLA [19]. It can provide the morphological information, such as long period (L_{ac}), the crystal layer thickness (L_c) and the amorphous layer thickness ($L_a = L_{ac} - L_c$). In order to obtain the morphological parameters, a single-dimensional correlation function is applied. The single-dimensional correlation function can be derived from the inverse Fourier transform of the intensity distribution I (q) is written as follows;

$$\gamma(z) = \frac{\int_0^\infty qI^2(q)\cos(qz)dq}{\int_0^\infty I(q)q^2dq} \qquad (5\text{-}3)$$

where z is the location distance, I (q) is the scattering intensity and q is the module of scattering vector. The scattering vector (q) can be expressed as;

$$q = \left(\frac{4\pi}{\lambda}\right) sin\ \theta \qquad (5\text{-}4)$$

where λ is the wavelength of the X-ray source and 2θ is the scattering angle.

As can be seen from Figure 5.3a that even after 40 min of crystallization time, no scattering peak was observed in the SAXS scattering pattern of neat PLA. However, when crystallization time equal to 50 min., a scattering peak appears at the scattering vector (q) of 0.30 nm which is corresponds to long spacing of approximately 20.9 nm. However, after crystallization for 60 min., the PLA lamellae are slightly thickened and L_{ac} increases to 21.7 nm. Although, similar SAXS profile is observed in the case of PLA/SNCs-g-LA nanocomposites, the scattering peaks start to get visible at a lower crystallization time. For instance, PLA/SNCs-g-LA (5 wt%) which was crystallized for 20 min, shows a very weak scattering peak with q about 0.33 nm, corresponding to the long spacing of ~ 19.9 nm, while; this scatting peak is absent in the both PLA/SNCs-g-LA (3 wt%) and PLA/SNCs-g-LA (7 wt%) nanocomposite samples which are crystallized for same crystallization time. The absence of the SAXS signals are due to longer induction time for crystallinity of PLA nanocomposites at low concentration of SNCs-g-LA (3 wt%), while impedes the effect of SNCs-g-LA at higher concentrations (7 wt%) notably by restricting the motion of the PLA chains and limiting their ordered arrangement for short range ordered structure. Subsequently, when crystallization time reaches to 30 min., or above, the presence of the considerable crystalline structure become a dominant factor contributing the SAXS signals (Figure 5.3). This result suggests that PLA crystals in PLA/SNCs-g-LA (3 wt%) samples are denser than

neat PLA and in line with the observed morphology of PLA/SNCs-g-LA (3 wt%) spherulites (Figure 5.4). However, the high content of SNCs-g-LA greatly suppress the ordered arrangement of PLA chains, giving rise to the looser and less perfect PLA spherulite as can be seen in Figure 5.5.

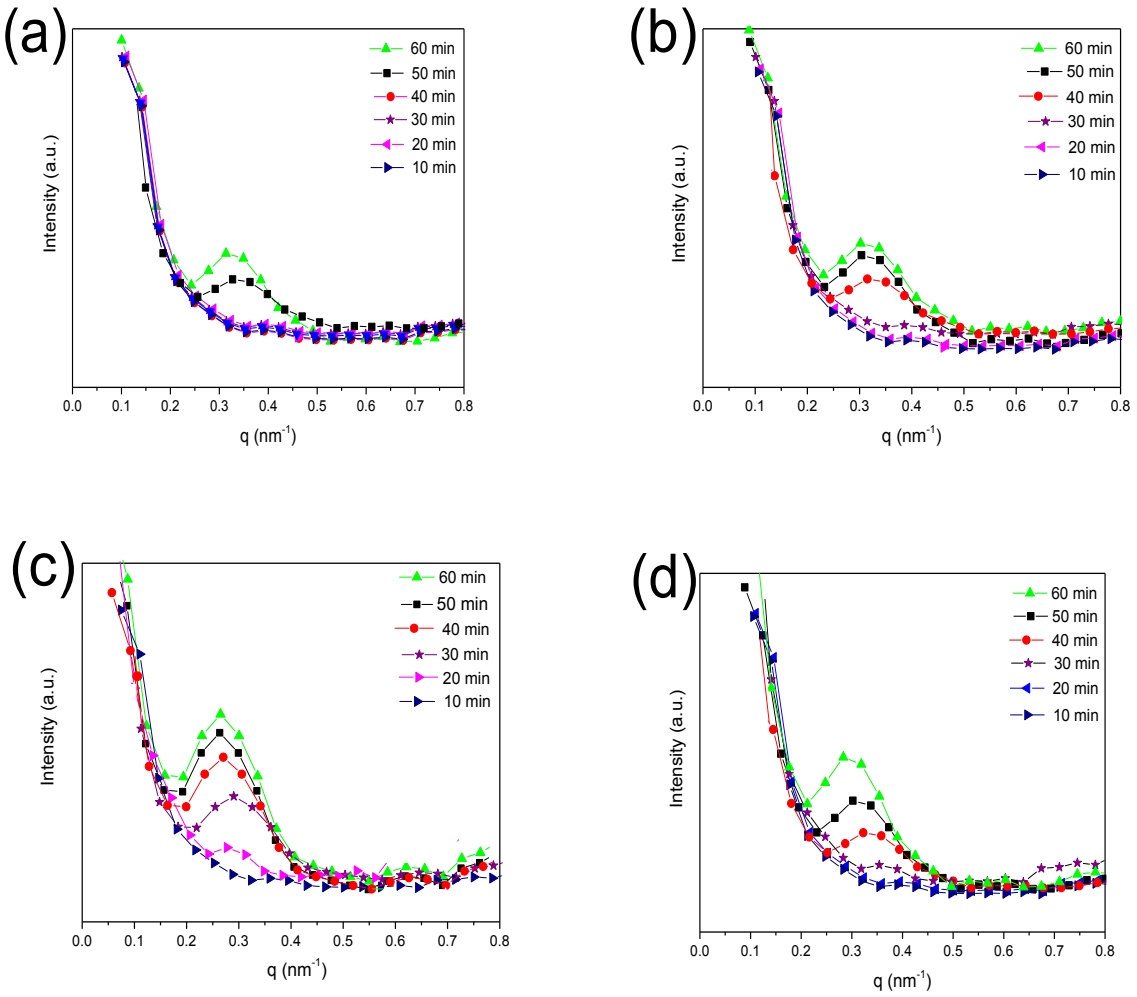

Figure 5.3. The SAXS analysis of a) neat PLA, b) PLA/SNCs-g-LA (3 wt%), c) PLA/SNCs-g-LA (5 wt%), b) PLA/SNCs-g-LA (7 wt%), nanocomposites which are crystallized at different crystallization time at T_c=130℃.

5.5.4. Spherulite Morphology of PLA/SNCs-g-LA Nanocomposites

Apart from the crystalline structures, the spherulite morphology is another important factor that can affect the gas permeability of PLA nanocomposites. Figure 5.4, shows the evaluation of

spherulite morphology of neat PLA and PLA/SNCs-g-LA nanocomposites during isothermal crystallization at **130** ℃. It can be seen from Figure 5.4, more PLA spherulites are formed in all PLA nanocomposites than compared to neat PLA at same isothermal crystallization time. This indicates that the evaluation of $\boldsymbol{\alpha}-$ crystal density in PLA nanocomposites is higher than that of neat PLA. However, the SNCs-g-LA has a different effect on the spherulite morphology based on the concentrations. In the case of PLA/SNCs-g-LA (3 wt%) nanocomposite, only small amount of SNCs-g-LA nanoparticles act as a heterogeneous surface area for growing of PLA molecular chain reducing the nucleating energy barrier and inducing the short-range ordered structure for PLA crystallization. However, when PLA was loaded with 5 wt% SNCs-g-LA show a denser and have smaller PLA spherulite morphology. This obviously is due to excellent heterogeneous nucleating ability of SNCs-g-LA nanoparticles, effectively increasing the $\boldsymbol{\alpha}-$nucleating density for PLA crystallization. However, addition of 7 wt% of SNCs-g-LA slows the motion of PLA chains substantially and restricts their relaxation. The optimum concentration of SNCs-g-LA nanoparticles to form a network structure in the PLA matrix was therefore estimated to be about 5 wt%. It is well documented that, the growth of polymer crystals is considered as a self-perfection and self-purification process, in which it is hardly possible for foreign matter to stay in the crystalline region. Therefore, it is rational to conjecture that addition of small amount of SNCs-g-LA can act as an efficient $\boldsymbol{\alpha}-$nucleating agents, the remaining SNCs-g-LA are excluded by PLA crystals, exhibiting random dispersion in the course of isothermal crystallization. However, the thickness of interlamellar amorphous layer calculated by one-dimensional electron density correlation function is less than 20 nm, which is much lower than that of the size of SNCs-g-LA (ranging from 80 to120 nm). Thus, most of the SNCs-g-LA are preferentially dispersed between PLA spherulites.

Sample	Time		
	10 min	30 min	60 min
PLA	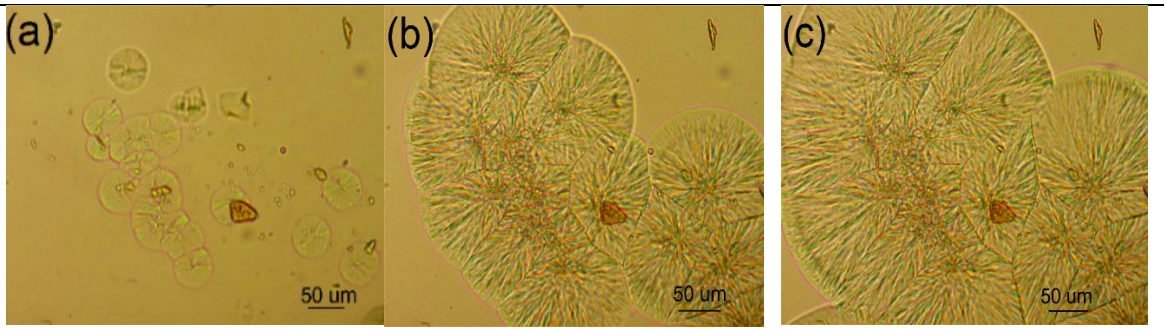		
PLA/SNCs-g-LA (3 wt%)	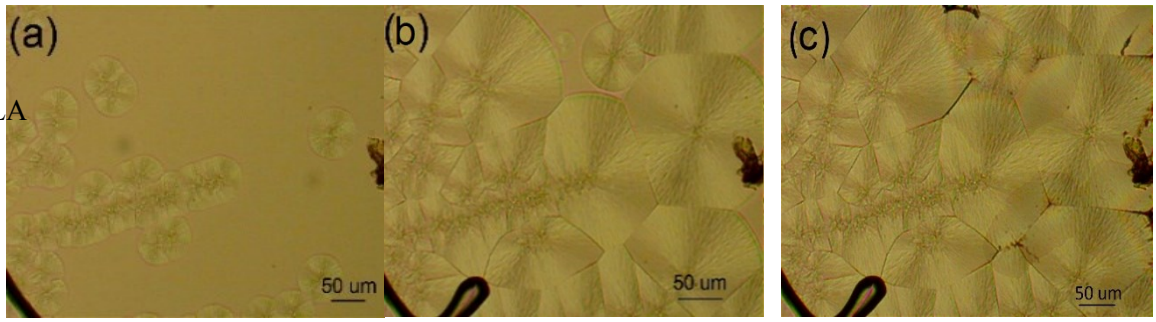		
PLA/SNCs-g-LA (5 wt%)	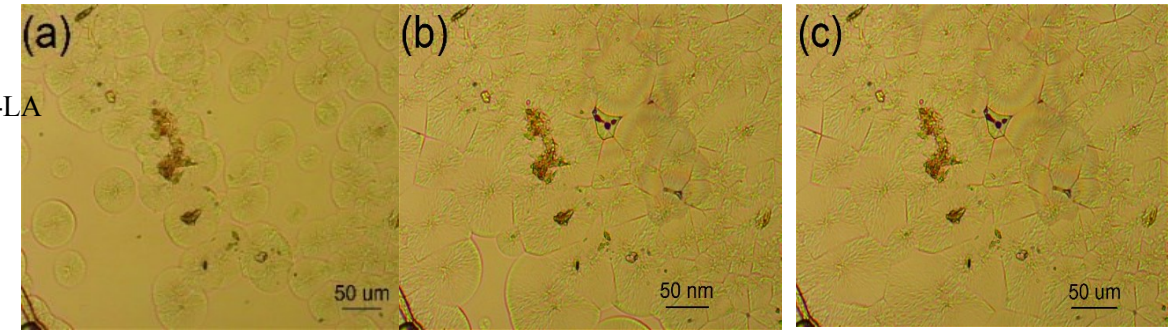		
PLA/SNCs-g-LA (7 wt%)	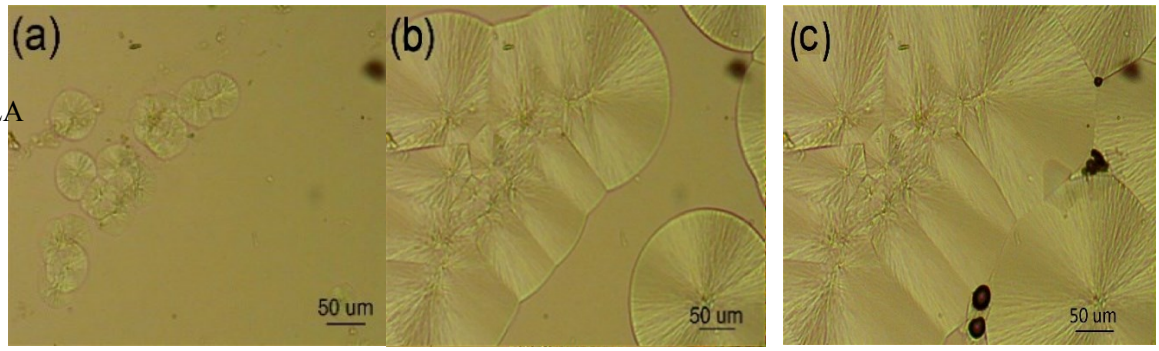		

Figure 5.4. Optical microscopic images of neat PLA at a) 10 min b) 20 min, c) 30 min d) 40 min and e) 60 min, and PLA/SNCs-g-LA (5 wt%) nanocomposite a') 10 min, b') 20 min, c') 40 min d') 80 min and e') 100 min.

5.5.5. Gas Transport Properties of PLA/SNCs-g-LA Nanocomposites

The oxygen and water vapor permeability of PLA and PLA/SNCs-g-LA nanocomposites were determined using oxygen and water permeability machine and the results are shown in Figure 5.5a and b respectively. As can be seen, gas permeability of all PLA nanocomposites are lower than neat PLA. Specifically, considerable enhancement in the gas permeability of PLA/SNCs-g-LA (5 wt%) was observed, the oxygen permeability was reduced by a factor of half, whereas; the permeability of water vapor was reduced by 70% compared to that of neat PLA. This improvement in the gas permeability of the PLA/SNCs-g-LA nanocomposites can be attributed to the presence of impermeable crystalline SNCs-g-LA nanoparticles as well as increase in crystalline phase in the PLA matrix [111,112]. Another possible explanation for enhancement of gas barrier property of PLA/SNCs-g-LA nanocomposites can be attributed to increase in the effective travel path of oxygen and water vapor which makes the path of water vapor and oxygen more tortuous and results in the decrease in gas diffusion and hence lower gas permeability. The maximum increase in crystallinity of PLA/SNCs-g-LA was observed when 5 wt% of SNCs-g-LA nanoparticles were loaded, the SNCs-g-LA content relates well with the observed improvement in the gas barrier properties of PLA nanocomposites and results in lower gas permeability (Figure 5.5). However, the addition of 7 wt% of SNCs-g-LA did not improve the gas permeability of PLA nanocomposite any further and instead results in lower gas barrier properties (Table 5.1). This is be due to the retarded crystal growth caused by SNCs-g-LA agglomerations at high loading levels [111,112]. As can be seen clearly in Figure 5.6, a homogeneous distribution of the SNCs-g-LA nanoparticles was observed in the PLA nanocomposites, regardless of the SNCs-g-LA nanoparticles up to 5 wt%. However, some agglomerations were observed in PLA/SNCs-g-LA (7 wt%) nanocomposite which confirms that at higher concentrations of SNCs-g-LA the nanoscale agglomeration occurs. Furthermore, crystalline structure (e.g., perfect α- crystals structure) and geometric size can also determine the intrinsic barrier performance of polymer lamellae. In our WAXS results, all samples display the same characteristic diffraction peaks of α- crystals structure of PLA, regardless of concentration levels of SNCs-g-LA and isothermal crystallization time (Figure 5.2). However, the SAXS profiles show no scattering signals in all samples when isothermal crystallization time was lower than 60 min. Thereafter the characteristic scattering signals develops more homogeneously with a further increase in isothermal crystallization time. This when

combined with the WAXS results (Figure 5.2), suggests that the occurrence of scattering signals may be attributed to PLA crystals causing electron density contrast.

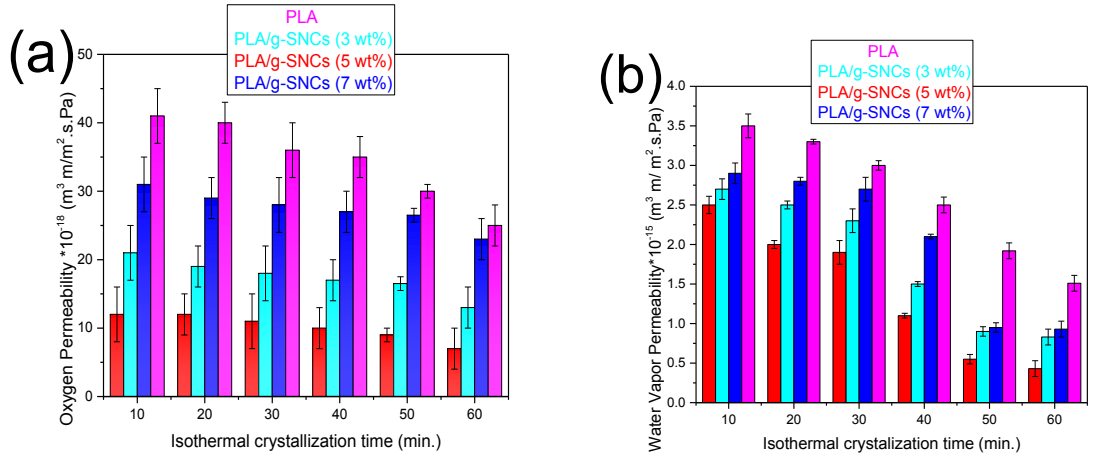

Figure 5.5. a) Oxygen and b) water vapor permeability of neat PLA and PLA/SNCs-g-LA nanocomposites which are crystallized at 130°C at various crystallization time.

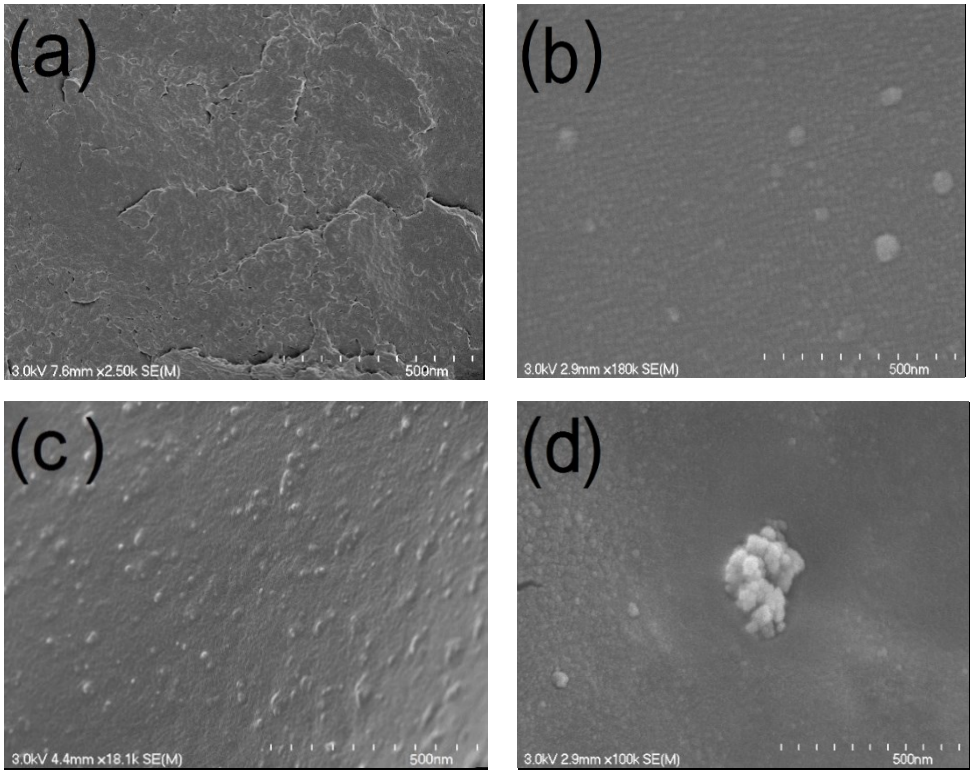

Figure 5.6. SEM images of; a) neat PLA, b) PLA/SNCs-g-LA (3 wt%), c) PLA/ SNCs-g-LA (5 wt%) and d) PLA/SNCs-g-LA (7 wt%) nanocomposites.

5.6. Conclusion

In this work, the effect of SNCs-g-LA varying in content (3-7 wt %) on the water vapor and oxygen permeability of PLA were investigated. All samples are isothermally crystallized at 130 ℃ for different crystallization time, where $\boldsymbol{\alpha}$ crystal structure was observed. It was found that the time of evaluation and content of $\boldsymbol{\alpha}$ −crystal structure were decreased and increased respectively in PLA/SNCs-g-LA nanocomposites. In addition, the PLA/ SNCs-g-LA nanocomposite film had a better barrier to both water and oxygen molecules irrespective of SNCs-g-LA content. This is attributed to the presence of highly crystalline SNCs-g-LA nanoparticles, which was increased the degree of crystallinity of the PLA nanocomposites and they acted as impermeable regions in the PLA matrix. Finally, the maximum improvements in water vapor permeability (50%) and oxygen permeability (70%) of PLA nanocomposites occurred when 5 wt% SNCs-g-LA nanoparticles were added into PLA matrix. However, higher content of the SNCs-g-LA nanoparticles (7 wt%) is negatively affected on the crystallinity and subsequently on barrier properties. To conclude that, the PLA/SNCs-g-LA nanocomposite films with better barrier performance developed in this study have tremendous potential for food packaging applications.

Chapter 6

6. Biodegradation of PLA/grafted SNCs Nanocomposite in Soil

Somayeh Sharafi Zamir[1], Babak Fathi[1], Abdellah Ajji[2], Mathieu Robert[1] and Said Elkoun[1*]

[1]Center for Innovation in Technological and Ecodesign (CITE), University of Sherbrooke, Sherbrooke, Qc, J1K 2R1, Canada.

[2]Chemical Engineering Department, Polytechnique Montreal, Montreal, Qc, H3C 3A7, Canada.

6.1. Résume

Dans ce travail, l'effet des nanocristaux d'amidon greffés avec de l'acide lactique (g-SNC) sur le taux de dégradation du poly (acide lactique) par le sol a été étudié par la mesure de la perte de poids, spectroscopie électronique aux rayons X (XPS), Spectroscopie infrarouge à transformée (FT-IR), microscopie électronique à balayage (MEB) et calorimétrie à balayage différentiel (DSC). Les résultats de perte de poids ont démontré que le taux de dégradation du PLA peut être accéléré en ajoutant des nanoparticules de g-SNC. Les résultats FTIR montrent que les intensités des liaisons C-O, C = O et C-H de PLA / g-SNC étaient plus faibles que celles de la PLA pure en augmentant le temps de dégradation de l'enfouissement du sol. De plus, la variation du pourcentage atomique de carbone interne était supérieure à celle de la surface, ce qui indique que le nanocomposite PLA / g-SNC était une dégradation en masse. L'analyse XPS a indiqué que la variation du rapport O / C était contrôlée par la biodégradation de l'amidon et l'hydrolyse du PLA. Il s'agissait d'un processus concomitant. Le degré de cristallinité mesuré par DSC a d'abord montré une tendance à la hausse, suivie d'une diminution de la tendance à la dégradation de l'enfouissement dans les nanocomposites de PLA. De plus, pendant la dégradation de l'enfouissement du sol, la température de transition vitreuse des nanocomposites PLA / SNCs-g-LA a évidemment diminué, tandis que celle-ci présentait une légère variation, ce qui indique que la dégradation des régions amorphes de PLA / SNCs-g-LA est antérieure . Les micrographies MEB montrent la formation de grandes fissures à la surface des nanocomposites PLA / g-SNC.

Mots clés: Poly (acide lactique) (PLA), nanocristaux d'amidon, dégradation du sol, cristallinité.

6.2. Abstract

In this work, the effect of lactic acid grafted starch nanocrystals (SNCs-g-LA) on the rate of soil burial degradation of Poly (lactic acid) was studied by means of the weight loss measurement (wt%), X-ray Photo Electron Spectroscopy (XPS), Fourier-Transform Infrared Spectroscopy (FT-IR), Scanning Electron Microscopy (SEM), and Differential Scanning Calorimetry (DSC). The weight loss results demonstrated that the degradation rate of PLA accelerated by adding SNCs-g-LA nanoparticles. The FT-IR analysis showed that the intensities of C-O, C=O, and C-H bond of PLA/SNCs-g-LA are higher than neat PLA that decreased further by increasing soil burial time. The XPS displayed that the atomic percentage of the O-C=O in PLA/SNCs-g-LA was reduced more than neat PLA after soil burial and the variation of O/C ratio controlled by SNCs-g-LA nanoparticles degradation due to the higher hydrolysis of SNCs-g-LA. In addition, the glass transition temperature and degree of crystallinity of PLA/SNCs-g-LA nanocomposites obviously decreased and increased respectively despite a slight variation for neat PLA. Regarding all above facts, it was hypothesized that the degradation rate of PLA in the presence of SNCs-g-LA is significantly accelerated.

Keywords: Poly lactic acid (PLA), grafted starch nanocrystals (SNCs-g-LA), soil degradation, crystallinity.

6.3. Introduction

Poly lactic acid (PLA) is an outstanding linear aliphatic thermoplastic polyester which possesses good mechanical properties (i.e. impact and tensile strength) and thermoplastic processing capacity [1]. PLA has been produced on a large scale and widely used in many applications such as food packaging, medical devices, agricultural films, and the automotive industries [2-3]. PLA is a bio-resourceable polymer that it is synthesized from the fermentation of native starch to lactic acid by the subsequent chemical polymerization [3,4]. However, PLA cannot easily degrade by microorganism due to the low vulnerability to bacterial attack in natural environments [119,121,124,196]. Usually, biodegradation studies are carried out in soil or compost. The biodegradation of PLA in soil occurs in three-steps. In the first step, water molecules diffuse into the PLA and hydrolyze the ester bonds of PLA backbone and then is followed by microbial degradation in which microorganisms break-down PLA molecular chains into oligomers and producing water, carbon dioxide, methane, mineral salts and etc., [119,121,124,196]. The rate of hydrolysis degradation is known to be influenced by temperature and catalyzed by free carboxylic groups of the hydrolyzed PLA terminal groups. Many studies have been focused on the soil burial biodegradation of PLA [119,121,124,196]. However, the degradation mechanism of PLA in soil is not clear so far. For examples, For example, Karamanlioglu et al., investigated the degradation of PLA under different environmental conditions and declared that the degradation mechanism of PLA in soil is unclear and remains controversial [198]. They also showed that microorganisms could increase the degradation rate of PLA and temperature was a key parameter for PLA soil degradation. Rudnik et al., also confirmed the degradation behavior of PLA in soil is a complex phenomenon and it is not controlled by Mediterranean climatic conditions [199]. Ho et al., buried PLA films with an average soil moisture of 80% and a temperature of 27 ℃ in an outdoor environment in Costa Rican soil. They found that the average degradation rate of PLA films in the soil of the banana field was 7675 M_w/week [118]. The degradation of PLLA films in south Finland soil for two years was also investigated by Gallet and his coworkers [120]. They reported that during the first year the PLLA films underwent just hydrolysis and in the second year microorganisms assimilated the small products of degradation. In addition, Calmon et al., found that weight losses of PLA varied from 0 to 100% after soil burial for 24 months depending on PLA type and location [119]. In contrast, the results obtained by Urayama et al., showed that

molecular weight of PLA (L-rich) samples was reduced only 20% after 20 months in soil [121]. Blending of PLA with natural fillers such as starch is considered as an effective technique to accelerate the biodegradation rate of PLA. It has been demonstrated that starch is more susceptible to biological attack under an environmental condition after use, hence, it enhances the degradation rate of PLA [124,125,196]. PLA also exhibits considerable advantages when it is blended with starch, such as reducing cost and improving physical and thermal properties of final PLA products. However, PLA and starch are immiscible, which would generally lead to poor interfacial adhesion between the two components. To overcome this problem, various chemical and physical modifications of PLA and/or starch have been developed to improve the interfacial adhesion between PLA and starch. The crystallinity, thermal and mechanical properties of PLA/starch blend with different chemical and physical modifications have been extensively studied [2,2,5]. However, there are a few reports considering the effect of these modifications on the biodegradation of a PLA/starch blend specifically in soil and compost conditions [123–125]. Shi et al., prepared a ternary blend of PLA, thermoplastic starch (TPS), and glycidyl methacrylate grafted poly (ethylene octene) (GPOE) [128]. They found that a GPOE compatibilizer can accelerate the PLA/TPS biodegradation rate by means of the radicals formed in the biodegradation of GPOE [128]. However, Pahetwarotai et al., reported that the compatibilization of PLA/starch with methylenediphenyl diisocyanate (MDI) decreased the biodegradation level of PLA due to the changes of the physical appearance of starch which led to lower water absorption [123]. Similar results about the role of compatibility on PLA/starch blend biodegradation were also reported by Iovino and his coworkers. They reported that the compatibilized PLA/starch blend revealed a lower biodegradation level due to the improved interface interaction [125]. The soil degradation mechanism of the esterified starch with malic anhydride (MA)/PLA composites was investigated by Zuo and his coworkers. They showed that the degradation of PLA/Starch composites took place at the carbonyl group linkage in starch structure and provided energy source for the microorganism to degrade the PLA matrix [58].

Even though the biodegradation of PLA/starch composite has been studied in a few reports in recent years, the effect of esterified SNCs on the degradation rate of PLA in soil has not been thoroughly analyzed. In the last work, the surface of SNCs was grafted by lactic acid (LA) through simple esterification reaction [23]. Then, the effect of grafted SNCs (SNCs-g-LA) nanoparticles and its concentrations on the crystallization behaviour and gas barrier properties (i.e. oxygen) were

determined. It was found that the SNCs-g-LA nanoparticles have considerable effect on the enhancing degree of crystallinity and oxygen barrier properties of PLA. Thus, it can enlarge the food packaging markets of PLA/SNCs-g-LA nanocomposites. This work is focused on the degradation of PLA nanocomposites with grafted SNCs by lactic acid (LA) under outdoor soil burial experiment. The weight loss, morphological changes, crystallinity, and thermal performances of the PLA/SNCs-g-LA nanocomposite during the degradation process in soil were thoroughly investigated and compared with neat PLA and PLA/neat SNCs nanocomposite.

6.4. Experimental

6.4.1. Materials

Corn starch was supplied by Sigma-Aldrich, Canada. It was dried in a vacuum oven at 40 ℃ for 24 hrs. before further modifications. The PLA pellets were purchased from Nature Works LLC (Minnesota, USA). The selected grade PLA (4032) was a semicrystalline grade and contained 2% D-units. The average molecular weight ($\mathbf{M_w}$) and polydispersity index ($\mathbf{M_w/M_n}$) of PLA pellets were about $\mathbf{109000g/mol}$ and $\mathbf{1.57}$ respectively.

6.4.2. Preparation of PLA Nanocomposite

Starch nanocrystals (SNCs) were extracted from native corn starch and successfully grafted with lactic acid (LA) as previously reported by authors [195]. The PLA/grafted SNCs (SNCs-g-LA) nanocomposite was prepared by the solvent casting process. Firstly, both PLA and grafted SNCs (SNCs-g-LA) were dried in a vacuum oven at 45 ℃ for 24 hrs. Subsequently, 0.2 g of grafted starch nanocrystals (SNCs-g-LA) and 3.8 g of PLA were dissolved in the 40 ml of dichloromethane as the solvent. The mixture was stirred for 24 hr., to obtain reaction solution. The solution of PLA/ SNCs-g-LA nanocomposite was cast by pouring the 40 mL of the solution onto glass Petri dishes (internal diameter 60 mm) and dried at room temperature for two days. Finally, the prepared films were vacuum dried overnight in order to remove the remained dichloromethane solvent. In addition, neat SNCs (without any modification) was mixed with PLA in the same way (named PLA/SNCs nanocomposite) in order to uses as a reference material.

6.4.3. Soil Burial Degradation Experiments

Biodegradation experiments were performed in outdoor soil conditions at the temperature and moisture of $\sim$15-25 ℃ and 70-80%, respectively. The samples of $50 \times 50 \times \mathbf{2\ mm}$ were cut and buried 15–25 cm depth under the soil surface for defined time periods (15, 30, 60 and 90 days).

Then, they were removed from soil, brushed softly, washed with distilled water and dried in a vacuum oven until a constant weight was reached.

6.4.4. Weight Loss

The weight loss of samples were measured by weighing the samples before and after biodegradation testing at different soil burial time (15, 30, 60 and 90 days). The weight loss of the samples with time was used to indicate the degradation rate in the soil burial test. Each sample had 3 parallel samples which buried in the same conditions and the average value was used as the weight loss. The weight loss percentage (wt %) of the samples was calculated with the following equation:

$$\text{Wt}\ (\%) = \frac{\mathbf{W_i - W_f}}{\mathbf{W_i}} \times \mathbf{100} \qquad (6\text{-}1)$$

Where $\mathbf{W_i}$ was the initial dry weight before degradation; $\mathbf{W_f}$ was the residual dry weight after degradation at an exposure time. An average of at least five measurements was calculated to obtain the reported results.

6.4.5. Fourier-Transform Infrared Spectroscopy (FT-IR)

Before and after degradation, the samples underwent an infrared spectroscopy using an attenuated total reflectance (ATR) Fourier Transform Infrared (FT-IR) analysis (JASCO-4600 Spectrometer). Scans were run at the resolution of 4 cm^{-1} in the range of $4000 - 600\ \text{cm}^{-1}$.

6.4.6. X-ray Photoelectron Spectroscopy (XPS)

The surface elemental composition was investigated by a X-ray Photoelectron Spectroscopy (XPS). A KRATOS Axis Ultra electron energy analyzer operating with an Al K_α monochromatic source were used to measure the different concentration of carbon and oxygen before and after soil burial degradation. The over viewing spectra were taken between 0 and 1400 eV with an energy step of 1 eV, while the details of the peaks of interest (C1s and O1s) were recorded with an energy step of 0.05 eV. Casa XPS version (2.3.16 Pre-rel 1, 4) was used as curve-fitting software. The overlapping peaks were resolved by the peak synthesis method, applying Gaussian-Lorentzian peak components after Shirley type background subtraction.

6.4.7. Scanning Electron Microscopy (SEM)

The morphology of the samples before and after biodegradation was investigated with Scanning Electron Microscopy (S-7500, Hitachi, Japan). After immersion of samples in liquid nitrogen, they were broken and coated with a thin layer of Pd-Au using a vapor deposition process before SEM characterization to avoid surface charging under an electron beam.

6.4.8. Differential Scanning Calorimetry (DSC)

The thermal properties of samples before and after soil degradation were characterized using Differential Scanning Calorimetry (DSC, Q2000, TA instrument). Samples (5-10 mg) were heated from 25 to 200 ℃ at 5℃/min and kept at 200 ℃ for 5 min. to eliminate the thermal history completely. Thereafter, the samples were quickly cooled down to room temperature and reheated again from room temperature to 200 ℃ at the rate of 5 ℃/min. The crystallinity degree of samples was calculated by using the following formulation;

$$\chi(\mathrm{x}) = \frac{\Delta \mathrm{H_m}}{(1-\mathrm{w})\,\Delta H_f^0} \times 100\% \qquad (6\text{-}2)$$

where w is the weight fraction of SNCs, ΔH_f^0 is the enthalpy of melting for fully crystalline PLA (93 J/g). An average of at least three measurements were performed to obtain the reported results.

6.4.9. Thermogravimetric Analysis (TGA)

The thermal stability of samples were studied by using a Thermogravimetric Analysis (TGA)-SETARMAN instrument under argon flow. Samples ($5-10$ mg) were heated from 25 to 700 ℃, at a heating rate of 10 ℃/min. Then, the corresponding loss of mass was noted.

6.5. Results and Discussion

6.5.1. Weight Loss Measurement

The weight loss measurement is a simple and valuable method used to estimate the degradation rate of polymers. Figure 6.1 displays the weight loss of neat PLA, PLA/SNCs and PLA/SNCs-g-LA nanocomposites at the end of each soil burial degradation period (15, 30, 60, and 90 days). As can be seen, the weight loss of neat PLA was almost negligible even after 90 days. However, the weight loss of both PLA nanocomposites were considerably higher than that of neat PLA. After 15 days, the weight loss of the PLA/SNCs-g-LA nanocomposite is considerably lower than PLA/SNCs nanocomposite. However, with increasing of soil burial time to 60 days the amount of

weight loss of both PLA/SNCs and PLA/SNCs-g-LA nanocomposites enhances considerably. With the increasing of soil burial time to 90 days, the extent of weight loss of both nanocomposites gradually slowed down. The higher degradation rate of PLA nanocomposites during the first 60 days can be related to the higher rate of SNCs degradation. The higher degradation rate of SNCs led to the disruption of the SNCs macromolecular chain arrangement and higher exposure of the amorphous phase of PLA which is more susceptible to microorganism degradation [123–125]. After 90 days, a large amount of the amorphous content decomposed and leaving mostly the crystalline component which decreased the rate of degradation. Generally, the weight loss of PLA/SNCs-g-LA was a bit lower than that of PLA/SNCs nanocomposites after 90 days. This is due to the hydrophobicity of SNCs-g-LA that increases the interfacial bonding between SNCs and PLA and effectively prevents water and microorganisms penetration into the PLA/g-SNCs nanocomposite [23].

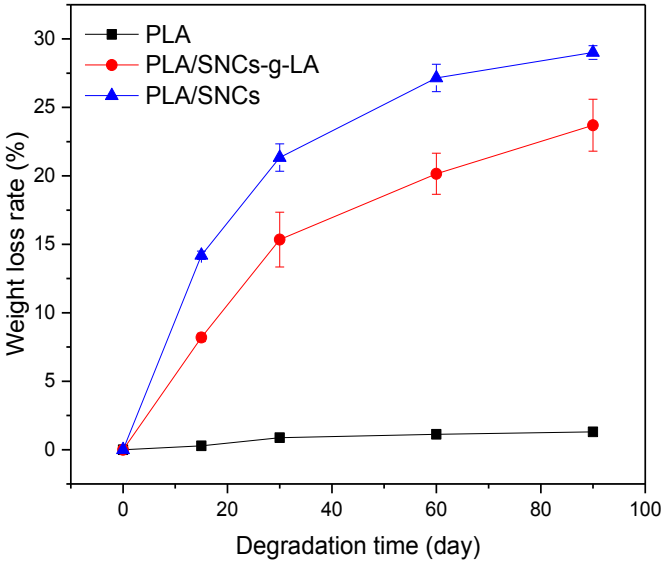

Figure 6.1. Weight loss of neat PLA, PLA/SNCs and PLA/SNCs-g-LA nanocomposites at different degradation time.

6.5.2. Morphological Properties

The morphological changes due to the soil degradation at different degradation times (15, 30, 60 and 90 days) were visualized by SEM and the micrographs are shown in Figure 6.2. The surface morphology of neat PLA was smooth before exposure to the soil and it becomes rough and some small pores were observed after degradation in soil for 90 days. However, the number of the pores

on the surface of PLA/SNCs-g-LA and PLA/SNCs nanocomposites were much higher than neat PLA at the same soil burial period. When the soil degradation time was 15 days, there was a certain degree of damage on the PLA/SNCs-g-LA nanocomposite surface but the extent of the damage was small. With the increasing of soil burial time to 30 days, the degree of disruption increased gradually in PLA/SNCs-g-LA nanocomposite. Finally, a large number of holes were observed after 90 days soil degration. However, the disruption of the surface of PLA/SNCs nanocomposite was much more obvious than PLA/SNCs-g-LA nanocomposite at the same degradation time. The SEM images showed that the surface of the PLA/SNCs nanocomposite was significantly eroded and random degradation caused many cavities with a large size on the surface of PLA/SNCs nanocomposite. With the increasing of soil burial time, the crack at the surface of PLA/SNCs nanocomposite increased abruptly. This can be due to the hydrolysis of SNCs by water which led to the surface damage and produced a rupture on the PLA/SNCs nanocomposite surface [124–126]. The presence of a large number of hydrophilic OH groups on the SNCs molecular structure led to a higher tendency of water molecules being absorbed. Therefore, SNCs absorbed moisture from the soil easily and produced a swelling phenomenon which led to a big crack on the PLA/SNCs nanocomposite surface. However, in PLA/SNCs-g-LA nanocomposite, some of the hydrophilic OH groups of the SNCs molecular chains were replaced by hydrophobic carbonyl groups with esterification reaction, as a result, the hydrophobicity of grafted SNCs was increased compared to SNCs. In addition, the interfacial compatibility or chemical affinity between esterified SNCs and PLA was better than that of neat SNCs and PLA. Therefore, it could effectively prevent water molecules to penetrate into the interface of PLA/SNCs-g-LA nanocomposite.

Time (day)	Samples		
	PLA	PLA/SNCs-g-LA	PLA/SNCs
0	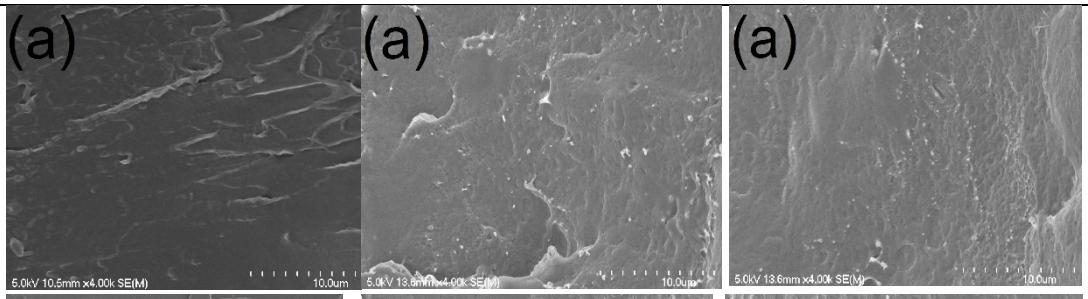		
15	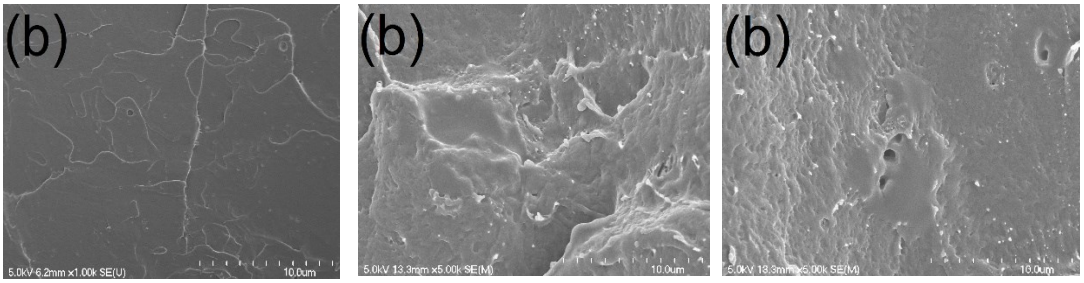		
30	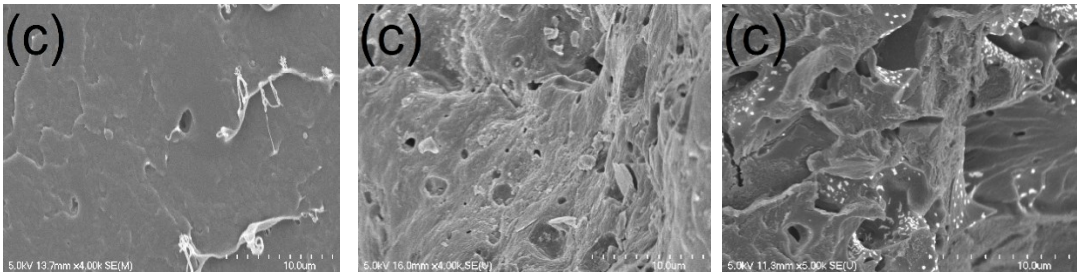		
60	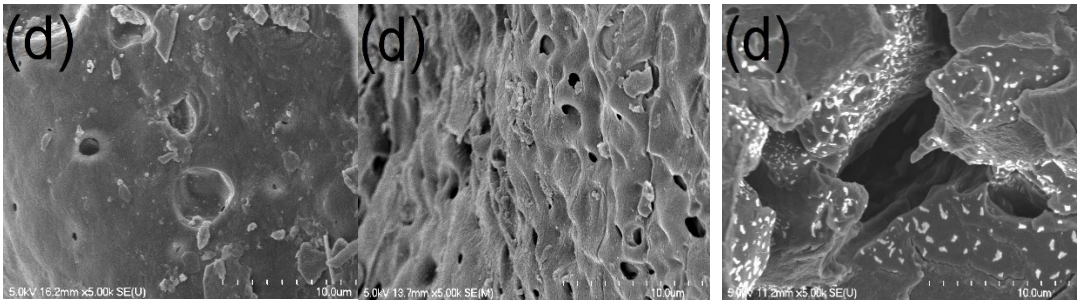		
90	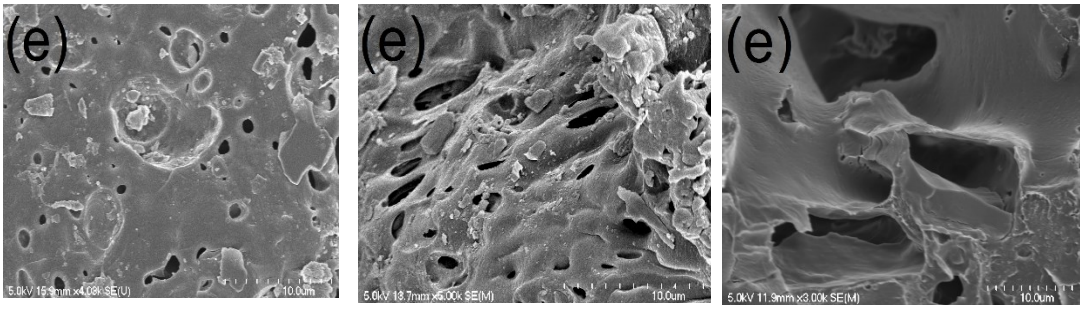		

Figure 6.2. The SEM images of neat PLA, PLA/SNCs and PLA/SNCs-g-LA nanocomposites at different degradation time.

6.5.3 XPS Analysis

The elemental surface analysis of samples was studied by XPS and the results were shown in Figure 6.3. The relative atomic percentages which were determined from high resolution C1s XPS peaks are summarized in Table 6.1. Deconvolution C1s peak shows the presence of $C-C/C-H, C=O$ and $O=C-O$ at binding energy of 285.0, 287.2, and 289.4 eV which is consistence with neat PLA [149]. In neat PLA, the intensity of all $C-C/C-H, C=O$, and $O=C-O$ peaks decreases after soil burial degradation. In addition, the atomic percentage of $O=C-O$ in PLA degraded for 90 days decreased from 14.2% to 13.1% [28]. This change occurring in $O=C-O$ peak can be owing to the hydrolysis of ester groups in PLA molecular chains. For the PLA/SNCs-g-LA nanocomposite, after degradation for 90 days, the intensities of $C-O$ and $O=C-O$ peaks decreased from 17.9% and 11.7% to 15.6% and 10.6% respectively. However, intensities of $C-O$ and $O=C-O$ peaks decreased much more in PLA/SNCs nanocomposite and decreased from 15.9 and 12.5% to 13.1% and 8.6%, respectively after degradation for 90 days. These can be attributed to the chains split of $C-O$ linkages between glucose rings in starch and $O=C-O$ linkages in PLA. The $O-C$ ratio of PLA decreased from 0.17 to 0.13, while the soil burial degradation decreased the $O-C$ ratio of PLA/SNCs-g-LA nanocomposite from 0.44 to 0.23. These results demonstrated that the degradation occurred in the oxygen-contained groups in the polymer structures and the nanocomposites degraded faster with the presence of neat SNCs compared to SNCs-g-LA.

Table 6.1. Deconvolution of C1s core level spectra in neat PLA, PLA/SNCs and PLA/SNCs-g-LA nanocomposites before and after soil burial degradation.

Peak BE (eV)	Chemical bonds	Relative atomic percentage (%)					
		PLA		PLA/SNCs		PLA/SNCs-g-LA	
		0 day	90 days	0 day	90 days	0 day	90 days
285.0	C-C/H	69.2	68.3	65.5	64.0	65.0	64.8
286.5	C-O	14.2	12.7	15.9	13.9	18.9	15.6
289.5	O-C=O	14.1	13.1	12.5	8.6	12.7	10.6

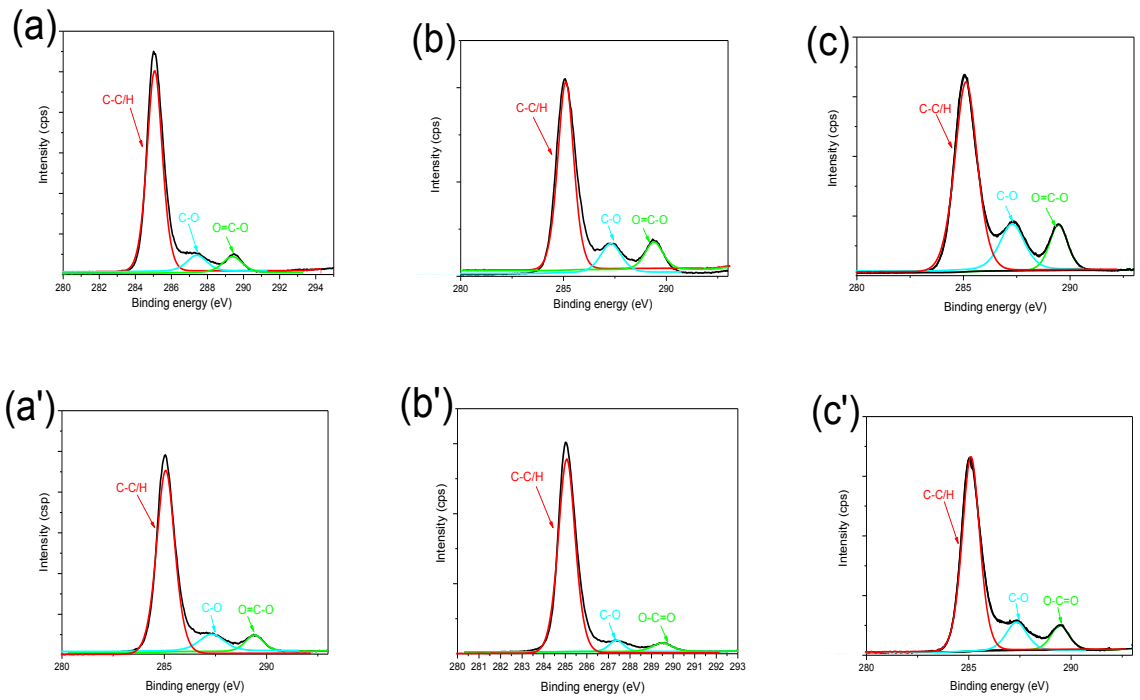

Figure 6.3. High resolution XPS C1s spectra of a) neat PLA, b) PLA/SNCs and c) PLA/SNCs-g-LA nanocomposites before degradation and a') neat PLA, b') PLA/SNCs and c') PLA/SNCs-g-LA nanocomposites after degradation for 90 days.

6.5.4. FT-IR Analysis

The chemical changes occurring on the surface of the samples during soil burial degradation is investigated by FTIR analysis (Figure 6.4). As can be seen from Figure 6.4, all spectra are similar and no new bands were observed during soil burial degradation suggesting that there were no byproducts emerging on the surface of the specimens. Although the characteristics absorption peak of FTIR spectra did not change after degradation, there were significant changes in the intensity of absorption peaks. Before soil burial degradation, the characteristics peak of 1079 and 1180 $\mathbf{cm^{-1}}$ were assigned to C-O stretching vibration, the peaks at 1448 and 1355 $\mathbf{cm^{-1}}$ were assigned to C-H deformation vibration, and finally, the peak at 1751 $\mathbf{cm^{-1}}$ was attributed to the C=O stretching vibration peaks. With the increasing of the degradation time, the intensity of the C-O stretching vibration peak, C-H vibration peaks, and C=O stretching vibration peaks weakened gradually. However, the intensities of C-O and C=O group absorption peaks in PLA/SNCs and PLA/SNCs-g-LA nanocomposites at the same soil burial degradation time decreased considerably and the intensity of C-O almost disappeared. This indicates that the degradation rate of PLA nanocomposites is higher than neat PLA. In addition, due to the fact that the surface modification reaction of SNCs by LA enhances the compatibility between SNCs and PLA which prevented the

composites decomposition, the degradation of PLA/SNCs is a bit higher than that of PLA/SNCs-g-LA (Section 6.4.3).

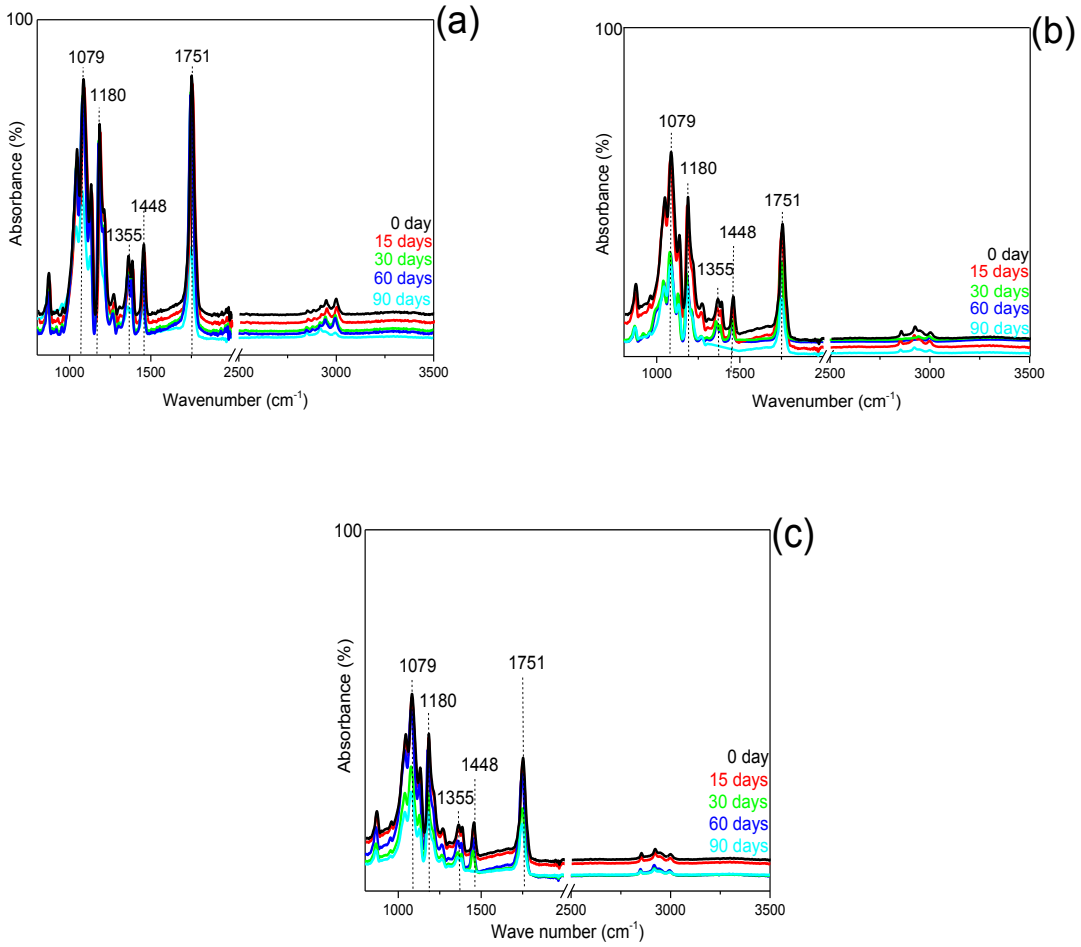

Figure 6.4. FTIR analysis of a) neat PLA, b) PLA/SNCs and c) PLA/SNCs-g-LA nanocomposites at different degradation time.

6.5.5. Thermal Properties

The thermal properties of neat PLA, PLA/SNCs and PLA/SNCs-g-LA nanocomposite samples before and after soil burial degradation were investigated by DSC analysis and the results are shown in Figure 6.5. In addition, glass transition temperature (T_g), cold crystallization temperature (T_{cc}), a double endothermic melting temperature (T_{m1} and T_{m2}) and the degree of crystallinity (X_c) were determined by DSC analysis and data were summarized in Table 6.2. Before soil burial degradation, the neat PLA exhibits a glass transition temperature around 61.8 ℃. However, after 15 days of soil burial, the T_g increased ~1 ℃ due to the biodegradation of the amorphous region.

However, the T_g of PLA decreases to 55.1℃ by further increasing soil burial degradation time to 60 days. It is well known that the PLA degradation at the temperature before the T_g happens slowly due to the change of molecular chains of the PLA from a glass-state to a rubber-state [7]. In addition, T_g of both PLA/SNCs and PLA/SNCs-g-LA nanocomposites was gradually decreased with increasing soil burial time. The T_g in PLA/SNCs started to decrease after 30 days, whereas, the T_g in PLA/SNCs-g-LA started to decrease after 60 days of soil burial. This means that the crystalline regions of PLA began to degrade earlier in PLA/SNCs nanocomposite compared to PLA/SNCs-g-LA nanocomposite thus weakening the interaction force between molecular chains. In addition, the T_{cc} of PLA/ SNCs shifted to a lower temperature and the area of the cold crystallization peak is much narrower than that of PLA/SNCs-g-LA nanocomposite. The decreases in T_{cc} of PLA/SNCs nanocomposite is probably due to the fact that more polymeric chains are involved in the crystallization process of PLA/SNCs nanocomposite as the degradation time increases [58,125]. The mentioned variation in burial time caused similar effect on the melting behavior, both PLA nanocomposites show higher T_m value than neat PLA which decreases when soil burial is longer. As expected, the variation in T_{cc} and T_m are accompanied by those in the X_c which took the same pathway of variation as the X_c. Among the studied samples, PLA shows the smallest crystallization degree which decreases with increasing soil burial degradation time. This variation can be due to the competition between the reorganization of polymer chains and degradation. However, both PLA nanocomposites show much higher crystallinity degree values than PLA and these values increased after soil burial with the highest values of 60 days of soil burial time. As can be seen in Table 6.2, the X_c of both PLA nanocomposites initially increases with increasing degradation time and then decreases with further increasing degradation time. For PLA/SNCs, the X_c started to decrease after 15 days of soil burial while this decline occurred after 30 days for PLA/SNCs-g-LA nanocomposite. The increase in X_c can be because of penetration of water and microorganisms from the soil which is firstly degrade amorphous phase, leading to an increase of the relative content of the crystalline phase in PLA nanocomposite. In addition, another reason can be due to the higher degradation rate of SNCs than SNCs-g-LA, therefore, the damage extent of nanocomposites was increased, leading to the extended degradation or decomposition of nanocomposite. For PLA/SNCs, the degree of crystallinity for PLA was 8.1% at the 15 days of burial time which was larger than that of PLA/SNCs-g-LA (6.9%). Moreover, the damage extent

and cracks of PLA/SNCs were larger than PLA/SNCs-g-LA and the degradation rate was higher than PLA/SNCs-g-LA. Thus, the crystalline regions of PLA in PLA/SNCs started to degrade in 15 days. However, the damage extent of PLA/SNCs-g-LA was smaller and began to degrade when the soil burial time was 30 days.

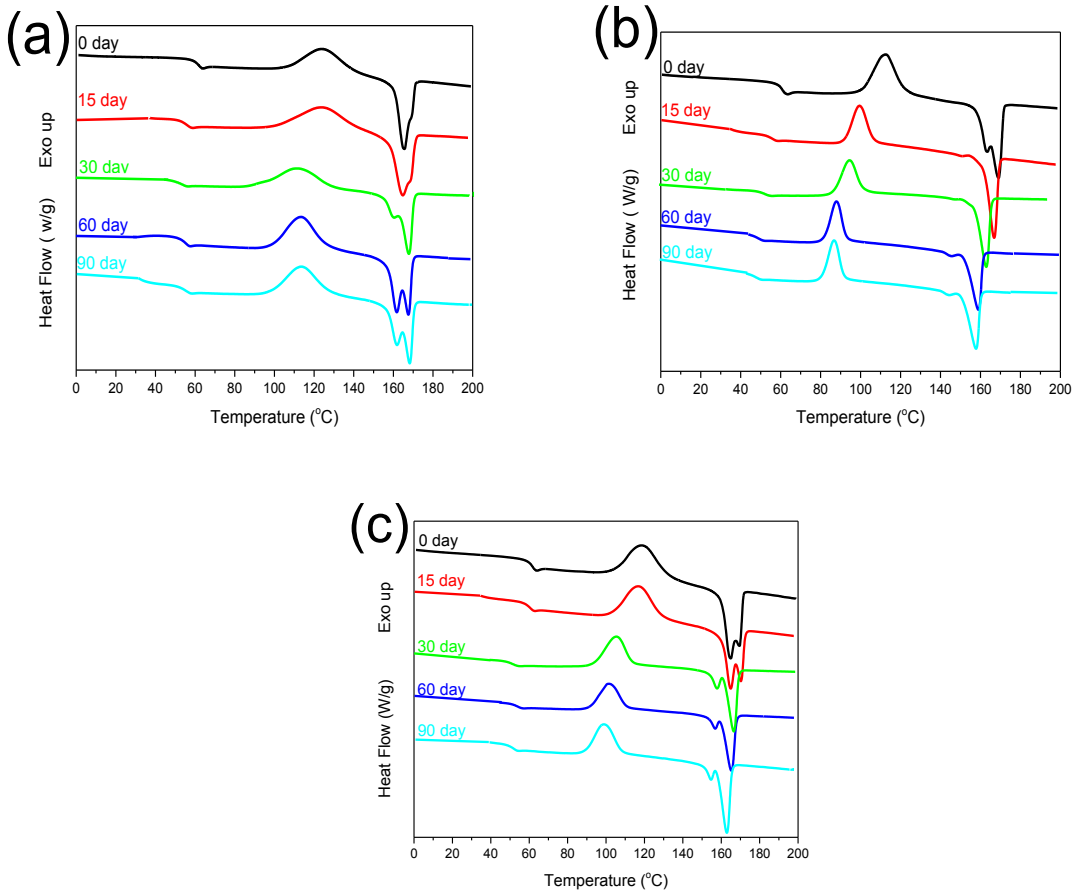

Figure 6.5. DSC analysis of a) neat PLA, b) PLA/SNCs and c) PLA/SNCs-g-LA nanocomposites at different degradation time.

Table 6.2. Thermal properties of a) neat PLA, b) PLA/SNCs and c) PLA/SNCs-g-LA nanocomposites at different degradation time.

samples	PLA					PLA/SNCs					PLA/SNCs-g-LA				
Time (days)	T_g (°C)	T_{cc} (°C)	ΔH_{cc} (J/g)	T_{m2} (°C)	X_c (%)	T_g (°C)	T_{cc} (°C)	ΔH_{cc} (J/g)	T_{m2} (°C)	X_c (%)	T_g (°C)	T_{cc} (°C)	ΔH_{cc} (J/g)	T_{m2} (°C)	X_c (%)
0	61.8	124.4	28.8	168.9	0.53	62.0	108.7	26.9	169.1	4.6	62.1	117.2	27.1	169.1	10.1
15	62.8	121.7	32.7	167.9	0.88	51.6	99.6	28.9	164.0	8.1	61.3	112.1	28.9	168.1	11.9
30	62.0	116.2	38.8	168.1	0.61	55.5	98.1	38.8	162.9	7.4	55.2	103.9	30.3	164.5	17.2
60	56.0	113.6	34.4	167.9	0.40	56.5	94.1	33.3	161.7	6.3	57.7	101.8	30.9	164.6	9.0
90	56.0	112.0	33.1	167.0	0.45	57.1	91.7	30.1	160.0	5.0	56.1	98.8	28.3	163.1	7.8

6.5.6. Thermal Stability

The influence of the biodegradation progression on the thermal stability of the neat PLA, PLA/SNCs, and PLA/SNCs-g-LA nanocomposites was studied by TGA and the thermograms are shown in Figure 6.6. The data are also summarized in Table 6.3. As demonstrated in Figure 6.6, when degradation time was increased from 0 to 90 days, the initial temperature of decomposition (T_i) and the final decomposition temperature (T_f) of neat PLA did not change considerably. Whereas, in the case of PLA/SNCs and PLA/SNCs-g-LA nanocomposite, both T_i and T_f decreased significantly with the extended degradation time. It is interesting that the variation of the final decomposition temperature was higher for PLA/SNCs-g-LA than that of PLA/SNCs nanocomposite. According to the thermal decomposition of SNCs and SNCs-g-LA, the decomposition temperature of SNCs was lower than that of SNCs-g-LA nanoparticles (Figure 6.6). This resulted in the considerable decrease of the decomposition temperature of PLA/SNCs nanocomposite during the 60 days of degradation. Besides, the crystallinity results showed that the crystallization of PLA in PLA/SNCs-g-LA was greater than that of PLA/SNCs nanocomposites. In theory, when there was a high degree of crystallization, the decomposition temperature (i.e. T_i andT_f) of PLA/SNCs-g-LA should be greater than that of PLA/SNCs. That means the degradation of SNCs-g-LA in PLA/SNCs-g-LA was less than PLA/SNCs and the relative content of PLA in PLA/SNCs-g-LA was greater than that of PLA/SNCs. Due to the fact that the thermal decomposition temperature of SNCs was significantly smaller than PLA, the thermal decomposition temperature of PLA/SNCs-g-LA was higher than PLA/SNCs.

Table 6.3. TGA data of neat PLA, PLA nanocomposites at different degradation time.

Samples	Time (day)	T_i (°C)	T_{max} (°C)	T_f (°C)
PLA	0	347.5	368.2	388.2
	15	346.3	365.1	380.9
	30	341.0	363.7	380.1
	60	337.9	363.1	380.1
	90	336.8	359.8	375.9
PLA/ SNCs	0	331.7	365.1	387.3
	15	317.1	355.4	379.1
	30	313.2	350.1	365.6
	60	310.0	340.7	360.7
	90	304.2	335.2	352.8
PLA/SNCs-g-LA	0	337.0	365.4	389.1
	15	322.7	362.8	382.5
	30	321.0	355.2	377.7
	60	320.2	347.6	374.1
	90	315.8	353.5	371.3

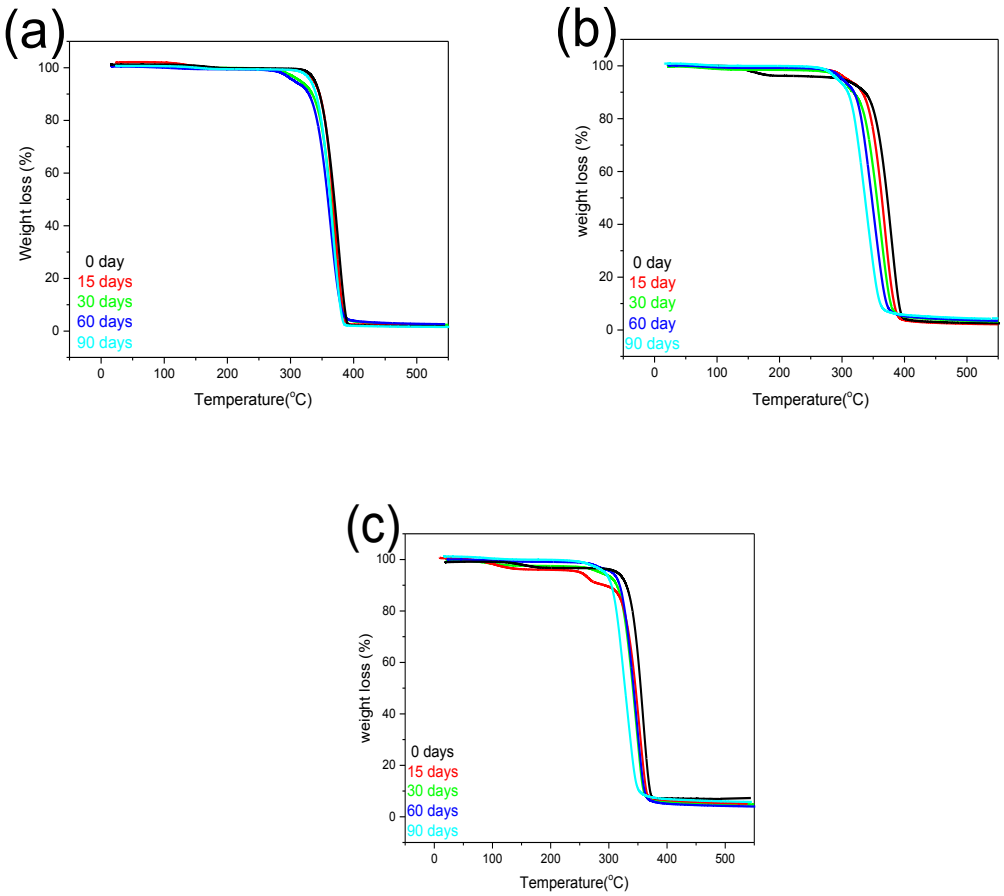

Figure 6.6. TGA curves of a) neat PLA, b) PLA/SNCs and c) PLA/SNCs-g-LA nanocomposites after different degradation time.

6.6. Conclusion

In this study the effect of grafted SNCs by LA on the soil burial degradation of PLA was studied. The surface chemical changes, morphology, and thermal properties evaluation were analyzed comprehensively. The results were also compared by the results of the soil degradation of PLA/SNCs nanocomposite. The results showed that the degradation of PLA/SNCs-g-LA nanocomposites is considerably higher than neat PLA. However, the rate of degradation at the surface and inside of PLA/SNCs-g-LA was somewhat less than that of PLA/SNCs. With increasing the degradation time, the chain breakage to the surface and inside of both nanocomposites showed an increased trend. The FTIR absorption peak intensities of C-O, C=O, and C-H were stronger in PLA/SNCs-g-LA compared to that of PLA/SNCs. The XPS showed that the reduction of atomic percentage of the O-C=O after 90 days in PLA/SNCs is higher than

PLA/SNCs-g-LA. In addition, DSC results showed, the degree of crystallization for PLA in PLA/SNCs-g-LA was higher than PLA/SNCs and degree of crystallinity first increases and then decreases by increasing soil burial degradation time. This is indicating that degradation first took place in the amorphous regions and then the crystalline regions. The more clear changes of T_g and thermal stability of the PLA/SNCs nanocomposite demonstrated that the PLA/SNCs nanocomposite degraded faster than the PLA/SNCs-g-LA in real soil conditions.

Chapter 7

7.1. Conclusion

Dans cette thèse, l'effet des nanoparticules de SNCs-g-LA sur la cristallisation et les propriétés de barrière aux gaz des PLA a été étudié. Dans la première phase du projet, les SNCs ont été greffés à l'acide lactique (SNCs-g-LA) afin de renforcer la compatibilité et la dispersion des SNCs à la matrice PLA. Ceci a été réalisé par une réaction d'estérification dans un solvant organique. De plus, l'effet des nanoparticules de SNCs-g-LA sur les propriétés thermiques et mécaniques de PLA/SNCs-g-LA a également été déterminé.

La première conclusion est que l'adhésion interfaciale entre le PLA et les nanoparticules de SNCs-g-LA augmente considérablement après la modification chimique des SNCs. De plus, les nanoparticules de SNCs-g-LA agissent en tant qu'agent de nucléation et fournissent des sites de nucléation optimaux pour la croissance cristalline. Ceci a renforcé la cristallisation à de faibles concentrations en SNCs-g-LA (5 wt%), tandis que les SNCs-g-LA ont contrecarré la cristallisation à des concentrations plus élevées. Dans la deuxième phase du projet, l'effet de différentes concentrations de SNCs-g-LA (3-7 wt%) sur la composition de phase, le comportement en transition de phase et le comportement de cristallisation isotherme du PLA a été étudié. Ceci a été réalisé par cristallisation de nanocomposites PLA/SNCs-g-LA à différentes Tc (80-130 ℃) où des structures cristallines α'de PLA ont été observées.

La deuxième conclusion importante est que les nanocomposites de PLA présentent une cinétique de cristallisation et un taux de croissance de la sphérulite plus rapides. La cinétique de caractérisation de la cristallisation a montré qu'en diminuant la concentration en SNCs-g-LA jusqu'à 5wt%, la densité de noyaux plus élevée et le cristal de sphérulite plus petits ont été observé. De plus, la formation de α-cristal dans les nanocomposites de PLA est plus probable que celle de α'-cristal et la vitesse de transition de phase dans les nanocomposites de PLA était supérieure à celle de PLA pur. Ce phénomène est plus important dans les nanocomposites de PLA avec 5wt% de nanoparticules de SNCs-g-LA. En ajoutant 5wt% de nanoparticules de SNCs-g-LA, le Ttrans des changements à une température plus basse et le degré de α-cristal des changements à une valeur supérieure à celle d'autres concentrations de nanoparticules de SNCs-g-LA. Par ailleurs, les sphérulites de PLA de phase-α ont été accélérées par la présence de nanoparticules de SNCs-g-LA. Le SGR où seulement le α-cristal formé a montré que la taille de la sphérulite était plus petite

dans le nanocomposite PLA/SNCs-g-LA (5 wt%) par rapport au PLA pur. De plus, la température de transition de phase diminue lorsque la concentration en SNCs-g-LA diminue jusqu'à 5wt%. En ajoutant seulement 5wt% de nanoparticules de SNCs-g-LA, la quantité de structures cristallines-α augmente dans la matrice de PLA. Dans la troisième partie du projet, il était prévu de déterminer l'effet des variants en SNCs-g-LA (3-7 wt %) sur la perméabilité à la vapeur d'eau et à l'oxygène du PLA. Tous les échantillons sont cristallisés de manière isothermique à 130℃ pendant différents temps de cristallisation, où la structure cristalline-α a été observée. Ensuite, la perméabilité à la vapeur d'eau et à l'oxygène de tous les nanocomposites de PLA a été mesurée. La troisième conclusion est que le temps d'évaluation et le contenu de la structure cristalline-α ont été diminué et augmenté respectivement dans les nanocomposites PLA/SNCs-g-LA. De plus, le film nanocomposite PLA/SNCs-g-LA présentait une meilleure barrière contre les molécules d'eau et d'oxygène, quel que soit le contenu en SNCs-g-LA. Ceci est attribué à la présence d'une structure hautement cristalline-α, augmentant le degré de cristallinité des nanocomposites de PLA et agissant comme des régions imperméables dans la matrice de PLA. Pour conclure, les films nanocomposites PLA/SNCs-g-LA avec une meilleure performance de barrière développés dans cette étude peuvent présenter un potentiel énorme pour les applications d'emballages alimentaires.

7.2. Conclusion

In this thesis, the oxygen and water vapor permeability of PLA/SNCs-g-LA nanocomposites and their dependency on the blend composition, crystallization behaviour, microstructure induced by changing the composition and crystallization kinetics were investigated. In the first phase of the project, SNCs were grafted by lactic acid (SNCs-g-LA) in order to enhance compatibility and dispersity of SNCs in PLA matrix. This was carried out by esterification reaction in an organic solvent. In addition, the effect of SNCs-g-LA nanoparticles on the thermal and mechanical properties of PLA/SNCs-g-LA were determined as well. The first conclusion is that LA molecules were successfully grafted on the SNCs surface and the interfacial adhesion between PLA and SNCs increases considerably after chemical modification of SNCs by LA. Besides that, the SNCs-g-LA nanoparticles act as a nucleating agent and provide optimal nucleation sites for crystal growth. This enhanced crystallization at low SNCs-g-LA concentration levels (5 wt%), while SNCs thwarted crystallization at higher concentrations (30 wt%). In the second phase of the project

the effect of different concentrations of SNCs-g-LA (3-7 wt%) on the phase composition, phase transition and isothermal crystallization behaviour of PLA were studied. Furthermore, the correlation between induced α and α' crystalline structures and gas permeability of PLA/SNCs-g-LA nanocomposites were examined. This was carried out by crystallization of PLA/SNCs-g-LA nanocomposites at diffrent T_c (80-130 ℃) where α and α' crystalline structures of PLA were observed. The second important conclusion is that PLA nanocomposites exhibited faster crystallization kinetics and spherulite growth rate than neat PLA. The kinetic of crystallization characterization showed that by decreasing SNCs-g-LA concentration to 5 wt% and higher nuclei density and smaller spherulite crystal were observed. The $t_{1/2}$ of PLA was minimum by adding 5 wt% SNCs-g-LA nanoparticles and it decreases from 10.4 min., to 3.9 min. Therefore, it can be concluded that, 5 wt% SNCs-g-LA is an optimum concentrations and it can help both thermodynamically and kinetically to form more stable crystalline structure of PLA. Additionally, the formation of $\alpha-$crystal in PLA nanocomposites is more likely than $\alpha'-$crystal and rate of phase transition in PLA nanocomposites was higher than neat PLA. This phenomenon is more prominent in PLA nanocomposites with 5 wt% SNCs-g-LA nanoparticles. By adding 5 wt% of SNCs-g-LA nanoparticles, the T_{trans} shifts to lower temperature (100 ℃) and the degree of $\alpha-$crystal shifts to higher value compared to other SNCs-g-LA nanoparticles concentrations. Moreover, PLA spherulites of $\alpha-$crystals were accelerated by the presence of SNCs-g-LA nanoparticles. The SGR where just $\alpha-$crystal was formed showed that the size of spherulite was smaller in PLA/SNCs-g-LA (5 wt%) nanocomposite compared to neat PLA. Additionally, the phase transition temperature decreases with decreasing SNCs-g-LA concentration to 5 wt%. By adding only 5 wt% SNCs-g-LA nanoparticles the quantity of α crystalline structures increases in PLA nanocomposites. The enhancement of the both α and α' crystal structures of PLA nanocomposites considerably decreased the oxygen (70%) and water vapor (50%) permeability of PLA nanocomposites. In the third part of project, it was intended to determine the effect of SNCs-g-LA varying in content (3-7 wt %) on the water vapor and oxygen permeability of PLA. All samples are isothermally crystallized at 130 ℃ for different crystallization time, where α crystal structure was observed. Then, the water vapor and oxygen permeability of all PLA nanocomposites were measured. The third conclusion is that the time of evaluation and content of $\alpha-$crystal structure were decreased and increased respectively in PLA/SNCs-g-LA nanocomposites. In addition, the PLA/SNCs-g-LA nanocomposite film had a better barrier to both water and oxygen

molecules irrespective of SNCs-g-LA content. This is attributed to the presence of highly α −crystal structure, which was increased the degree of crystallinity of the PLA nanocomposites and they acted as impermeable regions in the PLA matrix. To conclude that, the PLA/SNCs-g-LA nanocomposite films with better barrier performance developed in this study that can have tremendous potential for food packaging applications. Finally in the last part of this project, the effect of SNCs-g-LA (5 wt%) on the soil burial degradation of PLA was studied. The results showed that the degradation of PLA/SNCs-g-LA nanocomposites is higher than neat PLA. However, the degradation rate of PLA/SNCs-g-LA was slightly lower than PLA/SNCs and the disruption extending to the surface and inside of PLA/SNCs-g-LA was somewhat less than that of PLA/SNCs. With increasing the degradation time, the disruption extending to the surface and inside of both nanocomposites showed an increased trend.

8. Summary of Major Contributions (Publications)

1.S.S. Zamir, M.R. Frouzanmehr, M. Nagalakshmaiah, A. Ajji, M. Robert, S. Elkoun, Chemical compatibility of lactic acid-grafted starch nanocrystals (SNCs) with polylactic acid (PLA), Polym. Bull. (2018).

2. S.S.Zamir, A.Ajji, M.Robert and S.Elkoun, Phase transition and crystallization behaviour of grafted starch nanocrystals in PLA nanocomposites, polymer crystallinity (Under review).

3. S.S.Zamir, A.Ajji, M.Robert and S.Elkoun, Crystallinity and Gas permeability of Poly (lactic acid)/ Starch nanocrystals Nanocomposites, polymer composite (Under review).

4.S.S.Zamir, B.Fathi, A.Ajji, M.Robert and S.Elkoun, Biodegradation of PLA/grafted SNCs Nanocomposite in Soil, polymer degradation and stability (Under review).

9. Recommendation

The following topics are suggested for further investigation:

In this thesis, solvent casting was used to ensure the good dispersion of SNCs-g-LA in PLA matrix. However solvent casting is not cost effective process. Therefore, it would be interesting to develop an industrially viable cost-effective processing technology for manufacturing of PLA/SNCs-g-LA nanocomposites by making master batch of SNCs-g-LA nanoparticles and PLA nanocomposites and study different properties of shear flow-induced crystallization of PLA/SNCs-g-LA nanocomposite such as:

- ✓ Thermomechanical and rheological behaviour of shear flow-induced crystallization of PLA/SNCs-g-LA nanocomposite.
- ✓ Crystallinity and crystallization behaviour of shear flow-induced crystallization of PLA/SNCs-g-LA nanocomposite at different crystallization time and temperature and determine the optimum crystallization time and temperature.
- ✓ Oxygen and water vapor gas barrier properties of the shear flow-induced crystallization of PLA/SNCs-g-LA nanocomposite at the optimum crystallization time and temperature.
- ✓ Soil burial degradation of the shear flow-induced crystallization of PLA/SNCs-g-LA nanocomposite.

References

[1] B. Gupta, N. Revagade, J. Hilborn, Poly(lactic acid) fiber: An overview, Progress in Polymer Science. 32 (2007) 455–482.

[2] K. Madhavan Nampoothiri, N.R. Nair, R.P. John, An overview of the recent developments in polylactide (PLA) research, Bioresour. Technol. 101 (2010) 8493–8501.

[3] R. Mehta, V. Kumar, H. Bhunia, S.N. Upadhyay, Synthesis of Poly(Lactic Acid): A Review, Journal of Macromolecular Science, Part C: Polymer Reviews. 45 (2005) 325–349.

[4] T. Niranjana Prabhu, K. Prashantha, A review on present status and future challenges of starch based polymer films and their composites in food packaging applications, Polymer Composites. 39 (2018) 2499–2522.

[5] R. Auras, B. Harte, S. Selke, An Overview of Polylactides as Packaging Materials, Macromolecular Bioscience. 4 (2004) 835–864.

[6] V. Siracusa, P. Rocculi, S. Romani, M.D. Rosa, Biodegradable polymers for food packaging: a review, Trends in Food Science & Technology. 19 (2008) 634–643.

[7] D. LeCorre, J. Bras, A. Dufresne, Influence of botanic origin and amylose content on the morphology of starch nanocrystals, Journal of Nanoparticle Research. 13 (2011) 7193–7208. [8] A.V. Janorkar, A.T. Metters, D.E. Hirt, Modification of Poly(lactic acid) Films: Enhanced Wettability from Surface-Confined Photografting and Increased Degradation Rate Due to an Artifact of the Photografting Process, Macromolecules. 37 (2004) 9151–9159.

[9] H. Angellier, L. Choisnard, S. Molina-Boisseau, P. Ozil, A. Dufresne, Optimization of the Preparation of Aqueous Suspensions of Waxy Maize Starch Nanocrystals Using a Response Surface Methodology, Biomacromolecules. 5 (2004) 1545–1551.

[10] A. Dufresne, Polysaccharide nano crystal reinforced nanocomposites, Canadian Journal of Chemistry. 86 (2008) 484–494.

[11] T.N. Prabhu, K. Prashantha, A review on present status and future challenges of starch based polymer films and their composites in food packaging applications, Polymer Composites. 39 (2018) 2499–2522.

[12] S. Saeidlou, M.A. Huneault, H. Li, C.B. Park, Poly(lactic acid) crystallization, Progress in Polymer Science. 37 (2012) 1657–1677.

[13] J. Muller, C. González-Martínez, A. Chiralt, Combination of Poly(lactic) Acid and Starch for Biodegradable Food Packaging, Materials. 10 (2017) 952.

[14] M.L. Di Lorenzo, Crystallization behavior of poly(l-lactic acid), European Polymer Journal. 41 (2005) 569–575.

[15] Crystal Modifications and Thermal Behavior of Poly(l-lactic acid) Revealed by Infrared Spectroscopy - Macromolecules (ACS Publications), (n.d.). http://pubs.acs.org/doi/abs/10.1021/ma051232r (accessed August 1, 2016).

[16] J. Zhang, H. Tsuji, I. Noda, Y. Ozaki, Weak Intermolecular Interactions during the Melt Crystallization of Poly(L -lactide) Investigated by Two-Dimensional Infrared Correlation Spectroscopy, The Journal of Physical Chemistry B. 108 (2004) 11514–11520.

[17] J. Zhang, K. Tashiro, H. Tsuji, A.J. Domb, Disorder-to-Order Phase Transition and Multiple Melting Behavior of Poly(L -lactide) Investigated by Simultaneous Measurements of WAXD and DSC, Macromolecules. 41 (2008) 1352–1357.

[18] T. Kawai, N. Rahman, G. Matsuba, K. Nishida, T. Kanaya, M. Nakano, H. Okamoto, J. Kawada, A. Usuki, N. Honma, K. Nakajima, M. Matsuda, Crystallization and Melting Behavior of Poly (L -lactic Acid), Macromolecules. 40 (2007) 9463–9469.

[19] W. Hoogsteen, A.R. Postema, A.J. Pennings, G. Ten Brinke, P. Zugenmaier, Crystal structure, conformation and morphology of solution-spun poly(L-lactide) fibers, Macromolecules. 23 (1990) 634–642.
[20] R. Vasanthakumari, A.J. Pennings, Crystallization kinetics of poly(l-lactic acid), Polymer. 24 (1983) 175–178.
[21] H. Abe, Y. Kikkawa, Y. Inoue, Y. Doi, Morphological and Kinetic Analyses of Regime Transition for Poly[(*S*)-lactide] Crystal Growth, Biomacromolecules. 2 (2001) 1007–1014.
[22] M.L. Di Lorenzo, Determination of spherulite growth rates of poly(l-lactic acid) using combined isothermal and non-isothermal procedures, Polymer. 42 (2001) 9441–9446.
[23] H.D. Keith, F.J. Padden, A discussion of spherulitic crystallization and spherulitic morphology in high polymers, Polymer. 27 (1986) 1463–1471.
[24] M. Yasuniwa, T. Satou, Multiple melting behavior of poly(butylene succinate). I. Thermal analysis of melt-crystallized samples, Journal of Polymer Science Part B: Polymer Physics. 40 (2002) 2411–2420.
[25] M. Yasuniwa, S. Tsubakihara, K. Iura, Y. Ono, Y. Dan, K. Takahashi, Crystallization behavior of poly(l-lactic acid), Polymer. 47 (2006) 7554–7563.
[26] R. Androsch, C. Schick, M.L. Di Lorenzo, Kinetics of Nucleation and Growth of Crystals of Poly(l-lactic acid), in: Advances in Polymer Science, 2017.
[27] T. Liu, J. Petermann, C. He, Z. Liu, T.-S. Chung, Transmission Electron Microscopy Observations on Lamellar Melting of Cold-Crystallized Isotactic Polystyrene, Macromolecules. 34 (2001) 4305–4307.
[28] R.K. Verma, V. Velikov, R.G. Kander, H. Marand, B. Chu, B.S. Hsiao, SAXS studies of lamellar level morphological changes during crystallization and melting in PEEK, Polymer. 37 (1996) 5357–5365.
[29] M. Jamshidian, E.A. Tehrany, M. Imran, M. Jacquot, S. Desobry, Poly-Lactic Acid: Production, Applications, Nanocomposites, and Release Studies, Comprehensive Reviews in Food Science and Food Safety. 9 (2010) 552–571.
[30] P. Pan, W. Kai, B. Zhu, T. Dong, Y. Inoue, Polymorphous Crystallization and Multiple Melting Behavior of Poly(l-lactide): Molecular Weight Dependence, Macromolecules. 40 (2007) 6898–6905.
[31] M.L.D. Lorenzo, Calorimetric analysis of the multiple melting behavior of poly(L-lactic acid), Journal of Applied Polymer Science. 100 (2006) 3145–3151.
[32] L. Wu, H. Hou, Isothermal cold crystallization and melting behaviors of poly(L-lactic acid)s prepared by melt polycondensation, Journal of Applied Polymer Science. 115 (2010) 702–708.
[33] P. Pan, B. Zhu, W. Kai, S. Serizawa, M. Iji, Y. Inoue, Crystallization behavior and mechanical properties of bio-based green composites based on poly(L-lactide) and kenaf fiber, Journal of Applied Polymer Science. 105 (2007) 1511–1520.
[34] A. Guinault, C. Sollogoub, S. Domenek, A. Grandmontagne, V. Ducruet, Influence of crystallinity on gas barrier and mechanical properties of pla food packaging films, International Journal of Material Forming. 3 (2010) 603–606.
[35] J.J. Kolstad, Crystallization kinetics of poly(L-lactide-co-meso-lactide), Journal of Applied Polymer Science. 62 (1996) 1079–1091.
[36] A.M. Harris, E.C. Lee, Improving mechanical performance of injection molded PLA by controlling crystallinity, Journal of Applied Polymer Science. 107 (2008) 2246–2255.
[37] M. Nofar, W. Zhu, C.B. Park, J. Randall, Crystallization Kinetics of Linear and Long-Chain-Branched Polylactide, Industrial & Engineering Chemistry Research. 50 (2011) 13789–13798.
[38] N. Najafi, M.C. Heuzey, P.J. Carreau, Crystallization behavior and morphology of polylactide and PLA/clay nanocomposites in the presence of chain extenders, Polymer Engineering & Science. 53 (2013) 1053–1064.
[39] J.Y. Nam, S. Sinha Ray, M. Okamoto, Crystallization Behavior and Morphology of Biodegradable Polylactide/Layered Silicate Nanocomposite, Macromolecules. 36 (2003) 7126–7131.
[40] M. Pluta, Melt compounding of polylactide/organoclay: Structure and properties of nanocomposites, Journal of Polymer Science Part B: Polymer Physics. 44 (2006) 3392–3405.
[41] S. Barrau, C. Vanmansart, M. Moreau, A. Addad, G. Stoclet, J.-M. Lefebvre, R. Seguela, Crystallization Behavior of Carbon Nanotube−Polylactide Nanocomposites, Macromolecules. 44 (2011) 6496–6502.
[42] Z. Su, Y. Liu, W. Guo, Q. Li, C. Wu, Crystallization Behavior of Poly(Lactic Acid) Filled with Modified Carbon Black, Journal of Macromolecular Science, Part B. 48 (2009) 670–683.
[43] A.P. Mathew, K. Oksman, M. Sain, The effect of morphology and chemical characteristics of cellulose reinforcements on the crystallinity of polylactic acid, Journal of Applied Polymer Science. 101 (2006) 300–310.

[44] J. Bonilla, E. Fortunati, M. Vargas, A. Chiralt, J.M. Kenny, Effects of chitosan on the physicochemical and antimicrobial properties of PLA films, Journal of Food Engineering. 119 (2013) 236–243.
[45] T. Ke, X. Sun, Melting behavior and crystallization kinetics of starch and poly(lactic acid) composites, Journal of Applied Polymer Science. 89 (2003) 1203–1210.
[46] Z. Xiong, Y. Yang, J. Feng, X. Zhang, C. Zhang, Z. Tang, J. Zhu, Preparation and characterization of poly(lactic acid)/starch composites toughened with epoxidized soybean oil, Carbohydrate Polymers. 92 (2013) 810–816.
[47] H. Angellier, L. Choisnard, S. Molina-Boisseau, P. Ozil, A. Dufresne, Optimization of the Preparation of Aqueous Suspensions of Waxy Maize Starch Nanocrystals Using a Response Surface Methodology, Biomacromolecules. 5 (2004) 1545–1551.
[48] A. Dufresne, Polysaccharide nano crystal reinforced nanocomposites, Canadian Journal of Chemistry. 86 (2008) 484–494.
[49] N. Lin, J. Huang, P.R. Chang, D.P. Anderson, J. Yu, Preparation, Modification, and Application of Starch Nanocrystals in Nanomaterials: A Review, J. Nanomaterials. 2011 (2011) 20:1–20:13.
[50] L. Averous, N. Boquillon, Biocomposites based on plasticized starch: thermal and mechanical behaviours, Carbohydrate Polymers. 56 (2004) 111–122.
[51] A.H. Mistry, S.J. Schmidt, S.R. Eckhoff, J.W. Sutherland, Alkali Extraction of Starch from Corn Flour, Starch - Stärke. 44 (1992) 284–288.
[52] Starch nanocrystals and starch nanoparticles from waxy maize as nanoreinforcement: A comparative study - PDF Free Download, Kundoc.Com. (n.d.). https://kundoc.com/pdf-starch-nanocrystals-and-starch-nanoparticles-from-waxy-maize-as-nanoreinforcemen.html (accessed April 11, 2019).
[53] P.C. Belibi, T.J. Daou, J.M.B. Ndjaka, B. Nsom, L. Michelin, B. Durand, A Comparative Study of Some Properties of Cassava and Tree Cassava Starch Films, Physics Procedia. 55 (2014) 220–226.
[54] S. Bel Haaj, W. Thielemans, A. Magnin, S. Boufi, Starch nanocrystals and starch nanoparticles from waxy maize as nanoreinforcement: A comparative study, Carbohydr Polym. 143 (2016) 310–317.
[55] E. Kristo, C. Biliaderis, Physical properties of starch nanocrystal-reinforced pullulan films, Carbohydrate Polymers. 68 (2007) 146–158.
[56] W. Thielemans, M.N. Belgacem, A. Dufresne, Starch Nanocrystals with Large Chain Surface Modifications, Langmuir. 22 (2006) 4804–4810.
[57] W. Thitisomboon, P. Opaprakasit, N. Jaikaew, S. Boonyarattanakalin, Characterizations of modified cassava starch with long chain fatty acid chlorides obtained from esterification under low reaction temperature and its PLA blending, Journal of Macromolecular Science, Part A. 55 (2018) 253–259.
[58] Y.F. Zuo, J. Gu, Z. Qiao, H. Tan, J. Cao, Y. Zhang, Effects of dry method esterification of starch on the degradation characteristics of starch/polylactic acid composites, Int. J. Biol. Macromol. 72 (2015) 391–402.
[59] H. Wang, X. Sun, P. Seib, Mechanical properties of poly(lactic acid) and wheat starch blends with methylenediphenyl diisocyanate, Journal of Applied Polymer Science. 84 (2002) 1257–1262.
[60] E. Ojogbo, R. Blanchard, T. Mekonnen, Hydrophobic and Melt Processable Starch-Laurate Esters: Synthesis, Structure–Property Correlations, Journal of Polymer Science Part A: Polymer Chemistry. 56 (2018) 2611–2622.
[61] R. Acioli-Moura, X.S. Sun, Thermal degradation and physical aging of poly(lactic acid) and its blends with starch, Polymer Engineering & Science. 48 (2008) 829–836.
[62] Y. Zuo, J. Gu, L. Yang, Z. Qiao, H. Tan, Y. Zhang, Preparation and characterization of dry method esterified starch/polylactic acid composite materials, International Journal of Biological Macromolecules. 64 (2014) 174–180.
[63] V.H. Orozco, W. Brostow, W. Chonkaew, B.L. López, Preparation and Characterization of Poly(Lactic Acid)-g-Maleic Anhydride + Starch Blends, Macromolecular Symposia. 277 (2009) 69–80.
[64] S.W. Hwang, S.B. Lee, C.K. Lee, J.Y. Lee, J.K. Shim, S.E.M. Selke, H. Soto-Valdez, L. Matuana, M. Rubino, R. Auras, Grafting of maleic anhydride on poly(L-lactic acid). Effects on physical and mechanical properties, Polymer Testing. 31 (2012) 333–344.
[65] Z. Xiong, C. Li, S. Ma, J. Feng, Y. Yang, R. Zhang, J. Zhu, The properties of poly(lactic acid)/starch blends with a functionalized plant oil: Tung oil anhydride, Carbohydrate Polymers. 95 (2013) 77–84.
[66] Y. Ohya, S. Maruhashi, T. Ouchi, Preparation of poly(lactic acid)-grafted amylose through the trimethylsilyl protection method and its biodegradation, Macromolecular Chemistry and Physics. 199 (1998) 2017–2022.

[67] Q. Gong, L.-Q. Wang, K. Tu, In situ polymerization of starch with lactic acid in aqueous solution and the microstructure characterization, Carbohydrate Polymers. 64 (2006) 501–509.
[68] N. Le Bolay, A. Lamure, N. Gallego Leis, A. Subhani, How to combine a hydrophobic matrix and a hydrophilic filler without adding a compatibilizer – Co-grinding enhances use properties of Renewable PLA–starch composites, Chemical Engineering and Processing: Process Intensification. 56 (2012) 1–9.
[69] O.C. Wokadala, N.M. Emmambux, S.S. Ray, Inducing PLA/starch compatibility through butyl-etherification of waxy and high amylose starch, Carbohydrate Polymers. 112 (2014) 216–224.
[70] M.A. Huneault, H. Li, Preparation and properties of extruded thermoplastic starch/polymer blends, Journal of Applied Polymer Science. 126 (2012) E96–E108.
[71] O. Martin, L. Avérous, Poly(lactic acid): plasticization and properties of biodegradable multiphase systems, Polymer. 42 (2001) 6209–6219.
[72] W.Y. Jang, B.Y. Shin, T.J. Lee, R. Narayan, Thermal Properties and Morphology of Biodegradable PLA/Starch Compatibilized Blends, (n.d.) 8.
[73] J.W. Park, S.S. Im, S.H. Kim, Y.H. Kim, Biodegradable polymer blends of poly(L-lactic acid) and gelatinized starch, Polymer Engineering & Science. 40 (2000) 2539–2550.
[74] K.S. Kang, S.I. Lee, T.J. Lee, R. Narayan, B.Y. Shin, Effect of biobased and biodegradable nucleating agent on the isothermal crystallization of poly(lactic acid), Korean Journal of Chemical Engineering. 25 (2008) 599–608.
[75] J. Cai, M. Liu, L. Wang, K. Yao, S. Li, H. Xiong, Isothermal crystallization kinetics of thermoplastic starch/poly(lactic acid) composites, Carbohydrate Polymers. 86 (2011) 941–947.
[76] K. Hamad, M. Kaseem, H.W. Yang, F. Deri, Y.G. Ko, Properties and medical applications of polylactic acid: A review, Express Polymer Letters. 9 (2015) 435–455.
[77] J.R. Dorgan, H. Lehermeier, M. Mang, Thermal and Rheological Properties of Commercial-Grade Poly(Lactic Acid)s, Journal of Polymers and the Environment. 8 (2000) 1–9.
[78] S. Kanehashi, A. Kusakabe, S. Sato, K. Nagai, Analysis of permeability; solubility and diffusivity of carbon dioxide; oxygen; and nitrogen in crystalline and liquid crystalline polymers, Journal of Membrane Science. 365 (2010) 40–51.
[79] L. Bao, J.R. Dorgan, D. Knauss, S. Hait, N.S. Oliveira, I.M. Maruccho, Gas permeation properties of poly(lactic acid) revisited, Journal of Membrane Science. 285 (2006) 166–172.
[80] H. Sawada, Y. Takahashi, S. Miyata, S. Kanehashi, S. Sato, K. Nagai, Gas Transport Properties and Crystalline Structures of Poly(lactic acid) Membranes, Transactions of the Materials Research Society of Japan. 35 (2010) 241–246.
[81] G. Colomines, V. Ducruet, C. Courgneau, A. Guinault, S. Domenek, Barrier properties of poly(lactic acid) and its morphological changes induced by aroma compound sorption, Polymer International. 59 (2010) 818–826.
[82] M. Drieskens, R. Peeters, J. Mullens, D. Franco, P.J. Lemstra, D.G. Hristova-Bogaerds, Structure versus properties relationship of poly(lactic acid). I. Effect of crystallinity on barrier properties, Journal of Polymer Science Part B: Polymer Physics. 47 (2009) 2247–2258.
[83] M. Cocca, M.L.D. Lorenzo, M. Malinconico, V. Frezza, Influence of crystal polymorphism on mechanical and barrier properties of poly(l-lactic acid), European Polymer Journal. 47 (2011) 1073–1080.
[84] J.-H. Chang, Y.U. An, G.S. Sur, Poly(lactic acid) nanocomposites with various organoclays. I. Thermomechanical properties, morphology, and gas permeability, Journal of Polymer Science Part B: Polymer Physics. 41 (2003) 94–103.
[85] S. Sato, T. Nyuui, G. Matsuba, K. Nagai, Correlation between interlamellar amorphous structure and gas permeability in poly(lactic acid) films, Journal of Applied Polymer Science. 131 (2014).
[86] A. Sangroniz, A. Chaos, Y.M. Garcia, J. Fernández, M. Iriarte, A. Etxeberria, Improving the barrier character of polylactide/phenoxy immiscible blend using poly(lactide-co-ε-caprolactone) block copolymer as a compatibilizer, Journal of Applied Polymer Science. 134 (2017) 45396.
[87] Multi-scale analysis of the impact of polylactide morphology on gas barrier properties, Polymer. 108 (2017) 163–172.
[88] N.S. Oliveira, J. Dorgan, J. a. P. Coutinho, A. Ferreira, J.L. Daridon, I.M. Marrucho, Gas solubility of carbon dioxide in poly(lactic acid) at high pressures: Thermal treatment effect, Journal of Polymer Science Part B: Polymer Physics. 45 (2007) 616–625.

[89] R. Shogren, Water vapor permeability of biodegradable polymers, Journal of Environmental Polymer Degradation. 5 (1997) 91–95.
[90] Z. Duan, N.L. Thomas, Water vapour permeability of poly(lactic acid): Crystallinity and the tortuous path model, Journal of Applied Physics. 115 (2014) 064903.
[91] U. Sonchaeng, F. Iñiguez-Franco, R. Auras, S. Selke, M. Rubino, L.-T. Lim, Poly(lactic acid) mass transfer properties, Progress in Polymer Science. 86 (2018) 85–121.
[92] J.-W. Rhim, S.-I. Hong, C.-S. Ha, Tensile, water vapor barrier and antimicrobial properties of PLA/nanoclay composite films, LWT - Food Science and Technology. 42 (2009) 612–617.
[93] C. Thellen, C. Orroth, D. Froio, D. Ziegler, J. Lucciarini, R. Farrell, N.A. D'Souza, J.A. Ratto, Influence of montmorillonite layered silicate on plasticized poly(l-lactide) blown films, Polymer. 46 (2005) 11716–11727.
[94] C. Courgneau, S. Domenek, R. Lebossé, A. Guinault, L. Avérous, V. Ducruet, Effect of crystallization on barrier properties of formulated polylactide, Polymer International. 61 (2012) 180–189.
[95] B. Şengül, N. Dilsiz, Barrier properties of polylactic acid/layered silicate nanocomposites for food contact applications, Polymer Science Series A. 56 (2014) 896–906.
[96] L.D. Maio, P. Scarfato, M.R. Milana, R. Feliciani, M. Denaro, G. Padula, L. Incarnato, Bionanocomposite Polylactic Acid/Organoclay Films: Functional Properties and Measurement of Total and Lactic Acid Specific Migration, Packaging Technology and Science. 27 (2014) 535–547.
[97] E. Picard, E. Espuche, R. Fulchiron, Effect of an organo-modified montmorillonite on PLA crystallization and gas barrier properties, Applied Clay Science. 53 (2011) 58–65.
[98] H.W. Xiao, P. Li, X. Ren, T. Jiang, J.-T. Yeh, Isothermal crystallization kinetics and crystal structure of poly(lactic acid): Effect of triphenyl phosphate and talc, Journal of Applied Polymer Science. 118 (2010) 3558–3569.
[99] S. Jain, M.M. Reddy, A.K. Mohanty, M. Misra, A.K. Ghosh, A New Biodegradable Flexible Composite Sheet from Poly(lactic acid)/Poly(ε-caprolactone) Blends and Micro-Talc, Macromolecular Materials and Engineering. 295 (2010) 750–762.
[100] A. Šturcová, G.R. Davies, S.J. Eichhorn, Elastic Modulus and Stress-Transfer Properties of Tunicate Cellulose Whiskers, Biomacromolecules. 6 (2005) 1055–1061.
[101] E. Fortunati, M. Peltzer, I. Armentano, A. Jiménez, J.M. Kenny, Combined effects of cellulose nanocrystals and silver nanoparticles on the barrier and migration properties of PLA nano-biocomposites, Journal of Food Engineering. 118 (2013) 117–124.
[102] M.P. Arrieta, E. Fortunati, F. Dominici, E. Rayón, J. López, J.M. Kenny, PLA-PHB/cellulose based films: Mechanical, barrier and disintegration properties, Polymer Degradation and Stability. 107 (2014) 139–149.
[103] N.S. Murthy, A.M. Kotliar, J.P. Sibilia, W. Sacks, Structure and properties of talc-filled polyethylene and nylon 6 films, Journal of Applied Polymer Science. 31 (1986) 2569–2582.
[104] E. Fortunati, M. Peltzer, I. Armentano, L. Torre, A. Jiménez, J.M. Kenny, Effects of modified cellulose nanocrystals on the barrier and migration properties of PLA nano-biocomposites, Carbohydrate Polymers. 90 (2012) 948–956.
[105] D. Plackett, H. Anturi, M. Hedenqvist, M. Ankerfors, M. Gällstedt, T. Lindström, I. Siró, Physical properties and morphology of films prepared from microfibrillated cellulose and microfibrillated cellulose in combination with amylopectin, Journal of Applied Polymer Science. (2010) n/a-n/a.
[106] E. Espino-Pérez, J. Bras, V. Ducruet, A. Guinault, A. Dufresne, S. Domenek, Influence of chemical surface modification of cellulose nanowhiskers on thermal, mechanical, and barrier properties of poly(lactide) based bionanocomposites, European Polymer Journal. 49 (2013) 3144–3154.
[107] J. Trifol, D. Plackett, C. Sillard, P. Szabo, J. Bras, A.E. Daugaard, Hybrid poly(lactic acid)/nanocellulose/nanoclay composites with synergistically enhanced barrier properties and improved thermomechanical resistance: Hybrid poly(lactic acid)/nanocellulose/nanoclay composites, Polymer International. 65 (2016) 988–995.
[108] Y. Fan, H. Fukuzumi, T. Saito, A. Isogai, Comparative characterization of aqueous dispersions and cast films of different chitin nanowhiskers/nanofibers, International Journal of Biological Macromolecules. 50 (2012) 69–76.
[109] H. Angellier, S. Molina-Boisseau, L. Lebrun, A. Dufresne, Processing and Structural Properties of Waxy Maize Starch Nanocrystals Reinforced Natural Rubber, Macromolecules. 38 (2005) 3783–3792.

[110] N.L. García, L. Ribba, A. Dufresne, M.I. Aranguren, S. Goyanes, Physico-Mechanical Properties of Biodegradable Starch Nanocomposites, Macromolecular Materials and Engineering. 294 (2009) 169–177.
[111] Z. Yin, J. Zeng, C. Wang, Z. Pan, Preparation and Properties of Cross-Linked Starch Nanocrystals/Polylactic Acid Nanocomposites, International Journal of Polymer Science. 2015 (2015) 1–5.
[112] C.M.O. Müller, A.T.N. Pires, F. Yamashita, Characterization of thermoplastic starch/poly(lactic acid) blends obtained by extrusion and thermopressing, Journal of the Brazilian Chemical Society. (2012).
[113] M.L. Sanyang, S.M. Sapuan, M. Jawaid, M.R. Ishak, J. Sahari, Development and characterization of sugar palm starch and poly(lactic acid) bilayer films, Carbohydrate Polymers. 146 (2016) 36–45.
[114] J. Muller, C. González-Martínez, A. Chiralt, Poly(lactic) acid (PLA) and starch bilayer films, containing cinnamaldehyde, obtained by compression moulding, European Polymer Journal. 95 (2017) 56–70.
[115] R. Ortega-Toro, I. Morey, P. Talens, A. Chiralt, Active bilayer films of thermoplastic starch and polycaprolactone obtained by compression molding, Carbohydrate Polymers. 127 (2015) 282–290.
[116] D. Battegazzore, J. Alongi, A. Frache, Poly(lactic acid)-Based Composites Containing Natural Fillers: Thermal, Mechanical and Barrier Properties, Journal of Polymers and the Environment. 22 (2014) 88–98.
[117] A. Bher, I. Uysal Unalan, R. Auras, M. Rubino, C. Schvezov, Toughening of Poly(lactic acid) and Thermoplastic Cassava Starch Reactive Blends Using Graphene Nanoplatelets, Polymers. 10 (2018) 95.
[118] K.-L.G. Ho, A.L.P. Iii, A. Gadea-Rivas, J.A. Briceno, A. Rojas, Degradation of Polylactic Acid (PLA) Plastic in Costa Rican Soil and Iowa State University Compost Rows, (n.d.) 5.
[119] A. Calmon, S. Guillaume, V. Bellon-Maurel, P. Feuilloley, F. Silvestre, Evaluation of Material Biodegradability in Real Conditions-Development of a Burial Test and an Analysis Methodology Based on Numerical Vision, (n.d.) 10.
[120] G. Gallet, R. Lempiäinen, S. Karlsson, Characterisation by solid phase microextraction–gas chromatography–mass spectrometry of matrix changes of poly(l-lactide) exposed to outdoor soil environment, Polymer Degradation and Stability. 71 (2000) 147–151.
[121] H. Urayama, T. Kanamori, Y. Kimura, Properties and Biodegradability of Polymer Blends of Poly(L-lactide)s with Different Optical Purity of the Lactate Units, (n.d.) 6.
[122] R.L. Shogren, W.M. Doane, D. Garlotta, J.W. Lawton, J.L. Willett, Biodegradation of starch/polylactic acid/poly(hydroxyester-ether) composite bars in soil, Polymer Degradation and Stability. 79 (2003) 405–411.
[123] W. Phetwarotai, P. Potiyaraj, D. Aht-Ong, Biodegradation of Polylactide and Gelatinized Starch Blend Films Under Controlled Soil Burial Conditions, Journal of Polymers and the Environment. 21 (2013) 95–107.
[124] Q. Shi, C. Chen, L. Gao, L. Jiao, H. Xu, W. Guo, Physical and degradation properties of binary or ternary blends composed of poly (lactic acid), thermoplastic starch and GMA grafted POE, Polymer Degradation and Stability. 96 (2011) 175–182.
[125] R. Iovino, R. Zullo, M.A. Rao, L. Cassar, L. Gianfreda, Biodegradation of poly(lactic acid)/starch/coir biocomposites under controlled composting conditions, Polymer Degradation and Stability. 93 (2008) 147–157.
[126] Y. Zuo, J. Gu, L. Yang, Z. Qiao, H. Tan, Y. Zhang, Synthesis and characterization of maleic anhydride esterified corn starch by the dry method, International Journal of Biological Macromolecules. 62 (2013) 241–247.
[127] J.F. Jenck, F. Agterberg, M.J. Droescher, Products and processes for a sustainable chemical industry: a review of achievements and prospects, Green Chemistry. 6 (2004) 544.
[128] K. Kümmerer, Sustainable from the very beginning: rational design of molecules by life cycle engineering as an important approach for green pharmacy and green chemistry, Green Chemistry. 9 (2007) 899.
[129] R.A. Auras, B. Harte, S. Selke, R. Hernandez, Mechanical, Physical, and Barrier Properties of Poly(Lactide) Films, Journal of Plastic Film & Sheeting. 19 (2003) 123–135.
[130] R. P. Pawar, S. U. Tekale, S. U. Shisodia, J. T. Totre, A. J. Domb, Biomedical Applications of Poly(Lactic Acid), Recent Patents on Regenerative Medicine. 4 (2014) 40–51.
[131] B. Li, S.-C. Chen, Z.-C. Qiu, K.-K. Yang, S.-P. Tang, W. Yu, Y.-Z. Wang, Synthesis of poly(lactic acid-b-p-dioxanone) block copolymers from ring opening polymerization of p-dioxanone by poly(L-lactic acid) macroinitiators, Polymer Bulletin. 61 (2008) 139–146.
[132] M. Hirata, Y. Kimura, Thermomechanical properties of stereoblock poly(lactic acid)s with different PLLA/PDLA block compositions, Polymer. 49 (2008) 2656–2661.

[133] S.-Y. Gu, K. Zhang, J. Ren, H. Zhan, Melt rheology of polylactide/poly(butylene adipate-co-terephthalate) blends, Carbohydrate Polymers. 74 (2008) 79–85.
[134] G. Rohman, F. Lauprêtre, S. Boileau, P. Guérin, D. Grande, Poly(d,l-lactide)/poly(methyl methacrylate) interpenetrating polymer networks: Synthesis, characterization, and use as precursors to porous polymeric materials, Polymer. 48 (2007) 7017–7028.
[135] M. Pluta, J.K. Jeszka, G. Boiteux, Polylactide/montmorillonite nanocomposites: Structure, dielectric, viscoelastic and thermal properties, European Polymer Journal. 43 (2007) 2819–2835.
[136] K. Gorna, M. Hund, M. Vučak, F. Gröhn, G. Wegner, Amorphous calcium carbonate in form of spherical nanosized particles and its application as fillers for polymers, Materials Science and Engineering: A. 477 (2008) 217–225.
[137] N.C. Bleach, S.N. Nazhat, K.E. Tanner, M. Kellomäki, P. Törmälä, Effect of filler content on mechanical and dynamic mechanical properties of particulate biphasic calcium phosphate—polylactide composites, Biomaterials. 23 (2002) 1579–1585.
[138] R. Hoover, T. Hughes, H.J. Chung, Q. Liu, Composition, molecular structure, properties, and modification of pulse starches: A review, Food Research International. 43 (2010) 399–413.
[139] D. Le Corre, J. Bras, A. Dufresne, Starch Nanoparticles: A Review, Biomacromolecules. 11 (2010) 1139–1153.
[140] M.A. Huneault, H. Li, Morphology and properties of compatibilized polylactide/thermoplastic starch blends, Polymer. 48 (2007) 270–280.
[141] H. Namazi, A. Dadkhah, Convenient method for preparation of hydrophobically modified starch nanocrystals with using fatty acids, Carbohydrate Polymers. 79 (2010) 731–737.
[142] G. Moad, Chemical modification of starch by reactive extrusion, Progress in Polymer Science. 36 (2011) 218–237.
[143] H. Angellier, S. Molina-Boisseau, M.N. Belgacem, A. Dufresne, Surface Chemical Modification of Waxy Maize Starch Nanocrystals, Langmuir. 21 (2005) 2425–2433.
[144] T. Ouchi, T. Uchida, Y. Ohya, Synthesis of Poly(L-lactide) with One Terminal D-Glucose Residue and Wettability of Its Film Surface, Macromolecular Bioscience. 1 (2001) 371–375.
[145] G.F. Fanta, F.C. Felker, R.L. Shogren, Graft polymerization of acrylonitrile onto spherocrystals formed from jet cooked cornstarch, Carbohydrate Polymers. 56 (2004) 77–84.
[146] P. Dubois, M. Krishnan, R. Narayan, Aliphatic polyester-grafted starch-like polysaccharides by ring-opening polymerization, Polymer. 40 (1999) 3091–3100.
[147] M. Avella, E. Martuscelli, M. Raimo, Review Properties of blends and composites based on poly(3-hydroxy)butyrate (PHB) and poly(3-hydroxybutyrate-hydroxyvalerate) (PHBV) copolymers, Journal of Materials Science. 35 (2000) 523–545.
[148] L. Chen, Y. Ni, X. Bian, X. Qiu, X. Zhuang, X. Chen, X. Jing, A novel approach to grafting polymerization of ε-caprolactone onto starch granules, Carbohydrate Polymers. 60 (2005) 103–109.
[149] L. Chen, X. Qiu, M. Deng, Z. Hong, R. Luo, X. Chen, X. Jing, The starch grafted poly(l-lactide) and the physical properties of its blending composites, Polymer. 46 (2005) 5723–5729.
[150] H.-S. Xu, X.J. Dai, P.R. Lamb, Z.-M. Li, Poly(L-lactide) crystallization induced by multiwall carbon nanotubes at very low loading, Journal of Polymer Science Part B: Polymer Physics. 47 (2009) 2341–2352.
[151] S. Mattioli, M. Peltzer, E. Fortunati, I. Armentano, A. Jiménez, J.M. Kenny, Structure, gas-barrier properties and overall migration of poly(lactic acid) films coated with hydrogenated amorphous carbon layers, Carbon. 63 (2013) 274–282.
[152] R.A. Auras, S.P. Singh, J.J. Singh, Evaluation of oriented poly(lactide) polymers vs. existing PET and oriented PS for fresh food service containers, Packaging Technology and Science. 18 (2005) 207–216.
[153] R. Auras, B. Harte, S. Selke, Effect of water on the oxygen barrier properties of poly(ethylene terephthalate) and polylactide films, Journal of Applied Polymer Science. 92 (2004) 1790–1803.
[154] J. Zhang, H. Tsuji, I. Noda, Y. Ozaki, Structural Changes and Crystallization Dynamics of Poly(L -lactide) during the Cold-Crystallization Process Investigated by Infrared and Two-Dimensional Infrared Correlation Spectroscopy, Macromolecules. 37 (2004) 6433–6439.
[155] D. Sawai, T. Yokoyama, T. Kanamoto, M. Sungil, S.-H. Hyon, L.P. Myasnikova, Crystal Transformation and Development of Tensile Properties upon Drawing of Poly(L-lactic acid) by Solid-State Coextrusion: Effects of Molecular Weight, Macromolecular Symposia. 242 (2006) 93–103.

[156] C. Alemán, B. Lotz, J. Puiggali, Crystal Structure of the α-Form of Poly(L -lactide), Macromolecules. 34 (2001) 4795–4801.
[157] L. Bouapao, H. Tsuji, Stereocomplex Crystallization and Spherulite Growth of Low Molecular Weight Poly(L-lactide) and Poly(D-lactide) from the Melt, Macromolecular Chemistry and Physics. 210 (2009) 993–1002.
[158] Z. Qiu, Z. Li, Effect of Orotic Acid on the Crystallization Kinetics and Morphology of Biodegradable Poly(L -lactide) as an Efficient Nucleating Agent, Industrial & Engineering Chemistry Research. 50 (2011) 12299–12303.
[159] S. Jacobsen, H.G. Fritz, Plasticizing polylactide—the effect of different plasticizers on the mechanical properties, Polymer Engineering & Science. 39 (1999) 1303–1310.
[160] H. Xiao, L. Yang, X. Ren, T. Jiang, J.-T. Yeh, Kinetics and crystal structure of poly(lactic acid) crystallized nonisothermally: Effect of plasticizer and nucleating agent, Polymer Composites. 31 (2010) 2057–2068.
[161] B. Zhao, L. Li, F. Lu, Q. Zhai, B. Yang, C. Schick, Y. Gao, Phase transitions and nucleation mechanisms in metals studied by nanocalorimetry: A review, Thermochimica Acta. 603 (2015) 2–23.
[162] D. Libster, A. Aserin, N. Garti, Advanced nucleating agents for polypropylene, Polymers for Advanced Technologies. 18 (2007) 685–695.
[163] J. Varga, I. Mudra, G.W. Ehrenstein, Highly active thermally stable β-nucleating agents for isotactic polypropylene, Journal of Applied Polymer Science. 74 (n.d.) 2357–2368.
[164] C. Mathieu, A. Thierry, J.C. Wittmann, B. Lotz, Specificity and versatility of nucleating agents toward isotactic polypropylene crystal phases, Journal of Polymer Science Part B: Polymer Physics. 40 (n.d.) 2504–2515.
[165] M. Kristiansen, T. Tervoort, P. Smith, H. Goossens, Mechanical Properties of Sorbitol-Clarified Isotactic Polypropylene: Influence of Additive Concentration on Polymer Structure and Yield Behavior, Macromolecules. 38 (2005) 10461–10465.
[166] N. Mohmeyer, H.-W. Schmidt, P.M. Kristiansen, V. Altstädt, Influence of Chemical Structure and Solubility of Bisamide Additives on the Nucleation of Isotactic Polypropylene and the Improvement of Its Charge Storage Properties †, Macromolecules. 39 (2006) 5760–5767.
[167] F. Luo, K. Wang, N. Ning, C. Geng, H. Deng, F. Chen, Q. Fu, Y. Qian, D. Zheng, Dependence of mechanical properties on β-form content and crystalline morphology for β-nucleated isotactic polypropylene, Polymers for Advanced Technologies. 22 (n.d.) 2044–2054.
[168] H. Abe, Y. Kikkawa, Y. Inoue, Y. Doi, Morphological and Kinetic Analyses of Regime Transition for Poly[(*S*)-lactide] Crystal Growth, Biomacromolecules. 2 (2001) 1007–1014.
[169] T.-Y. Cho, G. Strobl, Temperature dependent variations in the lamellar structure of poly(l-lactide), Polymer. 47 (2006) 1036–1043.
[170] J.-Z. Xu, T. Chen, C.-L. Yang, Z.-M. Li, Y.-M. Mao, B.-Q. Zeng, B.S. Hsiao, Isothermal Crystallization of Poly(L -lactide) Induced by Graphene Nanosheets and Carbon Nanotubes: A Comparative Study, Macromolecules. 43 (2010) 5000–5008.
[171] W.-C. Lai, Thermal Behavior and Crystal Structure of Poly(L -lactic acid) with 1,3:2,4-Dibenzylidene- D -sorbitol, The Journal of Physical Chemistry B. 115 (2011) 11029–11037.
[172] P. Pan, Z. Liang, N. Nakamura, T. Miyagawa, Y. Inoue, Uracil as Nucleating Agent for Bacterial Poly[(3-Hydroxybutyrate)-co-(3-hydroxyhexanoate)] Copolymers, Macromolecular Bioscience. 9 (2009) 585–595.
[173] H.-Y. Kim, J.H. Lee, J.-Y. Kim, W.-J. Lim, S.-T. Lim, Characterization of nanoparticles prepared by acid hydrolysis of various starches, Starch - Stärke. 64 (n.d.) 367–373.
[174] H. Namazi, A. Dadkhah, Convenient method for preparation of hydrophobically modified starch nanocrystals with using fatty acids, Carbohydrate Polymers. 79 (2010) 731–737.
[175] J.-F. Zhang, X. Sun, Mechanical Properties of Poly(lactic acid)/Starch Composites Compatibilized by Maleic Anhydride, Biomacromolecules. 5 (2004) 1446–1451.
[176] J. Yu, F. Ai, A. Dufresne, S. Gao, J. Huang, P.R. Chang, Structure and Mechanical Properties of Poly(lactic acid) Filled with (Starch nanocrystal)-graft-poly(ε-caprolactone), Macromolecular Materials and Engineering. 293 (2008) 763–770.
[177] J.D. Hoffman, J.J. Weeks, Melting process and the equilibrium melting temperature of polychlorotrifluoroethylene, Journal of Research of the National Bureau of Standards Section A: Physics and Chemistry. 66A (1962) 13.

[178] M. Avrami, Kinetics of Phase Change. I General Theory, The Journal of Chemical Physics. 7 (1939) 1103–1112. doi:10.1063/1.1750380.
[179] M. Avrami, Kinetics of Phase Change. I General Theory, J. Chem. Phys. 7 (1939) 1103–1112.
[180] J.-W. Rhim, H.-M. Park, C.-S. Ha, Bio-nanocomposites for food packaging applications, Progress in Polymer Science. 38 (2013) 1629–1652.
[181] L. Yu, K. Dean, L. Li, Polymer blends and composites from renewable resources, Progress in Polymer Science. 31 (2006) 576–602.
[182] R.A. Auras, S.P. Singh, J.J. Singh, Evaluation of oriented poly(lactide) polymers vs. existing PET and oriented PS for fresh food service containers, Packaging Technology and Science. 18 (2005) 207–216.
[183] Y.S. Hu, R.Y.F. Liu, L.Q. Zhang, M. Rogunova, D.A. Schiraldi, S. Nazarenko, A. Hiltner, E. Baer, Oxygen Transport and Free Volume in Cold-Crystallized and Melt-Crystallized Poly(ethylene naphthalate), Macromolecules. 35 (2002) 7326–7337.
[184] S. Huang, H. Li, S. Jiang, X. Chen, L. An, Crystal structure and morphology influenced by shear effect of poly(l-lactide) and its melting behavior revealed by WAXD, DSC and in-situ POM, Polymer. (2011).
[185] P. Pan, Z. Liang, B. Zhu, T. Dong, Y. Inoue, Blending Effects on Polymorphic Crystallization of Poly(l-lactide), Macromolecules. 42 (2009) 3374–3380.
[186] J. Zhang, Y. Duan, H. Sato, H. Tsuji, I. Noda, S. Yan, Y. Ozaki, Crystal Modifications and Thermal Behavior of Poly(l-lactic acid) Revealed by Infrared Spectroscopy, 38 (2005) 10.
[187] A. Guinault, C. Sollogoub, S. Domenek, A. Grandmontagne, V. Ducruet, Influence of crystallinity on gas barrier and mechanical properties of pla food packaging films, Int J Mater Form. 3 (2010) 603–606.
[188] H. Abdillahi, E. Chabrat, A. Rouilly, L. Rigal, Influence of citric acid on thermoplastic wheat flour/poly(lactic acid) blends. II. Barrier properties and water vapor sorption isotherms, Industrial Crops and Products. 50 (2013) 104–111.
[189] A. Dufresne, Crystalline starch based nanoparticles, Current Opinion in Colloid & Interface Science. 19 (2014) 397–408.
[190] M. Râpă, A.C. Miteluţ, E.E. Tănase, E. Grosu, P. Popescu, M.E. Popa, J.T. Rosnes, M. Sivertsvik, R.N. Darie-Niţă, C. Vasile, Influence of chitosan on mechanical, thermal, barrier and antimicrobial properties of PLA-biocomposites for food packaging, Composites Part B: Engineering. 102 (2016) 112–121.
[191] M.D. Sanchez-Garcia, J.M. Lagaron, On the use of plant cellulose nanowhiskers to enhance the barrier properties of polylactic acid, Cellulose. 17 (2010) 987–1004.
[192] Y. Zhang, C. Rempel, Q. Liu, Thermoplastic Starch Processing and Characteristics—A Review, Critical Reviews in Food Science and Nutrition. 54 (2014) 1353–1370.
[193] M.B.K. Niazi, M. Zijlstra, A.A. Broekhuis, Influence of plasticizer with different functional groups on thermoplastic starch, Journal of Applied Polymer Science. 132 (2015).
[194] "Poly(Lactic Acid) (PLA), Poly(□-Caprolactone) (PCL) and Thermoplastic " by Rui Wang, (n.d.). https://scholarworks.rit.edu/theses/9933/ (accessed April 13, 2019).
[195] S.S. Zamir, M.R. Frouzanmehr, M. Nagalakshmaiah, A. Ajji, M. Robert, S. Elkoun, Chemical compatibility of lactic acid-grafted starch nanocrystals (SNCs) with polylactic acid (PLA), Polym. Bull. (2018).
[196] R.L. Shogren, W.M. Doane, D. Garlotta, J.W. Lawton, J.L. Willett, Biodegradation of starch/polylactic acid/poly(hydroxyester-ether) composite bars in soil, Polymer Degradation and Stability. 79 (2003) 405–411.
[197] S. Lv, Y. Zhang, J. Gu, H. Tan, Soil burial-induced chemical and thermal changes in starch/poly (lactic acid) composites, International Journal of Biological Macromolecules. 113 (2018) 338–344.
[198] Karamanlioglu M, Preziosi R, Robson GD: Abiotic and biotic environmental degradation of the bioplastic polymer poly(lactic acid): A review. Polym Degrad Stab 2017;137:122–130.
[199] Rudnik E, Briassoulis D: Degradation behaviour of poly(lactic acid) films and fibres in soil under Mediterranean field conditions and laboratory simulations testing. Ind Crops Prod 2011;33:648–658.